ALMA MATER STUDIORUM
UNIVERSITÀ DI BOLOGNA

DOTTORATO DI RICERCA IN

SCIENZE BIOMEDICHE E NEUROMOTORIE

Ciclo 36

Settore Concorsuale: 05/H2 - ISTOLOGIA

Settore Scientifico Disciplinare: BIO/17 - ISTOLOGIA

Pharmacological targeting of P-selectin to halt the progression of myelofibrosis in the *Gata1*^{low} mouse model

Presentata da: ***Paola Verachi***

Coordinatore Dottorato

Prof.ssa Matilde Yung Follo

Supervisore

Prof. Rocco Liguori

Co-supervisore

Prof.ssa Anna Rita Migliaccio

Esame finale anno 2024

Abstract

Primary myelofibrosis is a clonal hematopoietic disorder characterized by marked degrees of systemic inflammation. The release of pro-inflammatory factors by clonal hematopoietic cell populations cause the remodeling of a specialized microenvironment, defined niche, in which the hematopoietic stem cells reside. The main source of pro-inflammatory cytokines is represented by malignant megakaryocytes. The bone marrow and spleen from myelofibrosis patients, as well as those from the *Gata1*^{low} mouse model of the disease, contain increased number of abnormal megakaryocytes. These cells express on their surface high levels of the adhesion receptor P-selectin that, by triggering a pathological megakaryocyte-neutrophil emperipolesis, lead to increased bioavailability of TGF-β1 in the microenvironment and disease progression. *Gata1*^{low} mice develop with age a phenotype similar to that of patients with myelofibrosis. We previously demonstrated that deletion of the P-selectin gene in *Gata1*^{low} mice prevented the development of the myelofibrotic phenotype in these mice. In the current study, we tested the hypothesis that pharmacological inhibition of P-selectin may rescue the fibrotic phenotype of *Gata1*^{low} mice. To test this hypothesis, we have investigated the phenotype expressed by old *Gata1*^{low} mice treated with the anti-mouse monoclonal antibody against P-selectin RB40.34, alone or in combination with the JAK2 inhibitor Ruxolitinib. The results showed that the combined therapy normalized the phenotype of *Gata1*^{low} mice with limited toxicity by reducing fibrosis, TGF-β1 and CXCL1 content in the BM and spleen and by restoring hematopoiesis in the bone marrow and the normal architecture of the spleen. In conclusion, pharmacological inhibition of P-selectin was effective in targeting malignant megakaryocytes and the microenvironmental abnormalities that affect the hematopoietic stem cell compartment in this model. These results suggest that P-selectin and JAK1/2 inhibitors in combination may represent a valid therapeutic option for patients with myelofibrosis.

Table of Contents

1. Introduction

1.1 Primary Mielofibrosis

1.1.1 Pathogenetic Insights

Primary Myelofibrosis (PMF) is the most severe of Philadelphia chromosome negative myeloproliferative neoplasms (MPN), a group of hematological disorders correlated by morphological and molecular genetic features that includes also Polycythemia Vera (PV) and Essential Trombocytemia (ET) [1]. They are all clonal disorders characterized by an excessive proliferation of myeloid progenitors, resulting in an aberrant production of mature functional blood cells [2]. In 2005 several studies shed the light on the genetic landscape of MPN by the discovery of a Janus kinase 2 (*JAK2*, located on chromosome 9p24) gain of-function mutation ($JAK2^{V617F}$) at the stem cell compartment, resulting in aberrant clonal myeloproliferation [3–6]. JAK2 is a tyrosine kinase that participates in the signal transduction of all the hematopoietic superfamily receptors such as the IL-3 receptor family (IL-3R, IL-5R, and GM-CSF receptor), and single-chain receptors such as erythropoietin receptor (EPO) and thrombopoietin (TPO) receptor [7].

The $JAK2^{V617F}$ is a point mutation located at the JH2 pseudokinase domain (exon 14) and occurs in PV, ET and PMF with frequencies of ~98%, 50% and 60%, respectively [8]. The mutation results in the loss of the inhibitory effect of the JH2 domain on the kinase activity and consequently in the constitutive activation of JAK2 and downstream signaling cascades, including molecules such as STAT5 (signal transducer and activator of transcription 5) and ERK (extracellular signal-regulated kinase) [4]. Additional MPN driver mutations include *MPL* (Myeloproliferative Leukemia Protein) and *CARL* (Calreticulin) mutations, which also lead to constitutive activation of the JAK2/STAT pathway, but through different mechanisms.

Regardless of the driver mutation, PMF is characterized by the coexistence of an inflammatory state with aberrant cytokine production and megakaryocytes (MKs) proliferation and it is currently established that these factors contribute to bone marrow (BM) and splenic stromal reaction (including reticulin/collagen fibrosis and neoangiogensis), ineffective erythropoiesis with extramedullary hematopoiesis (EMH) and constitutional symptoms [1,9,10]. Moreover, the concurrence of these phenomena in the pathogenesis of the disease can explain the ineffectiveness of pharmacologic therapy with JAK1/2 inhibitors in eradicating the neoplastic clone in myelofibrosis (MF). Indeed, current drug therapy, including the use of JAK1/2 inhibitors, is mostly palliative and has not been shown to modify the natural course of the disease or prolong survival.

In this regard, it is currently assumed that the complex phenotype and phenotypic differences among patients are also related to other co-occurring mutations, including those of epigenetic regulators, that cooperate with driver mutations to facilitate disease progression and leukemic transformation. These mutations occur with frequency of 10% or higher and include *ASXL1* (additional sex combs-like 1), *TET2* (TET oncogene family member 2) and *DNMT3A* (DNA cytosine methyltransferase 3a) [11–13]. More recent observations include impaired MKs maturation associated with reduced GATA1 expression that might arise from ribosomal deficiency [14].

At present, the only cure for PMF remains allogeneic hematopoietic stem cell transplant (AHSCT), a therapeutic option limited to a small number of patients and associated with high mortality and morbidity. Thus, PMF is still an unmet clinical need and the current studies are focusing on finding new therapeutic strategies targeting the malignant clone and the microenvironmental abnormalities that contribute to fibrosis and disease progression.

1.1.2 Disease Manifestations

The complex phenotype of PMF includes fibrosis and hematopoietic failure in BM, stem and progenitor cells mobilization, development of EMH with splenomegaly and its clinical course is associated with an increased risk of thrombosis, bleeding and evolution to acute leukemia that occurs in approximately 20% of patients. Prominent clinical features include anemia due to ineffective erythropoiesis, those associated with splenomegaly such as abdominal distention and pain, early satiety, dyspnea, and diarrhea and constitutional symptoms including fatigue, low-grade fever and cachexia. Most patients die from the disease with a median survival ranging between 5 and 7 years [15].

In 2016, the World Health Organization (WHO) provided the diagnostic criteria for PMF that include a combination of clinical, morphological and molecular genetic features [16]. The WHO subclassifies PMF into prefibrofic/early PMF (pre-PMF) and overt PMF stages. Diagnosis of pre-PMF, as well as overt PMF, requires meeting all three major criteria and at least one minor criterion (**Table 1**).

Table 1. WHO diagnostic criteria for PMF. Table adapted from Barbui T et al. Blood Cancer J. 2018 Feb 9;8(2):15 [16]

PMF	
Pre-PMF	**Overt PMF**
Major criteria • Megakaryocytic proliferation and atypia, without reticulin fibrosis grade 1, accompanied by increased age-adjusted BM cellularity, granulocytic proliferation, and often decreased erythropoiesis • Not meeting the WHO criteria for BCR-ABL1+, chronic myeloid leukemia (CML), PV, ET, myelodysplastic syndromes, or other myeloid neoplasms • Presence of *JAK2*, *CALR*, or *MPL* mutation or in the absence of these mutations, presence of another clonal marker or absence of minor reactive BM reticulin fibrosis	*Major criteria* • Presence of megakaryocytic proliferation and atypia, accompanied by either reticulin and/or collagen fibrosis grades 2 or 3 • Not meeting WHO criteria for BCR-ABL1+, chronic myeloid leukemia (CML), PV, ET myelodysplastic syndromes, or other myeloid neoplasms • Presence of *JAK2*, *CALR*, or *MPL* mutation or in the absence of these mutations, presence of another clonal marker, or absence of reactive myelofibrosis
Minor criteria • Anemia not attributed to a comorbid condition • Leukocytosis ≥11000/μL • Palpable splenomegaly • LDH increased to above upper normal limit of institutional reference range	*Minor criteria* • Anemia not attributed to a comorbid condition • Leukocytosis ≥11000/μL • Palpable splenomegaly • LDH increased to above upper normal limit of institutional reference range • Leukoerythroblastosis

1.1.3 Conventional Symptomatic Therapies for PMF

As already mentioned, AHSCT currently remains the only treatment modality to cure PMF. However, transplant-related complications are not trivial and are associated with high morbidity and mortality [17]. At present, choice of drug strategies for PMF is mostly based on managing anemia, splenomegaly and constitutional symptoms. For anemia, the drugs of choice are androgens, prednisone, danazol or immunomodulatory drugs such as thalidomide. For splenomegaly, clinicians opt for hydroxyurea [18]. Ruxolitinib (Rux) and fedratinib are JAK2 inhibitors approved by the Food and Drug Administration (FDA) for their use in PMF and are considered effective treatment options for countering splenomegaly and constitutional symptoms in hydoxyurea-refractory patients, with response rates of 30% to 50%. However, treatment with this drugs is associated with treatment-emergent anemia and thrombocytopenia [19]. Moreover, long-term treatment with Rux is associated with high rate of treatment discontinuation, withdrawal syndrome during treatment discontinuation

that is characterized by acute relapse of constitutional symptoms, rapid worsening of splenomegaly and cytopenias [20–22]. Several reports associated the use of Rux with the onset of opportunistic infections and poor response to COVID vaccines. Recently introduced JAK1/2 inhibitors, such as pacritinib and momelotinib, have markedly different toxicity profiles and momelotinib have also shown erythropoietic benefits [23].

However, Rux nor the other JAK1/2 inhibitors currently available for PMF have antitumor activity and none of them has been proven to reverse BM fibrosis or induce complete or partial remissions. In addition, long-term follow-up of patients treated with JAK1/2 inhibitors showed no evidence of survival advantage. At present, new agents targeting outside of the JAK-STAT pathway, alone or in combination with Rux, are currently under investigation to optimize clinical response of PMF patients.

1.2 The Pathogenetic Role of Megakaryocytes in Myelofibrosis

1.2.1 Normal Megakaryopoiesis

MKs are large polyploid cells (50–100 μm) with polylobulated nuclei and represent the 0.05% of the total BM population. Traditionally, MKs are produced from hematopoietic stem cells (HSCs) under the control of TPO signaling and have the major function to produce and release platelets into the circulation. Megakaryopoiesis initiates with HSCs giving rise to multipotent progenitors (MPP), which generate the common myeloid progenitor (CMP). CMP then produce the megakaryocyte erythrocyte progenitor (MEP), which gives rise to both erythroid cells and MKs [24,25]. Beyond the TPO signaling, megakaryopoiesis is controlled by several transcription factors, including *RUNX1*, *GATA1*, *GFI1B* and several *ETS* factors [26,27].

On the basis of ultrastructural features, MKs precursors can be divided into four classes: the promegakaryoblast, a small mononuclear cell; the megakaryoblast (stage I MK), a cell with oval or kidney-shaped nucleus and several nucleoli; the promegakaryocyte (stage II MK), a cell with an irregularly shaped nucleus and abundant cytoplasm; and mature MK (stage III MK) that contain a multilobed nucleus with abundant cytoplasm [28].

Upon stimulation, immature MKs undergo multiple endomitotic cycles and cytoskeletal rearrangements to generate proplatelets, which enter the peripheral blood and produce platelets. During the final stage of maturation, the MKs cytoplasm develops a complex system of membranes, defined the demarcation membrane system (DMS), and different types of granules including lysosomes, dense granules and α-granules [29]. MKs α-granules are the most abundant and contain several types of adhesive proteins, such as β-thromboglobulin, CXCL4 (platelet factor 4, PF4),

thrombospondin, fibronectin, von Willebrand factor (vWF) and P-selectin (P-sel). Moreover, α-granules contain growth factors including Platelet Derived Growth Factor (PDGF), Transforming Growth Factor-β1 (TGF-β1), Epidermal Growth Factor (EGF) and Insulin Growth Factor (IGF) [30].

1.2.2 Megakaryopoiesis in PMF is Abnormal

Regardless of the driver mutation, the BM and spleen from PMF patients contain a high number of atypical MKs that display morphological abnormalities such as hypo-lobulated nuclei and clustering. Previous studies demonstrated that CD34pos cells from PMF patients had an increased capacity to generate MKs in culture. In particular, these MKs are immature with reduced ploidy and have higher proliferative rate [31–33]. These observations were further supported by single cell studies demonstrating that HSCs from PMF patients express MKs-specific genes, suggesting their bias toward this lineage [34,35].

In normal megakaryopoiesis, TPO binds to its receptor MPL and induces JAK/STAT, MAPK/ERK and PI3K/AKT activation in HSCs, MKs and platelets [36]. Mice lacking TPO or MPL are thrombocytopenic with decreased number of MKs and progenitors [37,38]. Numerous reports have defined the role of enhanced TPO-MPL signaling in PMF by demonstrating that the serum from PMF contains elevate levels of TPO and overexpression of TPO in the BM induce fibrosis in mice [39,40]. Beyond the abnormalities in the TPO signaling, in 2005 Vannucchi et al., reported that malignant MKs showed an impaired maturation that was associated with low levels of the transcription factor GATA1 [41,42]. In PMF, the loss of GATA1 protein is a post-transcriptional event since the *GATA1* mRNA levels are modestly elevated or unchanged relative to control MKs [14]. Indeed, by gene-expression analysis Gilles et al., revealed the presence of a ribosomal protein S14 (RPS14)-deficient gene signature (RPS14_DN.V1_UP), which is associated with defective ribosomal protein function, suggesting that ribosomal deficiency contributes to impaired megakaryopoiesis in PMF [14].

1.2.3 The Malignant Megakaryocytes as Drivers of PMF

The crucial of role of MKs in the pathogenesis of the disease was proven by several studies on PMF patients and murine models indicating that: i) all driver mutations in MPN result in abnormal proliferation of malignant MKs [43]; ii) the MKs-restricted expression of $JAK2^{V617F}$ mutation is sufficient to induce MF in mice [44]; iii) patients and rats treated with TPO mimetics develop BM fibrosis [45]; iv) high TPO production by transduced hematopoietic cells, as well as impaired expression of the transcription factor GATA1, result in the development of MF in mice [46,47]; v) patients with Grey Platelet Syndrome, a rare inherited bleeding disorder characterized by

macrothrombocytopenia and agranular MKs and platelets, manifest myelofibrosis and splenomegaly [48].

In PMF, MKs are supposed to be the main source of pro-inflammatory cytokines that contribute to fibroblast proliferation, fibrotic evolution, neoangiogensis and osteosclerosis [31]. Among these cytokines, TGF-β1 plays a crucial role in the development of BM fibrosis. Once activated, TGF-β1 initiates the fibrosis by increasing the synthesis of types I, III and IV collagen, fibronectin, proteoglycans and tenascin, and by decreasing extracellular matrix (ECM) degradation through down-regulation of metalloproteinases (MMPs) and up-regulation of tissue MMPs inhibitors [49,50]. Moreover, previous studies demonstrated that TGF-β1 restrained HSCs proliferation and induced endothelial to mesenchymal transition in fibrotic diseases [51].

Of note, TGF-β1 and its receptors are abnormally expressed in MKs, platelet and CD34pos cells from PMF patients. In addition, Ciaffoni et al., reported an activation of the non-canonical TGF-β1 signaling in the BM and spleen from PMF patients [52]. The contribution of TGF-β1 in the pathogenesis of PMF was supported by observations indicating that genetic ablation of the gene or treatment with the TGF-β receptor-1(R1) kinase inhibitor SB43154 cure several mouse models of the disease [52–56].

Other MKs-derived cytokines/chemokines potentially involved in fibrosis progression in the BM are CXCL4, PDGF, Fibroblast Growth Factor (FGF), Vascular Endothelial Growth Factor (VEGF) and Interleukin-8 (IL-8). In particular, IL-8 binds to CXC chemokine receptor 1 (CXCR1) and 2 (CXCR2) and exhibits many biological functions in inflammation by stimulating neutrophils chemotaxis, HSCs proliferation and neoangiogensis. High levels of circulating IL-8 were found in the plasma and serum from PMF patients [57]. In addition, Dunbar et al., demonstrated that the malignant CD34pos clones from a subset of PMF patients secreted high levels of IL-8 *in vitro* which was associated with adverse clinical outcome and increased marrow fibrosis [58].

The potential mechanisms underlying the aberrant release of MKs content in BM fibrosis have been previously described and may be related to: i) an aberrant assembly and secretion of granules stored within the MKs; ii) an aberrant release of microvescicles; iii) a pathological cell-cell interaction between MKs and polymorphonuclear (PMN) cells that lead to the death of MKs by para-apoptosis and to the consequent release of the MKs content [59].

1.2.4 Megakaryocytes as Inducers of the Microenvironmental Abnormalities in PMF

Recent advances by single cell expression profiling showed that, in addition to traditional MKs committed to generate platelets, there are at least three other MKs subpopulations, each one exerting different functions: the niche-poised MKs, which are responsible for producing the ECM; the immune-poised MKs, which can be activated in response to inflammatory signals and exert immune functions by secreting effectors molecules such as IL-8; the HSCs-supporting MKs, which reside in the BM in close proximity to the vascular niches and regulate HCSs quiescence and proliferation during both steady-state and stress hematopoiesis [60–63].

The role of MKs as shapers of hematopoietic niches has been proven by the fact that conditional ablation of MKs in murine models resulted in increased HSCs frequency and cycling in the BM, suggesting that MKs normally regulate HSCs quiescence through the production of CXCL4 and TGF-β1 [64,65]. MKs also participate in HSCs niche remodeling by promoting osteoblast expansion [66,67] and activate HSCs proliferation under stress conditions by releasing fibroblast growth factor 1 (FGF1), PDGF-β, and TGF-β1 [65,68].

In light of these recent discoveries indicating that MKs are an heterogeneous population exerting several functions beyond platelet production, it has been suggested that, in pathologic conditions, malignant MKs are responsible to induce microenvironment dysfunctions which sustain hematologic malignancies, including MPN [69].

Firstly, it is widely recognized that PMF-MKs support and regulate the malignant HSCs-supporting microenvironment by secreting several pro-inflammatory cytokines, including TGF-β1, and forcing fibroblasts to produce ECM in the disease. Indeed, patients with MF have dramatically increased levels of TGF-β1 from plasma and MKs cultures in comparison to the healthy donors, and this condition supports the prevalence of MF-HSCs by altering the hematopoietic microenvironment and inducing the quiescence of a reservoir of normal HSCs [70,71].

Finally, abnormal MKs interactions with other cell types have been described in PMF: i) Zhan et al., reported that mice expressing the $JAK2^{V617F}$ mutation specifically in endothelial cells exhibit thrombocytosis and clusters of MKs preferentially located near sinusoids, associated with reticulin fibrosis [44]; ii) Karagianni et al., extensively described the role of MKs on bone homeostasis, suggesting that these cells promote osteosclerosis by activating osteoblasts proliferation while inhibiting the development and the activity of osteoclasts [76].

1.3 The *Gata1*^{low} Mouse Model of PMF

Regardless of the driver mutation, the PMF has a unique cellular signature: the BM and spleen of PMF patients, as well as those from murine models of the disease, contain a great number of defective MKs carrying several abnormalities including an increased proliferation with delayed maturation [28,77]. The driver role of malignant MKs in the pathogenesis of the disease has been proven by the fact that MKs-restricted expression of *JAK2*^{V617} mutation in mice is sufficient to induce enhanced erythropoiesis and promote fibrosis, leading to a myeloproliferative state with expansion of mutant and non-mutant hematopoietic cells [44]. It is well established that impaired MKs maturation in PMF is associated with reduced expression of GATA1, whose downregulation has been associated to ribosomal deficiency for defective *RPS14* gene signature [14,41].

GATA1 is a transcription factor that exerts a key role in erythroid and megakaryocytic cell differentiation and its importance in hematopoiesis has been proven by the fact that mice lacking the gene by targeted mutation die in utero of severe anemia [78,79]. The clinical relevance of this transcription factor has been characterized several years after the discovery of the gene, when *GATA1* mutations has been associated with inherited human disorders characterized by MKs abnormalities such as dyserythropoietic anemia, X-linked thrombocytopenia, and thalassemia [80–83].

In particular, the role of GATA1 in megakaryopoiesis has been demonstrated by the observation that transgenic mice expressing reduced levels of this transcription factor or lacking for the GATA1 partner FOG-1 are thrombocytopenic [84–86]. Indeed, *GATA1* deficiency leads to a marked increase of small and immature MKs that fail to complete the differentiation program and this results in a lower number of circulating platelets with structural and functional abnormalities. Morphologically, platelets from mice expressing low levels of GATA1 are bigger and spherical with low density of α-granules. Moreover, impaired platelet activation and prolonged bleeding times has been reported. Low levels of GATA1 lead to an hyperproliferation of MKs precursors, reduced expression of lineage-specific genes (e.g. *Pf4*, *Mpl*) and ultrastructural abnormalities including presence of excessive rough endoplasmic reticulum RER and disorganized DMS [84,86].

In 2002, the Migliaccio's laboratory was the first to describe the transgenic *Gata1*^{low} mice lacking of the first enhancer (DNase hypersensitive site I) and the *Gata1* distal promoter as a suitable model for PMF [47]. These mice were originally generated by McDevitt et al., to define the mechanisms that govern the transcriptional regulation of *Gata1*. The upstream region of the *Gata1* locus comprises two short nonconding 5'-exons and their promoters, and a DNase I hypersensitive site (HS) region. By homologous recombination, the ≈8 kb upstream region including the DNase I HS was replaced by a loxP-flanked neomycin-resistance cassette. The disruption of the region of interest was obtained

by using a targeting vector containing a loxP site-flanked neomycin resistant gene driven by the mouse phosphoglycerate kinase promoter and herpes simplex virus thymidine kinase gene. The construct was electroporated into 129S4/SvJae-derived J1 embryonic stem cells which were themselves injected into C57BL/6 blastocysts [87].

The resulting hypomorphic mutation leads to anemia due to an impairment in erythroid maturation. Moreover, *Gata1^{low}* mice are severely thrombocytopenic because MKs remain immature and release few abnormally large platelets. At the ultrastructural level, the MKs maturation is blocked between the stage I and II, the α-granules show a reduced expression of several proteins including the vWF and an atypical localization of the adhesion molecule P-sel that is found on DMS rather than within the α-granules. The proliferative rate of *Gata1^{low}* MKs is increased, while their expression of lineage-specific genes (e.g. *Tpo*, *Mpl*) is reduced.

In the C57BL/6 strain the mortality was above the 90% of mutants around birth; when the mutation was introduced in the CD1 background by the Migliaccio's laboratory, most of the mice reached adulthood and recovered from the severe anemia within the first month but remained thrombocytopenic.

Mice harboring the *Gata1^{low}* mutation develop with age all the pathological features of human PMF including anemia, progenitor cells in the peripheral blood (stem and progenitor cells mobilization), collagen and reticulin deposition in the BM and in the spleen and splenic EMH with consequent splenomegaly [47]. The major difference between this model and other murine models developed for the study of PMF is represented by the slow rate of progression of the disease in the *Gata1^{low}* mice, which resembles the natural history of human PMF [47].

During their first 12 months, *Gata1^{low}* mice exhibit only thrombocytopenia and splenomegaly due to the expansion of MKs lineage. After the first month, they recover from anemia but the high rate of erythroid progenitor cell apoptosis persists. *Gata1^{low}* mice manifest the first symptoms at 8 to 12 months of age, whereas a complete myelofibrotic phenotype is not observed until 15 months of age. The first signs of the myelofibrotic phase are: reticulin deposition in the BM with medullary aplasia, splenomegaly, EMH in the liver, moderate leukocytosis and immature myeloid cells in the peripheral blood [47]. However, few of the *Gata1^{low}* mice survive more than 2 to 4 months after the manifestation of first symptoms. Similarly, human PMF is usually diagnosed in the second half of life with the final exitus within 4.5 years.

1.4 Role of P-selectin/TGF-β Circuit in the Progression of PMF

1.4.1 Role of TGF-β1 in PMF

As already mentioned, TGF-β1 contributes to the pathogenesis of the PMF by promoting collagen/reticulin deposition and fibrosis. TGF-β1 is a cytokine involved in tissue development and repair and its dysregulation has been observed in several forms of cancer. Expression of TGF-β1 is regulated by TGF-β1 itself, while its activity is promoted by proteases that convert the latent complex into its active form. Active forms of TGF-β1 bind to a membrane receptor serine/threonine kinase complex that phosphorylates SMAD2 and SMAD3, which translocate in the nucleus where they form a complex with SMAD4 to regulate target gene expression [88]. TGF-β1 can also signal through non-canonical pathways, including ERK, p-38, MAPK and JNK activation [89,90].

This growth factor maintains tissue homeostasis and exhibits tumor-suppressive effects by regulating not only cellular proliferation, differentiation, survival, and adhesion but also the cellular microenvironment. On the other hand, pathological alterations of the TGF-β1 signaling pathway promote cell invasion, immune regulation, and microenvironment modification that malignant cells may exploit to their advantage [88]. In this regard, several studies reported that serum, CD34pos cells, and MKs from PMF patients contain levels of total and bioactive TGF-β1 2-fold higher than normal. As well as human patients, *Gata1*^{low} mice express normal levels of total TGF-β1 in plasma and 2-fold higher than normal in the BM. Of note, Zingariello et al., demonstrated that the TGF-β1 content of MKs from the BM and spleen from PMF patients and from *Gata1*^{low} mice was 5- to 10 fold higher than normal [52]. In the same study, they observed that the BM and spleen from *Gata1*^{low} mice expressed distinctive alterations in TGF-β1 signaling profile with up- or down-regulation of genes involved in hematopoietic functions [52]. In particular, David-assisted pathway analysis of the two altered signatures predicted osteopetrosis and hematopoietic failure in the BM and activation of hematopoiesis in the spleen, a pattern that reflected the phenotype of *Gata1*^{low} mice. The contribution of this cytokine in the development of myelofibrosis in *Gata1*^{low} mice was further supported by observations indicating that treatment with the TGF-β receptor-1(R1) kinase inhibitor SB43154 prevented the development of the myelofibrotic phenotype in this murine model. In particular, the SB43154-treatment in *Gata1*^{low} mice normalized the TGF-β1 signaling, restoring the hematopoiesis and reducing the fibrosis, osteogenesis and neoangiogensis in the BM while reducing EMH in the spleen [52]. Moreover, Varricchio et al., demonstrated that the TGF-β1 protein trap AVID200 beneficially affected hematopoiesis and BM fibrosis in PMF. In this study, they demonstrated that this drug reduced the proliferation of human mesenchymal stromal cells (MSCs), decreased phosphorylation of SMAD2, and inhibited the ability of TGF-β1 to induce collagen expression. The

in vivo effects of AVID200 were tested on *Gata1^{low}* mice and resulted in a reduction of BM fibrosis and an increase in BM cellularity and in the frequency and numbers of murine progenitor cells as well as short-term and long-term HSCs [70]. Collectively, these data strongly support the prominent role of TGF-β in the pathogenesis of the disease and encourage the use of therapeutic agents targeting the TGF-β1 and/or elements involved in its release for the cure of PMF.

1.4.2 P-selectin as a Driver of the Pathological Megakaryocyte-Neutrophil Emperipolesis Observed in PMF

Several studies have described the pathological mechanisms underlying the massive release of TGF-β1 by malignant MKs. In particular, by using mice overexpressing TPO, which develop a disease resembling human PMF, Schmitt et al., were the first to demonstrate that the aberrant release of growth factors stored in the MKs granules, including TGF-β1, was promoted by a pathological emperipolesis between MKs and neutrophilic and eosinophilic PMN cells [77].

The term emperipolesis was originally used to define a random passage of one cell through the cytoplasm of another one with no physiologic consequences for either of them [91]. Normally this process occurs in MKs with a frequency of 5% and an increase of this frequency was observed in patients with severe thrombocytosis, whether myeloproliferative or reactive, and was not necessarily associated with marrow fibrosis. *In vitro* modeling and *in vivo* studies have proven that emperipolesis is a distinctive form of cell-cell interaction different from phagocytosis, entosis or transcellular migration and involves the active cytoskeletal engagement by both cell types. By electron microscopy and immunofluorescence studies, Cunin et al., proposed a multi-steps process of MK-neutrophil emperipolesis: (1) neutrophils expressing β2 integrin binds to ICAM-1 expressed by MKs, inducing the translocation and clustering of ICAM-1 and ezrin; (2) neutrophils enter into MKs vacuole, called emperisome, in an actin-dependent manner; (3) the emperisome contracts and neutrophil and emperisomes membranes enter in close contact; (4) the emperisome membrane disappear and neutrophils translocate to the DMS where membrane fusion occurs; (5) after a period of residence, neutrophils exit the host cell without evident harm to either cell [92].

In the above-mentioned study, Schimitt et al., provided evidences of extensive emperipolesis in BM biopsy specimens from PMF patients as well as in TPO mice. The rate of emperipolesis in PMF patients was correlated with the amount of reticulin deposition and thus associated with the severity of the disease and with poor prognosis. Ultrastructural studies on BM samples from TPO mice showed a marked alteration of both the host MKs and the engulfed PMN cells. PMN cells had apoptotic-like nuclei and disrupted plasma membranes. MKs had myeloperoxidase-positive granules

scattered in their cytoplasm, associated with cytoplasmic alterations, vacuoles, dystrophic DMS, and ruptured α-granule. Of note, the resulting morphologic alterations detected in MKs and PMN cells were observed in parallel with abnormal P-sel expression and subcellular distribution, in particular on the DMS near engulfed PMN cells [77]. Since PMN cells express the P-sel ligand PSLG-1 on their surface [93,94], the authors suggested that the binding of this receptor to the P-sel expressed on the DMS of MKs might be responsible for the pathological emperipolesis between these cells. This destructive mutual cell interaction may result in the pathological release of TGF-β1 in microenvironment, leading to fibroblast activation and collagen deposition in the BM. According with this hypothesis, the same abnormalities in P-sel localization were observed in the BM from patients with idiopathic MF.

According to these observations, Centuriore et al., detected an increased rate of emperipolesis also in the BM and spleen from *Gata1*^{low} mice [28]. The authors observed that mutant MKs were surrounded by myeloperoxidase-positive neutrophils, some of which had their membranes in close contact with those of the DMS. Although apoptotic MKs were not found in *Gata1*^{low} myelofibrotic tissues, the 50% of MKs had a shrunken and damaged morphology and the 16% (in the spleen) to 34% (in the BM) of them contained 1 to 3 degranulated neutrophils embedded in a vacuolated cytoplasm. In parallel, the authors observed an abnormal distribution of P-sel. Indeed, low levels of GATA1 block the MKs maturation between stage I and II and halt proper assembly of α-granules [28]. This was demonstrated by immunolabeling studies showing that vWF was barely detectable in *Gata1*^{low} MKs, whereas P-sel, although normally expressed, was mostly delocalized to the DMS. Moreover, vWF and P-sel were barely detectable in *Gata1*^{low} platelets [95].

Collectively, these observations suggest that P-sel distribution to the DMS may represent an element upstream to TGF-β1 in the pathobiology of PMF.

To further support this hypothesis, Spangrude et al., evaluated the consequences of P-sel deficiency by using *Gata1*^{low} mice carrying a deletion of the P-sel gene (*Gata1*^{low}*/P-sel*^{null}) and comparing their phenotype with that of *Gata1*^{low} single mutants as they aged [96]. First, BM of *Gata1*^{low}*/P-sel*^{null} did not present fibrosis and the degree of osteosclerosis was inferior of that expressed by *Gata1*^{low} mice. Spleen from double mutant mice did not appear enlarged and showed reduced fibrosis. Deletion of the P-sel gene increased the survival of double mutants, extending their lives approximately 3 months longer than their *Gata1*^{low} littermates. Moreover, most *Gata1*^{low}*/P-sel*^{null} mutants survived splenectomy while 75% of *Gata1*^{low} mice died of profound anemia. In agreement with the observation that splenic hematopoiesis is dispensable for survival of *Gata1*^{low} */P-sel*^{null} mice, the P-sel deletion restored the abnormal distribution of *Gata1*^{low} HSCs and their ability to mature in BM.

As expected, loss-of-funtction of P-sel disrupted emperipolesis between MKs and neutrophils and prevented TGF-β1 accumulation in the microenvironment. Interestingly, MKs from *Gata1*^{low}*/P-sel*^{null} mice remained higher than normal and with an immature morphology, suggesting that, since the myelofibrotic phenotype is rescued in these mice, the P-sel/TGF-β1 circuitry may initiate the fibrotic progression. In conclusion, this study provided genetic evidence that disease progression is sustained by P-sel/TGF-β1 axis that increase TGF-β1 content in MKs and favor establishment of a microenvironment that supports MF-related HSCs niches in spleen.

1.4.3 Role of CXCL1 in Neutrophils Chemotaxis

Most of the scientific literature concerning emperipolesis was the result of transmission electron microscopy studies, but until then mechanisms that drive this process in MF remained poorly understood. The main limitation of transmission electron microscopy in studying this phenomenon is that this technique requires the use of thin sections (3 μm) whereas the diameter of MKs and neutrophils is 50-100 μm and 10–20 μm, respectively, and thus this method does not allow to unequivocally confirm the presence of engulfed neutrophils within MKs. With the recent development of confocal microscopy, which allows three-dimensional reconstruction of cells, Cunin et al., provided new insights about the mechanism underlying this process. Of note, they discovered that emperipolesis occurs in fast and slow forms that differ morphologically: approximately half of neutrophils exited the MKs rapidly, displaying amoeboid morphology as they passed through the host cell (fast emperipolesis), while the remaining neutrophils assumed a sessile morphology, remaining within the MKs for at least 60 minutes (slow emperipolesis). However, in both processes, the cell membranes of the MKs and neutrophils remain intact [92].

Recently, encouraged by this recent study, we revisited the pathological emperipolesis occurring in *Gata1*^{low} murine model of MF. First, we validated confocal microscopy observations with antibodies specific for the MKs and the neutrophils as a method to detect emperipolesis in the BM. As expected, BM sections from *Gata1*^{low} mice, as well as those from PMF patients, contained a high number of MKs and neutrophils that were preferentially located around or within MKs [97].

Then, we assessed whether the treatment with Reparixin, an allosteric inhibitor of CXCR1/R2, was effective in reducing this pathological cell interaction between MKs and neutrophils. The rationale for this study was provided by previous studies demonstrating that the levels of CXCL1, the murine equivalent of IL-8, and its ligands CXCR1/R2, were elevated in MKs from *Gata1*^{low} mice, according to recent findings indicating that high levels of circulating IL-8 are predictive of poor prognosis in

patients with PMF [58,98]. Moreover, it is well known that CXCL1 signaling triggers neutrophils chemotaxis, a process that reasonably precedes the emperipolesis between MKs and neutrophils.
Treatment with Reparixin did not affect the frequency of MKs in the BM from *Gata1*^{low} mice but significantly decreased that of neutrophils, including that around or within MKs [97].
In conclusion, these data suggested that CXCL1 may be responsible for the massive neutrophil infiltration and the consequent emperipolesis with malignant MKs, leading to the mutual destruction of these cells and the release of TGF-β1 in the microenvironment. This hypothesis was further supported by the fact that treatment with Reparixin was also able to reduce the TGF-β1 content and the degree of fibrosis in *Gata1*^{low} mice.

2. Aim of the study

At present, the only cure for PMF is represented by AHSCT since conventional therapies ameliorate constitutional symptoms but do not significantly impact disease progression. Several studies demonstrated that microenvironmental abnormalities and high levels of pro-inflammatory cytokines contribute to the BM stromal reaction and the progression of the disease, paving the way for novel therapeutic agents that may target these abnormalities.

Recent studies have suggested that the adhesion receptor P-sel may represent an element upstream to TGF-β1 pathway in the pathobiological mechanism underlying myelofibrosis. This hypothesis has been mechanistically demonstrated by the observation that the TGF-β1 content in the BM of *Gata1*^{low} mice lacking the P-sel gene was normal and that the double mutants *Gata1*^{low}*/P-sel*^{null} did not develop a myelofibrotic phenotype and showed an increased survival compared to their *Gata1*^{low} littermates.

Recently, the P-sel inhibitor crizanlizumab (SEG101) has been demonstrated to reduce the frequency of vaso-occlusive crises in patients with sickle cell disease with a low incidence of adverse events and in 2019 was approved by the FDA for clinical use.

The rationale for the clinical use of crizanlizumab has been provided by a preclinical study that evaluated the effects of the commercially available monoclonal antibody RB40.34 against the murine P-sel as an antithrombotic agent in a murine model of sickle cell disease. The aim of this study was to test the hypothesis that pharmacologic inhibition of P-sel, alone or in combination with Rux, might be more effective than Rux alone in reverting the myelofibrotic phenotype expressed by *Gata1*^{low} mice. First, we evaluated the ability of the antibody to reach the myelofibrotic tissues from *Gata1*^{low} mice and to target the malignant MKs that contain abnormal levels of P-sel. Then, by histological, flow cytometry and biochemical analyses we determined the short-term and long-term effects of the treatments. The results obtained indicated that the two drugs in combination reduced fibrosis, bone deposition and neoangiogensis while restoring hematopoiesis in BM and reducing hematopoiesis in spleen more effectively than the single agents.

3. Results

3.1. "Preclinical studies on the use of a P-selectin-blocking monoclonal antibody to halt progression of myelofibrosis in the *Gata1*^{low} mouse model"

The results of this study were published: **Verachi P**, Gobbo F, Martelli F, et al. *Preclinical studies on the use of a P-selectin-blocking monoclonal antibody to halt progression of myelofibrosis in the Gata1^{low} mouse model*. Exp Hematol. 2023;117:43-61. doi:10.1016/j.exphem.2022.09.004

The PDF of the published article is below.

ARTICLE

Preclinical studies on the use of a P-selectin-blocking monoclonal antibody to halt progression of myelofibrosis in the *Gata1^{low}* mouse model

Paola Verachi[a], Francesca Gobbo[a,b], Fabrizio Martelli[c], Mario Falchi[d], Antonio di Virgilio[e], Giuseppe Sarli[b], Celine Wilke[f], Andreas Bruederle[f], Anirudh Prahallad[f], Francesca Arciprete[g], Maria Zingariello[g], and Anna Rita Migliaccio[g,h]*

[a]*Department of Biomedical and Neuromotor Sciences, University of Bologna, Italy;* [b]*Department of Veterinary Medical Sciences, University of Bologna, Italy;* [c]*National Center for Preclinical and Clinical Research and Evaluation of Pharmaceutical Drugs, Istituto Superiore di Sanità, Rome, Italy;* [d]*National Center for HIV/AIDS Research, Istituto Superiore di Sanità, Rome, Italy;* [e]*Center for Animal Experimentation and Well-being, Istituto Superiore di Santà, Rome, Italy;* [f]*Novartis (United States), East Hanover, NJ, USA;* [g]*Unit of Microscopic and Ultrastructural Anatomy, University Campus Bio-Medico, Rome, Italy;* [h]*Altius Institute for Biomedical Sciences, Seattle, WA, USA*

The bone marrow (BM) and spleen from patients with myelofibrosis (MF), as well as those from the *Gata1^{low}* mouse model of the disease contain increased number of abnormal megakaryocytes. These cells express high levels of the adhesion receptor P-selectin on their surface, which triggers a pathologic neutrophil emperipolesis, leading to increased bioavailability of transforming growth factor-β (TGF-β) in the microenvironment and disease progression. With age, *Gata1^{low}* mice develop a phenotype similar to that of patients with MF, which is the most severe of the Philadelphia-negative myeloproliferative neoplasms. We previously demonstrated that *Gata1^{low}* mice lacking the *P-selectin* gene do not develop MF. In the current study, we tested the hypothesis that pharmacologic inhibition of P-selectin may normalize the phenotype of *Gata1^{low}* mice that have already developed MF. To test this hypothesis, we have investigated the phenotype expressed by aged *Gata1^{low}* mice treated with the antimouse monoclonal antibody RB40.34, alone and also in combination with ruxolitinib. The results indicated that RB40.34 in combination with ruxolitinib normalizes the phenotype of *Gata1^{low}* mice with limited toxicity by reducing fibrosis and the content of TGF-β and CXCL1 (two drivers of fibrosis in this model) in the BM and spleen and by restoring hematopoiesis in the BM and the architecture of the spleen. In conclusion, we provide preclinical evidence that treatment with an antibody against P-selectin in combination with ruxolitinib may be more effective than ruxolitinib alone to treat MF in patients.

HIGHLIGHTS

- Treatment with RB40.34 targeting murine P-selectin and ruxolitinib, in combination, is more effective than either drug alone in rescuing myelofibrosis in Gata1low mice.
- This drug combination reduced fibrosis, bone deposition and neoangiogenesis while restoring hematopoiesis in bone marrow and reducing hematopoiesis in spleen.
- Mechanistically, the drug combination may have exerted their effects by reducing the TGF-β and CXCL1 content of the bone marrow.
- These data provide pre-clinical evidence that P-selectin antibodies and Ruxolitinib in combination may be more effective than Ruxulotinib alone to treat myelofibrosis.

Myelofibrosis (MF) is the most severe of Philadelphia chromosome −negative myeloproliferative neoplasms (MPN). The complex phenotype of patients with MF includes fibrosis and hematopoietic failure in bone marrow (BM), stem/progenitor cell mobilization, and development of extramedullary hematopoiesis with splenomegaly, and their clinical course is associated with an increased risk of thrombosis, bleeding, and evolution to acute leukemia [1−4]. MF may be driven by gain of function mutations in several genes of the thrombopoietin axes, such as *MPL*, the thrombopoietin receptor; *JAK2*, the first element of the MPL signaling; and calreticulin, a chaperon protein, which when mutated binds MPL on the cell surface, inducing conformational changes, leading to ligand-independent constitutive activation of the receptor [5]. Regardless of the driver mutation, it has been recognized that MF has a distinctive cellular signature. In fact,

Offprint requests to: Anna Rita Migliaccio, Altius Institute for Biomedical Sciences, 2211 Elliott Avenue, 6th Floor, Suite 410, Seattle, WA 98121.; E-mail: amigliaccio@altius.org.

0301-472X/

https://doi.org/10.1016/j.exphem.2022.09.004

both the BM and spleen of such patients contain numerous clusters of morphologically immature megakaryocytes (MKs) [6] endowed with great proliferation potential [7,8]. In MF, MKs are retained immature by a mutation-driven RSP14 ribosomopathy that impairs the translation of the mRNA for GATA1 [9,10], the transcription factor that plays a pivotal role in the progression of MK maturation [11]. The causative role of the resulting abnormal MKs in the pathogenesis of this disease is strongly supported by experiments in mice, indicating that those carrying a hypomorphic mutation, which selectively reduces GATA1 in MKs (*Gata1*^{low} mice), develop MF with age [12], whereas transgenic mice expressing *JAK2*V617F, one of the driver mutations of the disease [1–4], only in MKs develop MF even if their hematopoietic stem cells (HSCs) are normal [13,14]. As first hypothesized by Schmitt et al. [7], mechanistically, malignant MKs are thought to drive MF by engaging in a pathologic process of emperipolesis with the neutrophils, increasing the bioavailability of transforming growth factor-β (TGF-β) and possibly other proinflammatory cytokines in the BM of patients with MF and animal models [8,15–17]. The pathobiological role of TGF-β in the development of MF has been further confirmed by the observation that in animal models, the development of MF is prevented by genetic ablation of the *TGF-β* gene [17,18] and reverted by treating MF mice with small TGF-β receptor-1 kinase inhibitors [19] or with the TGF-β trap AVID200 [20]. The TGF-β trap AVID200 is currently in phase I/II clinical trials for patients with MF who are resistant to therapy with the JAK1/2 inhibitor ruxolitinib (Rux) [21].

Later studies have indicated that the adhesion receptor P-selectin (P-SEL) may represent an element upstream to TGF-β in the pathobiological pathway leading to MF. In fact, the MK abnormalities observed in this disease include abnormal cytoplasmic trafficking of P-SEL, which was displayed on the cell surface instead of being partitioned into granules [22]. It has been hypothesized that P-SEL, which is found in high levels on the cell surface, interacting with its ligand P-selectin glycoprotein ligand-1 (PSGL-1) expressed by the neutrophils [23,24], drives a process of pathologic emperipolesis between the neutrophils and the MKs, which leads to the death of the MKs by para-apoptosis and release of TGF-β in the microenvironment [25,26].This hypothesis has been mechanistically demonstrated by the observation that the TGF-β bioavailability in the BM of *Gata1*^{low} mice lacking the *P-sel* gene is normal and that these mice do not develop MF with age and live on average 2 months longer than their *Gata1*^{low} littermates [27]. These findings support the hypothesis that in MF, the disease is established, and it progresses because of a pathologic P-SEL/TGF-β circuit established by the malignant MKs [28]. Whether inhibition of P-SEL would also be effective in reverting to normal MF once the disease is established has not been demonstrated as yet.

Recently, the P-SEL inhibitor crizanlizumab (SEG101) has been demonstrated to reduce the frequency of vaso-occlusive crises in patients with sickle cell disease with limited toxicity [29]. Based on these observations, in November 2019, the Federal Drug Administration approved the use of crizanlizumab for the treatment of pain crises in sickle cell disease. The rationale for the clinical study with crizanlizumab had been provided by a preclinical study that evaluated the effects of the commercially available monoclonal antibody RB40.34 targeting the murine P-SEL as an antithrombotic agent in a mouse model of sickle cell disease [30]. Because crizanlizumab had already been approved for clinical use and conditions for effective treatment of mice with RB40.34 had already been described, in this study, we tested the hypothesis that pharmacologic inhibition of P-SEL with RB40.34, alone and in combination with Rux, is effective in reverting the myelofibrotic phenotype expressed by *Gata1*^{low} mice.

METHODS

Mice

Gata1^{low} mice were bred in the animal facility of Istituto Superiore di Sanità as previously described [31]. Littermates were genotyped at birth by polymerase chain reaction, and those who were found not to carry the mutation were used as wild type (WT) controls. All the experiments, including the size of the experimental groups, were performed according to the protocols (D9997.121) approved by the Italian Ministry of Health on September 2, 2021, and according to the European Directive 86/609/EEC.

Treatments

A total of 47 *Gata1*^{low} mice were implanted with 14-mm microchips (one chip per mouse) (AVID) and divided into two separate experimental groups (Supplementary Figure E1). In the first experimental group, 24 11-month-old mice were randomly divided into four groups (three males and three females each), which were treated as follows: Group 1: vehicle (2% v/v Dimethyl sulfoxide by gavage, negative control for groups 3 and 4); Group 2: biotin-conjugated rat anti-mouse CD62P (RB40.34, catalog number 553743, BD Pharmigen; 30 μg/mouse/day $\times$ 3 days/week by IV, as described in [30], until day 45, and then IP); Group 3: Rux (Novartis Pharma AG; 45 mg/kg twice/day $\times$ 5 days a week by gavage as described in [32]); and Group 4: biotin-labeled RB40.34 and Rux in combination. On Day 5, all the mice were weighed and bled for blood cell count determination and detection of RB34.40 on platelets. The mice were sacrificed on day 5 (males) and day 12 (females), and BM and spleen were collected for cell signaling and histopathologic determinations. In the second experimental group, 23 8-month-old *Gata1*^{low} mice were divided into the same groups described above and treated for 7 weeks. In this experimental group, we used the purified RB40.34 (catalog number 553742, BD Pharmigen). The treatment was interrupted for 2 weeks during the holiday break (from day 24 to day 43). On day 54, all the mice were weighed, bled for blood count determination, and sacrificed for histopathology observations of their BM and spleen.

Blood Count Determination

Mice were topically anesthetized with Novesina (catalog number s01ha02, Novartis; one drop/eye), and blood was collected from the retro-orbital plexus into heparinized microcapillary tubes. Blood counts were evaluated on deidentified samples by an accredited commercial laboratory, which provides diagnostic services for laboratory animals (Plaisant Laboratory).

Flow Cytometry

Binding of RB40.34 to platelets. Platelet-enriched plasma was prepared by centrifugation of 200 μL heparinized blood (10,000 rpm for 20 min with the Eppendorf Centrifuge 5425/5425 R,

Eppendorf), and the binding of biotinylated RB40.34 to platelets was measured by flow cytometry following incubation with PE–Cy7–streptavidin (catalog number 557598, BD Pharmingen). Platelets were identified based on size (forward scatter) and internal cell complexity (side scatter), as described previously [22].

MK identification and binding to RB40.34. BM and spleen cells were resuspended in Ca^{++} Mg^{++}-free PBS containing 0.5% (v/v) fetal bovine serum (catalog number F7524, Sigma-Aldrich) and incubated with PE–CD41, FITC–CD61, and PE–Cy7–streptavidin. Cells were then divided by flow cytometry into four populations, corresponding to non-MK ($CD41^{neg}/CD61^{neg}$), immature MK ($CD41^{neg}/CD61^{high}$), mature MK ($CD41^{high}/CD61^{high}$), and very mature MK ($CD41^{high}/CD61^{neg}$), as described previously [19]. The levels of PE-Cy7–streptavidin staining were assessed as a measure of biotinylated RB40.34 binding to the MK.

Hematopoietic stem or progenitor cell determinations. Mononuclear BM and spleen suspensions were incubated with a cocktail of antibodies, including APC–CD117, APC–Cy7–Sca1, PE–Cy7–CD150, biotin-labeled anti-mouse CD48, and biotin-labeled anti-lineage antibodies. After 30 min of incubation on ice, cells were washed and incubated with streptavidin–PE–Cy5 (all from BD Pharmingen). Hematopoietic progenitor cells were defined as lineage-negative cells (Lin–). HSCs were defined as LSK ($Lin-/CD48^{neg}/c\text{-}Kit^{pos}/Sca\text{-}1^{pos}$), whereas long-term repopulating HSCs were defined as SLAM ($Lin-/CD48^{neg}/c\text{-}Kit^{pos}/Sca\text{-}1^{pos}/CD150^{pos}$) as described previously [27,33]. Nonspecific signals and dead cells were excluded, respectively, by appropriate fluorochrome-conjugated isotype and propidium iodide staining. All the flow cytometry analyses were performed using the Gallios analyzer (Beckman Coulter), and the results were analyzed using the Kaluza analysis program, version 2.1 (Beckman Coulter).

Western Blot Analysis

BM and spleen of *Gata1*^{low} mice treated for 5 days were dissolved in lysis buffer containing protease and phosphatase inhibitors and stored at −80°C. Protein extracts were separated by electrophoresis under denaturing conditions using 7.5%–10% mini-Protean TGX precasted gels (Bio-Rad) and transferred to nitrocellulose filters with the Trans-blot-Turbo system (Bio-Rad). Filters were probed with antibodies against proteins of the canonical (SMAD2/3, catalog number 8685, Cell Signaling), p-SMAD2/3 (catalog number 8828, Cell Signaling), TGF-βRII (catalog number ab186838, Abcam), and noncanonical (p38, catalog number 9212; p-p38, catalog number 4511; ERK1/2, catalog number 9102; and p-ERK1/2, catalog number 9101; all from Cell Signaling) TGF-β signaling and JAK2 (catalog number 3230, Cell Signaling), STAT5 (catalog number sc-74442), pJAK2 (Phospho-Tyr1007/1008 JAK2, catalog number 3771, Cell Signaling), and p-STAT5 (catalog number 9351, Cell Signaling) of JAK/STAT signaling. GAPDH (catalog number G9545, Sigma–Aldrich) was used as a loading control. The bands were quantified using ImageJ 1.52q software (National Institutes of Health) and normalized against GAPDH. Stoichiometry determinations of phosphoprotein levels were obtained by normalizing the content of the phosphoprotein with that of the corresponding total protein.

Histologic Analyses

Femurs were fixed in formaldehyde (10% v/v with neutral buffer), treated for 1 hour with a decalcifying kit (Osteodec; Bio-Optica), and embedded in paraffin. Spleens were fixed in formaldehyde and then embedded in paraffin [19]. Paraffin-embedded tissues were cut into consecutive 3-μm sections and stained either with hematoxylin–eosin (H&E; catalog number 01HEMH2500 and 01EOY101000, respectively; Histo-Line Laboratories), Gomori silver, or reticulin staining and Mallory trichrome staining (catalog numbers 04-040801, 04-040802, and 04-020802, respectively; Bio-Optica). For immunofluorescence microscopy, BM sections were incubated with anti-CXCL1 (catalog number ab86436, Abcam) and anti-TGF-β1 (catalog number sc-130348, Santa Cruz Biotechnology) antibodies, and reactions were detected by avidin–biotin immune-peroxidase staining and 3,3′-diaminobenzidine (0.05% w/v) (Vectastain Elite ABC Kit, Vector Laboratories). Slides were counterstained with Papanicolaou's hematoxylin (Histo-Line Laboratories). Images were acquired with the optical microscope Eclipse E600 (Nikon) equipped with the Imaging Source "33" Series USB 3.0 Camera (catalog number DFK 33UX264), and the signal was quantified acquiring at least five different areas/femur/mouse from at least four mice per group using ImageJ program (version 1.52t) (National Institutes of Health), as described previously [34,35]. For immunofluorescence microscopy determinations, 3-μm-thick BM sections were dewaxed in xylene, and antigens were retrieved by treatment with EDTA buffer (pH = 8) for 20 min in a pressure cooker (110°C–120°C, high pressure) and incubated with antibodies against CD42b (catalog number ab183345, Abcam), GATA1 (catalog number sc-265, Santa Cruz), CD3 (catalog number ab16669, Abcam), and CD45R/B220 (catalog number 553085, BD-Pharmingen) overnight at 4°C. Primary antibodies were visualized with the secondary antibody goat anti-rat Alexa Fluor 488 (catalog number ab150165, Abcam) or goat anti-rabbit Alexa Fluor 555 (catalog number ab150078, Abcam). All sections were counterstained with 4′,6-Diamidino-2-phenylindole (catalog number D9542-5MG, Sigma–Aldrich), mounted with Fluor-shield histology mounting medium (catalog number F6182-10MG, Sigma–Aldrich), and examined using a Nikon Eclipse Ni microscope equipped with filters appropriate for the fluorochrome to be analyzed. Images were recorded with a Nikon DS-Qi1Nc digital camera and NIS 190 Elements software BR 4.20.01 and quantified with ImageJ program by counting the number of cells that exceeded the intensity set as the threshold, as described previously [35]. Reconstruction of the image of all the femurs was obtained by combining the entire set of stack images (15 images at 20 × or 34 images at 63 ×) with the Zen Blue software (Zeiss). Microvessel density was determined by incubating BM and spleen sections with anti-CD34 (catalog number MAB7100, AbNova, primary), Alexa Fluor 568-conjugated donkey anti-rat (Invitrogen, secondary), and Hoechst 33342 (ThermoFisher Scientific).

Data Analysis

Data were analyzed and plotted using GraphPad Prism 8.0.2 software (GraphPad Software) and presented as mean (±SD) or as box charts, as more appropriate. All the data had normal distribution, as assessed using the Shapiro–Wilk *t* test. Values between two groups were compared using *t* test, whereas those among multiple groups were compared using Tukey's multiple comparisons test or analysis of variance, as indicated. Kaplan–Meier survival curves were compared by log-

rank (Mantel–Cox) test. Differences were considered statistically significant at $p < 0.05$.

RESULTS

The RB40.34 Antibody Readily Binds to Platelets in the Blood and Reaches the Fibrotic BM of *Gata1^{low}* Mice

Because the underlying fibrosis in the BM of *Gata1^{low}* mice may restrain the RB40.34 antibody to reach the BM, we conducted a feasibility study to determine whether the biotinylated-RB40.34 was detectable in BM sections of mice treated for 5 days. In addition, because we and others have demonstrated that platelets of *Gata1^{low}* mice express greater levels of P-SEL on their surface [22,36], we determined whether biotinylated-RB40.34 was detectable on platelets present in the blood 5 hours after its administration as control of the persistence of the antibody in the circulation after its injection (Figure 1). Biotin is produced in the liver and is present, albeit at low levels, in several cell types [37]. Therefore, it is not surprising that the APC–Cy7–streptavidin signal was also detected on platelets and BM sections of mice in the vehicle and Rux groups, which did not receive biotinylated-RB40.34. However, the signals on platelets and BM sections of mice that had received biotinylated-RB40.34 was greater than background levels (Figure 1).

Five-Day Treatment with RB40.34 in Combination with Rux Reduces TGF-β Signaling in the BM and JAK2/STAT5 Signaling in the Spleen of *Gata1^{low}* Mice

To investigate the effects of the treatments on the signaling state of the BM and spleen of *Gata1^{low}* mice, western blot analyses of these organs from untreated *Gata1^{low}* mice and mice treated for 5 days were performed. These studies used a panel of antibodies that target SMAD2/3 and TGF-βRII (canonical TGF-β signaling); p38, p-p38,

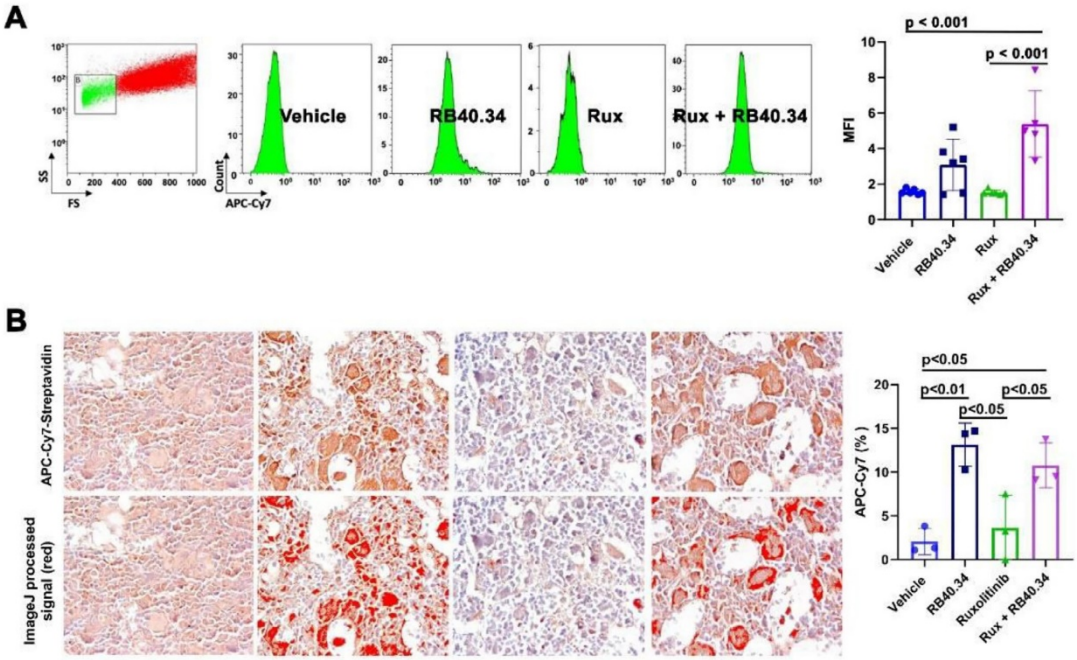

Figure 1 On day 5, RB40.34 is readily detected on the platelets present in the blood and on sections of bone marrow (BM) of *Gata1^{low}* mice. **(A)** Flow cytometry analyses with APC–Cy7–streptavidin of platelets present in the blood of *Gata1^{low}* mice after 5 days of treatment. The different groups of mice had been treated 5 hours earlier with the vehicle, biotinylated-RB40.34, Rux, and the two drugs in combination, as indicated. Platelets are recognized based on size (FS: forward scatter) and internal cell complexity (SS: side scatter). Representative FS or SS gating and histograms of the APC–Cy7–streptavidin staining are presented on the left. The mean fluorescence intensity (±SD) of APC–Cy7–streptavidin staining and values in individual mice (each symbol a mouse) are presented on the right. *p* values were calculated using Tukey's multiple comparison test, and significant differences are indicated in the panels. **(B)** Representative sections of BM of *Gata1^{low}* mice treated with vehicle (first panel) or biotinylated-RB40.34, Rux, and Rux and biotinylated-RB40.34 incubated with APC–Cy7–streptavidin (top panels). The panel on the bottom shows the computer-generated signal specific for mAb RB40.34 obtained by subtracting the background from the vehicle using ImageJ program. Areas exceeding the threshold are artificially labeled in red. Details of the ImageJ processing of the images are provided in **Supplementary Figure E2**. Magnification, 40 ×. The intensities of APC–Cy7 staining as a percentage of areas above the threshold in sections from the BM of multiple mice are presented on the right.

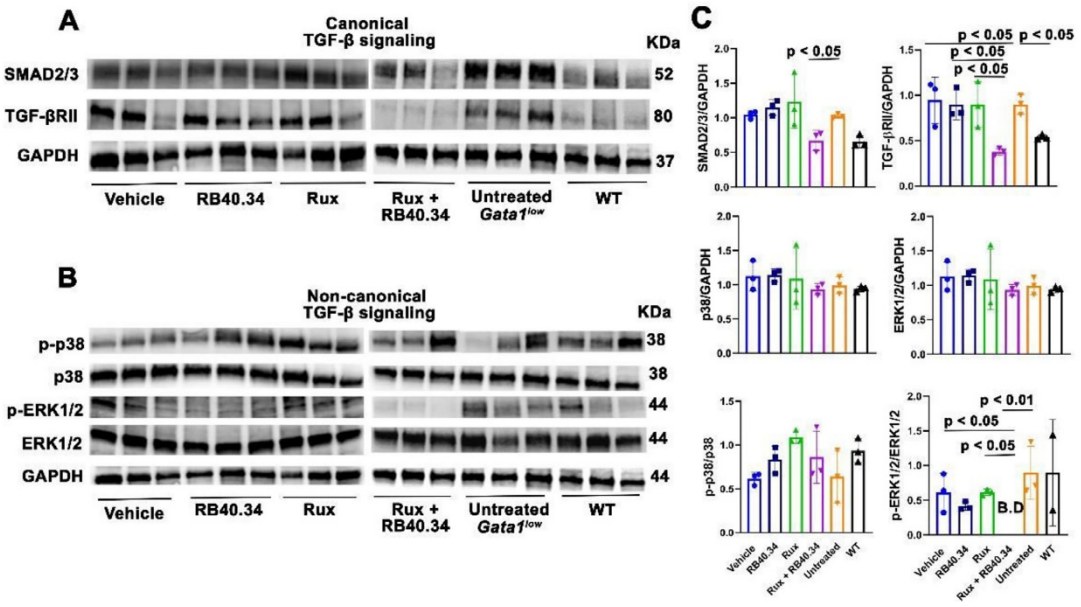

Figure 2 Treatment with RB40.34 in combination with Rux restores the abnormal canonical and noncanonical TGF-β signaling observed in the bone marrow (BM) of *Gata1*^{low} mice. **(A–C)** Western blot analyses for the content of elements downstream to the canonical and noncanonical TGF-β signaling of the BM of untreated wild-type (WT) and *Gata1*^{low} mice and of *Gata1*^{low} treated with vehicle, RB40.34, Rux, and the two drugs in combination, as indicated. Blots are presented on the right and quantifications on the left. Quantitative values are presented as mean (±SD) and as individual values for each mouse. Total protein levels are normalized toward the corresponding GPDH levels, whereas to take into account differences in total protein, the levels of the phosphoproteins are expressed stoichiometrically as a ratio to the total level of the corresponding protein. *p* values were calculated using Tukey's multiple comparison test, and statistically significant differences are indicated in the panels.

ERK1/2, and p-ERK1/2 (noncanonical TGF-β signaling); and JAK2 and STAT5 (JAK/STAT signaling). Untreated WT mice were analyzed in parallel as control (Figures 2 and 3 and Supplementary Figure E3). pJAK2 and pSTAT5 were not investigated because the phosphorylation of these two proteins in extracts from primary tissues was very sensitive to degradation upon storage (Supplementary Figure E4).

The BM from untreated *Gata1*^{low} mice expresses levels of TGF-βRII significantly greater than that in WT mice, which is likely a reflection of the increased number of MKs present in this organ. Treatment with RB40.34 or Rux alone had no effect on the levels of SMAD2/3 and TGF-βRII proteins, which remained similar to that of untreated *Gata1*^{low} mice. By contrast, treatment with RB40.34 in combination with Rux reduced the content of SMAD2/3 and TGF-βRII in the BM down to levels expressed by BM from WT mice, suggesting that the treatment reduced canonical TGF-β signaling in this organ (Figure 2A,C). The levels of total ERK and p38, which are two elements of the mitogen-activated protein kinase-dependent noncanonical TGF-β signaling [38], and their phosphorylated forms in the BM of untreated *Gata1*^{low} mice were not significantly greater than those of the normal mice. Although none of the treatments affected the p38 content/activation state, treatment with RB40.34 in combination with Rux reduces the activation of p-ERK to barely detectable levels, an indication that this treatment reduces the noncanonical TGF-β signaling possibly responsible for fibrosis in the BM (Figure 2B,C). By contrast, the content and activation state of canonical and noncanonical TGF-β signaling in the spleen from untreated *Gata1*^{low} mice are similar to that of the spleen from WT mice and are not significantly affected by any of the treatments (Supplementary Figure E3).

JAK2 was not detected in the BM of untreated *Gata1*^{low} and WT littermates and, except for two out of three mice in the vehicle and Rux-alone groups, remained undetectable in the BM of the treated groups as well. The content of STAT5 in the BM was instead robust and not statistically different across all groups (Figure 3A,C). By contrast, the content of JAK2 and STAT5 in the spleen of untreated *Gata1*^{low} mice was significantly greater than that of the WT littermates (Figure 3B,D), possibly reflecting the great levels of extramedullary hematopoiesis occurring in the spleen of the mutant animals [39]. The levels of STAT5 in the spleen of *Gata1*^{low} mice remained robust after treatment with either Rux or RB40.34 alone or in combination. By contrast, the levels of JAK2 in the spleen of the mutant mice were drastically reduced upon the combined treatment with Rux and RB40.34 but not with either of the drugs alone. These data suggest that the combination of Rux and RB40.34 targets the extramedullary hematopoiesis in the spleen.

These data indicate that treatment for only 5 days with Rux and RB03.34 in combination induces detectable biochemical changes in the BM and spleen of *Gata1*^{low} mice. Additional experiments, associated with expression profiling of individual cell populations, are necessary to assess whether these biochemical changes are due to

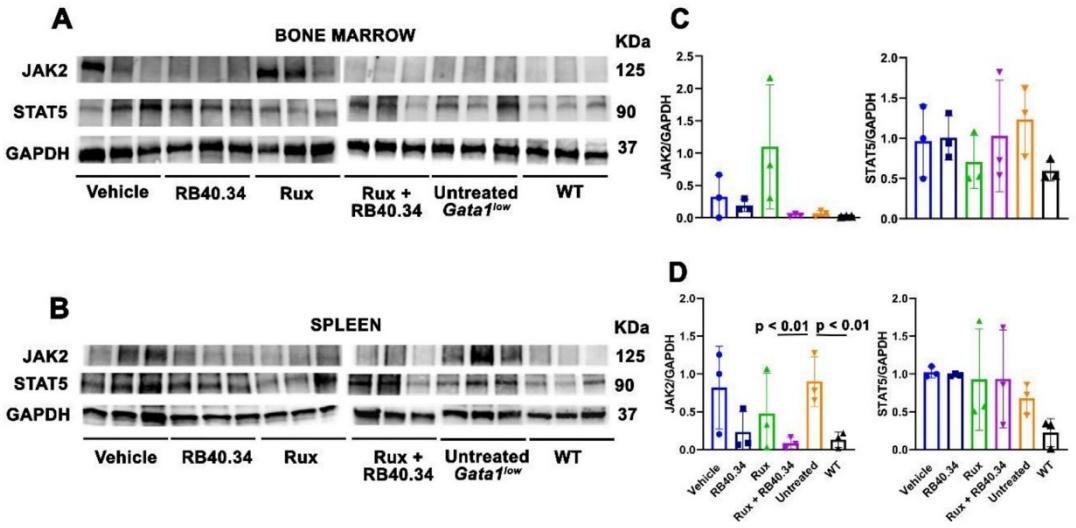

Figure 3 Treatment with RB40.34 in combination with Rux restores the abnormal JAK2/STAT5 signaling observed in the spleen of *Gata1*^{low} mice. Western blot analyses for JAK2, STAT5, and GAPDH (as loading control) of bone marrow **(A, C)** and spleen **(B, D)** from untreated wild-type (WT) and *Gata1*^{low} mice and *Gata1*^{low} mice treated with vehicle, RB40.34, and Rux, alone and in combination. Blots are presented on the right and quantifications on the left. In **(C, D)**, quantitative values are presented as mean (±SD) and as individual values for each mouse. *p* values were calculated using Tukey's multiple comparison test, and statistically significant differences are indicated in the panels.

alterations in cell composition and/or in the signaling cascade of individual cell populations in these organs.

All the Treatments Were Well Tolerated, with No Significant Effects on Survival and Body Weight

Encouraged by the results described above, we performed longer treatments (day 12 and day 54) to assess whether these drugs may affect the MF phenotype expressed by *Gata1*^{low} mice. To determine safety, all the treated mice were monitored daily by a veterinarian, who recorded no significant modifications in physical activity and behavior (no lethargy, no excessive grooming, and no change in coat luster) during the observation period. None of the treatments affected the weight of the animals in all the experimental groups (Supplementary Figure E5A). Although few deaths were recorded during the treatment period (Supplementary Table E1), the overall log-rank test of the Kaplan–Meier survival curves of the treated *Gata1*^{low} mice showed no significant difference in the death rate among groups (Supplementary Figure E5B).

RB40.34, Alone and in Combination with Rux, Reduces Anisocytosis and Lymphocyte Counts

Hematocrit (%) levels remained within normal ranges in all experimental groups for the duration of the treatments (Table 1). A significant increase in red blood cell (RBC) distribution width (RDW) at levels that meet the criteria for anisocytosis was observed in some of the mice treated with vehicle and in all those treated with Rux for 54 days, whereas the RDW in the groups treated with RB40.34 alone and in combination with Rux was within normal ranges (Figure 4A).

None of the treatments rescued the platelet deficiency of *Gata1*^{low} mice, which remained significantly lower than normal in all the groups (Table 1).

The difference in white blood cell (WBC) counts between untreated *Gata1*^{low} and WT littermates was not statistically significant (Table 1). None of the drugs that were investigated induced significant changes in the WBC counts because even the twofold reductions observed on day 54 in the Rux and RB40.54 plus Rux groups were not statistically significant, as shown by Tukey's multiple comparison test, compared with those of untreated mice. However, a comparison of the frequencies of the different WBC subpopulations revealed that RB40.34 in combination with Rux significantly decreased the lymphocyte counts by day 54 (Figure 4B).

In conclusion, none of the treatments induced anemia nor rescued thrombocytopenia of *Gata1*^{low} mice. However, treatment for 54 days with RB40.34 in combination with Rux reduced anisocytosis and lymphocyte counts.

Treatment with RB40.34 in Combination with Rux Reduces Fibrosis and Restores Hematopoiesis in the BM of *Gata1*^{low} Mice

By 8–11 months of age, the femurs of *Gata1*^{low} mice are hypocellular and contain great levels of fibrosis (Supplementary Figure E6). None of the treatments alters the BM cellularity (which remains lower than normal) and the level of fibrosis observed by day 5. By day 12, however, although the BM of all the groups remained hypocellular, the level of fibrosis in the diaphysis of the femurs of mice treated with RB40.34 and Rux in combination was reduced (Supplementary Figure E7), suggesting that this combination was starting to be effective. In agreement with this

Table 1 Hematocrit (%), platelet count, and white blood cell count determinations at days 5, 12, and 54 in *Gata1*^{low} mice treated with vehicle, RB40.34, Rux, and with a combination of the drugs

Hct (%)				
	Controls	Day 5	Day 12	Day 54
WT	39.65 ± 0.49 (2)			
Gata1^{low} untreated	21.10 ± 6.64 (16)			
Vehicle		33.03 ± 4.23 (6)	44.30 ± 0.10 (3)	33.52 ± 3.08 (5)
RB40.34		32.15 ± 5.51 (6)	43.25 ± 0.21 (2)	33.47 ± 0.23 (3)
Rux		38.12 ± 1.46 (6)	44.43 ± 0.81 (3)	29.46 ± 5.00 (5)
Rux + RB40.34		38.00 ± 1.58 (6)	44.07 ± 0.58 (2)	29.19 ± 1.23 (3)

Plt ($10^3/\mu$L)	Controls	Day 5	Day 12	Day 54
WT	775 ± 466.69 (2)			
Gata1^{low} untreated	115.06 ± 42.10 (16)			
Vehicle		138.67 ± 40.23 (6)	100.67 ± 17.67 (3)	92.40 ± 26.34 (5)
RB40.34		111 ± 46.23 (6)	79 ± 19.80 (2)	65.00 ± 28.48 (3)
Rux		137.83 ± 33.81 (6)	105.33 ± 26.41 (3)	94.60 ± 59.32 (5)
Rux + RB40.34		142.60 ± 26.45 (6)	123 ± 31.43 (2)	126.33 ± 34.59 (3)

Plt ($10^3/\mu$L)	Controls	Day 5	Day 12	Day 54
WT	775 ± 466.69 (2)			
Gata1^{low} untreated	115.06 ± 42.10 (16)			
Vehicle		138.67 ± 40.23 (6)	100.67 ± 17.67 (3)	92.40 ± 26.34 (5)
RB40.34		111 ± 46.23 (6)	79 ± 19.80 (2)	65.00 ± 28.48 (3)
Rux		137.83 ± 33.81 (6)	105.33 ± 26.41 (3)	94.60 ± 59.32 (5)
Rux + RB40.34		142.60 ± 26.45 (6)	123 ± 31.43 (2)	126.33 ± 34.59 (3)

Historical values of *Gata1*^{low} untreated mice and WT littermates are reported.
(n): number of mice.
Values among the treatment groups are not statistically different by Tukey's multiple comparison test.
Hct=hematocrit; *Plt*=platelets; *WT*=wild type.

hypothesis, by day 54, the femur of mice of the RB40.36 plus Rux group appeared reddish, a sign of improved erythropoiesis (Figure 5A), and contained a significantly greater number of cells than that of the vehicle group (Figure 5B). This increased cellularity was also evident by H&E staining of the BM sections (Figure 5C). In addition, reticulin staining indicated strong reductions of fibrosis in the BM of the entire femurs of mice treated with RB40.34 + Rux for 54 days (Figure 5C,D). By contrast, a single treatment with RB40.34 significantly reduces fibrosis but does not increase BM cellularity, whereas, as previously reported [32], treatment with Rux alone does not increase BM cellularity and does not reduce fibrosis in *Gata1*^{low} mice. The reason why, in contrast with our data, Rux is effective in reducing fibrosis in the *JAK2*^{V617F}-driven mouse model [40] is unclear and deserves to be investigated further.

The abnormal *Gata1*^{low} MKs release several bone morphogenic proteins that are responsible for increased bone formation starting at 1 month of age [12,41,42]. Despite the increased collagen deposition, the bone of *Gata1*^{low} mice remained immature with poor Ca^{++} deposition and, similar to what was observed in patients with MF, the mice developed osteopetrosis [43,44]. Differences in the integrity of the femurs of mice treated with the different drug combinations (Figure 5C) suggest possible differences in the levels of osteopetrosis expressed in the four experimental groups. To test this hypothesis, we used Mallory trichrome staining to analyze femurs of untreated WT and *Gata1*^{low} littermates and *Gata1*^{low} mice treated with a different drug combination (Supplementary Figure E8). As expected, the cortical bone of WT mice was characterized by red-mature lamellar bone with limited blue areas of osteoids rich in collagen fibers but poor in Ca^{++}. By contrast, the cortical bone of both the epiphysis and the diaphysis of *Gata1*^{low} mice contained large blue areas with unmineralized osteoids and limited areas of red-mature lamellar bone. The diaphysis of the mutant mice also contained large areas of trabecular unmineralized bone protruding in the medulla. These results are similar to those published previously [40,41]. After 54 days of treatment, the histopathology of the femur of the vehicle and RB40.34 group was similar to that of untreated *Gata1*^{low} mice of comparable age. However, the medulla of the femurs of the mice treated with Rux,

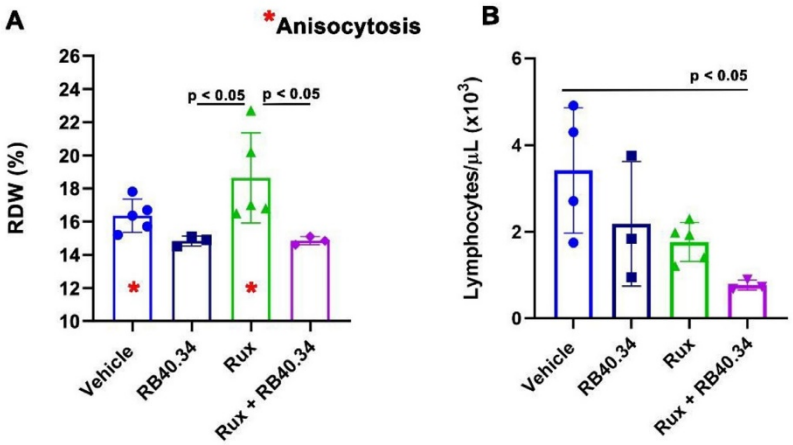

Figure 4 Treatment for 54 days with RB40.34 in combination with Rux reduces the frequency of red blood cell anisocytosis and lymphocyte counts in the blood of *Gata1*^{low} mice. **(A)** Red blood cell distribution width (RDW, in %) detected in the blood of *Gata1*^{low} mice treated with vehicle, RB40.34, Rux, and the two drugs in combination for 54 days, as indicated. Data are presented as mean (±SD) and as individual values for each mouse. The asterisks indicate the groups containing the deidentified samples flagged for anisocytosis by the accredited laboratory. **(B)** Lymphocyte counts observed in the blood of *Gata1*^{low} mice treated with vehicle, RB40.34, Rux, and the two drugs in combination for 54 days, as indicated. Data are presented as mean (± SD) and as individual values from each mouse. *p* values were calculated using Tukey's multiple comparison test, and statistically significant differences ($p < 0.05$) are indicated in the panels.

alone and in combination with RB40.34, contained significantly fewer areas of neo-bone formation, whereas the maturation of the cortical bone from the femurs of mice treated with Rux was normal (Supplementary Figure E8).

Another of the features associated with MF that is conserved in animal models is increased neoangiogenesis [12]. To assess whether the treatments had reduced neoangiogenesis in the BM and spleen of *Gata1*^{low} mice, confocal microscopy studies with CD34, which in mice recognize endothelial cells, and Hoechst, to identify the nucleated cells, were performed (Figure 6). Indeed, by day 54, the vessel density of all the treatment groups was significantly lower than that in the vehicle.

The BM hematopoietic failure associated with the myelofibrotic phenotype of *Gata1*^{low} mice includes barely detectable levels of hematopoietic stem/progenitor cells in this organ [27]. To confirm that RB40.34 in combination with Rux improves hematopoiesis in BM, the frequency and total numbers of progenitor (Lin−) and short-term (LSK) and long-term (SLAM) repopulating stem cells in the BM of mice treated for 54 days with the various drug combinations were evaluated (Figure 5E and Supplementary Figure E9). Indeed, the BM of mice treated with RB40.34 in combination with Rux contains a significantly greater frequency of Lin− and LSK and greater total numbers of all three populations than that of the vehicle-treated group.

Treatment with RB40.34 in Combination with Rux Reduces Fibrosis and Extramedullary Hematopoiesis and Restores the Architecture of the Spleen of Gata1^{low} Mice

Given the great relevance of JAK2 signaling in hematopoiesis [45], the observation that treatment with RB40.34 and Rux in combination greatly reduces the JAK2 content in the spleen suggests that this treatment decreases hematopoiesis in this organ. In agreement with this hypothesis, we observed marked reductions of fibrosis in the spleen of *Gata1*^{low} mice treated with RB40.34 + Rux for only 12 days (Supplementary Figure E7). By day 54, a trend toward reduction in spleen size (weight, ratio between spleen weight and body weight, and cell numbers) was observed in the group treated with RB40.34 1+ Rux (Figure 7A −C). Furthermore, a significant reduction in the total number of hematopoietic progenitor cells (Lin− cells) was observed on day 54 in the spleen of this group (Figure 7D and Supplementary Figure E9), supporting the hypothesis that RB40.34 and Rux in combination reduce extramedullary hematopoiesis in this organ.

The architecture of the spleen of *Gata1*^{low} mice is greatly altered by fibrosis and underlying extramedullary hematopoiesis (Figure 8A,B,D). Significant reductions in fibrosis were observed in mice treated with RB40.34 alone, Rux alone, and RB40.34 and Rux in combination, although greater reductions were observed in mice treated with the combination (Figure 8C,E). As expected [46], CD45R/CD3 staining indicates that the architecture of the spleen in WT mice is characterized by the presence of large aggregates of lymphoid cells and a well-developed white pulp. RBCs are embedded in the reticular connective tissue, which contains few MKs and supporting trabeculae. The T (CD3pos, in red) and B (CD45Rpos, in green) lymphocytes were numerous and localized around the central arterioles: T lymphocytes formed a sleeve around the central arteriole, the periarteriolar lymphoid sheath, whereas B lymphocytes were mainly localized in the outer region of the white pulp, defined as the marginal zone. By contrast, the spleen of *Gata1*^{low} mice contains a hypoplastic white pulp, and its periarteriolar lymphoid sheath contains a markedly reduced number of T cells. In addition, the red pulp appears disorganized by the presence of numerous MKs

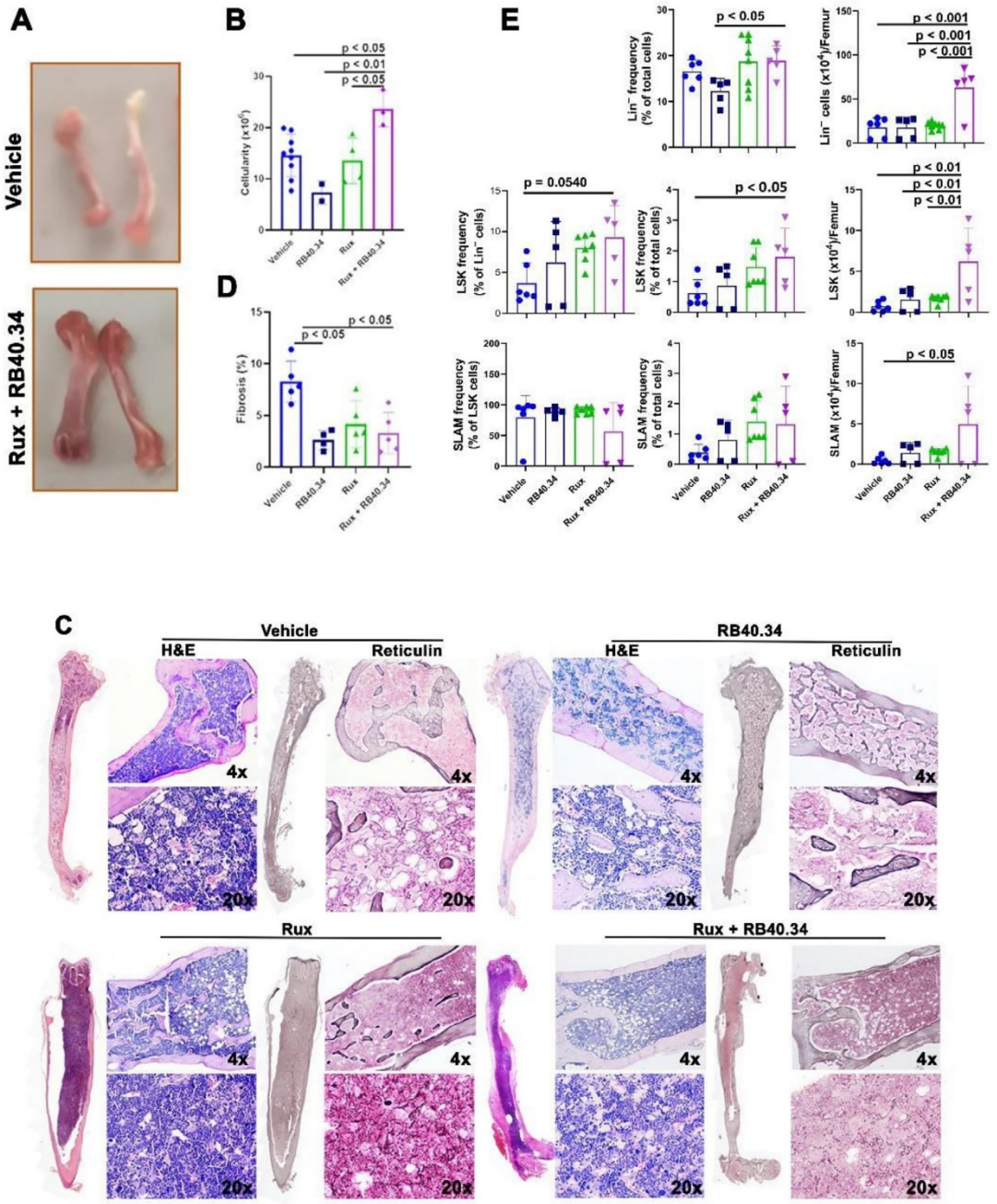

Figure 5 Treatment for 54 days with RB40.34 in combination with Rux increases the cellularity, reduces fibrosis, and restores hematopoiesis in the bone marrow (BM) of *Gata1^{low}* mice. **(A)** Photographs of the femur and tibia from representative mice treated for 54 days with vehicle and RB40.34 in combination with Rux, as indicated. **(B)** Number of cells per femur observed at day 54 in *Gata1^{low}* mice treated with vehicle, RB40.34, Rux, and the two drugs in combination. **(C)** Hematoxylin and eosin (H&E) and reticulin staining of femurs of representative *Gata1^{low}* mice treated for 54 days with vehicle, RB40.34, Rux, and the two drugs in combination, as indicated. The femurs are presented as stack images (at 4 ×) and as representative sections at 4 × and 20 × magnification, as indicated. **(D)** Levels of fibrosis quantified by image analyses of the reticulin staining of BM sections of *Gata1^{low}* mice treated for 54 days as

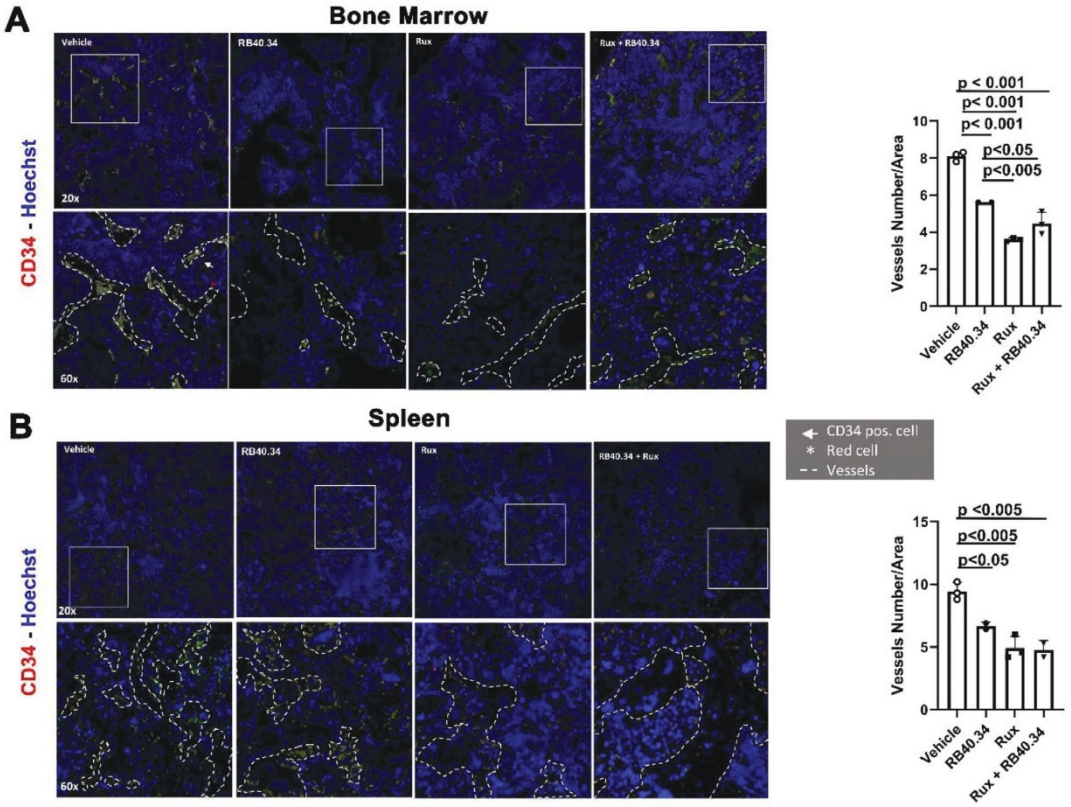

Figure 6 Treatment for 54 days with RB40.34 and Rux, alone and in combination, reduces the vessel density in the bone and spleen of *Gata1^{low}* mice. Confocal microscopy with CD34 and Hoechst (to counterstain the nuclei) of bone marrow **(A)** and spleen **(B)** sections of *Gata1^{low}* mice treated for 54 days with either vehicle or with RB40.34 and Rux alone and in combination. The panels in the first and third lanes are at 20 × magnification, and the area depicted in the rectangles is shown at 60 × in the corresponding panels in the second and third lanes. At 60 × magnification, microvessels (dashed lines) are identified as structures surrounded by CD34pos cells (indicated by arrows) and containing red cells (autofluorescent cells not counterstained by Hoechst, asterisks). Quantitative results are shown on the right as mean (±SD) and as values per individual mice (each symbol a mouse). Statistical analysis was performed using Tukey's multiple comparisons test, and significant *p* values are indicated within the panels.

and fibrosis (Figure 8A–C). Treatment of *Gata1^{low}* mice with RB40.34 and Rux in combination, and to a lesser extent by the two drugs as single agents, restored the normal architecture of the spleen with a great expansion of white pulp and a nearly normal organization of the periarteriolar lymphoid sheath and the marginal zone (Figure 8C).

RB40.34 in Combination with Rux for 54 days Improves MK Maturation but Does Not Decrease the MK Content in the BM and Spleen of *Gata1^{low}* Mice

The process of terminal MK maturation involves a series of precursors that progressively acquire features of mature cells that release platelets [16,47]. As these precursors progress along the maturation pathway, they express increased levels of CD41 and CD61 on their surface [47,48]. Therefore, flow cytometry analyses for CD41 and CD61 expression divides MK precursors into three classes: immature (CD41negCD61pos), mature (CD41posCD61pos), and very mature (CD41posCD61low), whereas non-MKs are negative for both markers. Based on this flow cytometry criteria, we determined whether the treatments rescued the defective MK maturation of *Gata1^{low}* mice (Figure 9). Because the BM of *Gata1^{low}* mice contains a great number of MKs [12], it is not surprising that CD61pos cells represent almost 30% of the total cell population of BM and spleen of mutant mice (Figure 9). The total frequency of the

indicated above. **(E)** Frequency and the total number of Lin−, LSK, and SLAM cells in the femur of *Gata1^{low}* mice treated with the various drug combinations. In **(B–E)**, results are presented as mean (±SD) and as values per individual mice (each symbol a mouse) and were analyzed using Tukey's multiple comparisons test. Statistically significant groups are indicated within the panels.

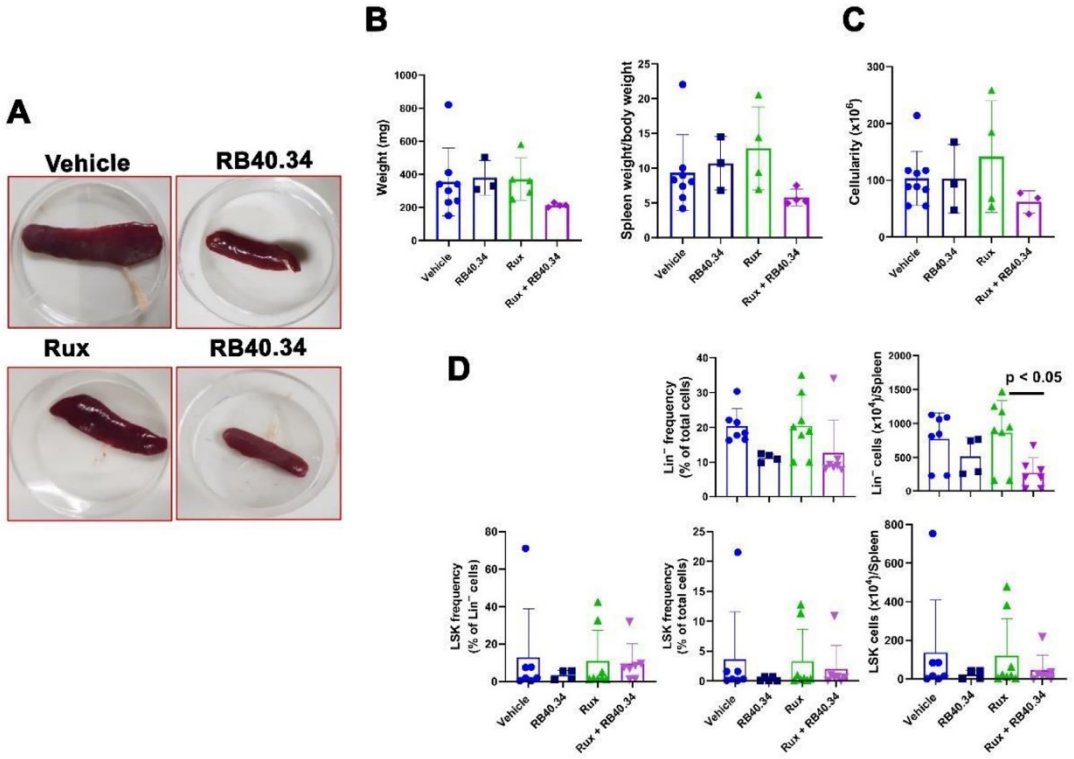

Figure 7 Treatment for 54 days with RB40.34 in combination with Rux decreases hematopoiesis of the spleen of *Gata1*^{low} mice. **(A)** Photographs of representative spleens treated for 54 days with the various drug combinations, as indicated. **(B, C)** Spleen size, as weight and ratio between spleen weight and body weight **(B)**, and total cell numbers **(C)**, of mice treated for 54 days with the various drug combinations. **(D)** Frequency and the total number of Lin− and LSK cells in the spleen of *Gata*1^{low} mice treated with the various drug combinations. SLAM cells are not presented because they are almost 100% of the LSK cells detected in the spleen (**Supplementary Figure E9**). In **(B–D)**, results are presented as mean (±SD) and as values per individual mice (each symbol a mouse). They were analyzed using Tukey's multiple comparisons test. Statistically significant groups are indicated within the panels.

CD61pos cells in the BM and spleen of all the experimental groups remained high for the total duration of the treatments. By days 5 and 12, very few of the MKs in the BM and spleen of *Gata1*^{low} mice in all the experimental groups had the very mature CD41bposCD61low phenotype. The frequency of very mature CD41bposCD61low MKs was low and that of the immature CD41bnegCD61pos MKs was high in the BM and spleen of mice treated with vehicle for 54 days. By contrast, by day 54, the frequency of MKs with the very mature and immature phenotypes in the groups treated with RB40.34, Rux, or RB40.34 and Rux in combination was significantly greater and lower, respectively, than that in the vehicle group. These results suggest that the drugs, although ineffective in reducing the proliferation of the MKs, are improving the cell maturation.

The abnormal maturation of MKs from mouse models and patients with MF includes localization of P-SEL on the demarcation membrane system (DMS) instead of in the α-granules [22,25,26]. Because the DMS increases with maturation, the amount of P-SEL exposed to the extracellular space also increases during this process. Therefore, the biotinylated RB40.34 that reaches the BM should bind large numbers of *Gata1*^{low} MKs and its binding should be greater as these cells mature. To assess whether the improved MK maturation induced by the treatments for 54 days included the rescue of the altered cell surface expression of P-SEL, the binding of PE–Cy7–streptavidin to MKs from the BM and spleen of mice treated for 5, 12, or 54 days was determined (Figure 9A–C). As expected, PE–Cy7–streptavidin binding was barely detected on BM and spleen cells of mice treated with either vehicle or Rux alone, which had not received the antibody at any of the time points. The low levels of PE–Cy7–streptavidin binding observed in these groups probably represent background signals due to endogenously produced biotin and are not informative on the levels of P-SEL expressed by MKs. By days 5 and 12, PE–Cy7–streptavidin binding was detected in cells both in the non-MK and MK gate. The binding of PE–Cy7–streptavidin to the non-MK cells is possibly related to the presence of endothelial cells in this population, which are also known to express P-SEL [17]. By days 5 and 12, large numbers of MKs from the BM and spleen of mice treated with RB40.34 alone and in combination with Rux bound PE–Cy7–streptavidin. As expected, the mean fluorescence intensity (MFI) of the binding increases in cells with a more mature phenotype, a reflection of the

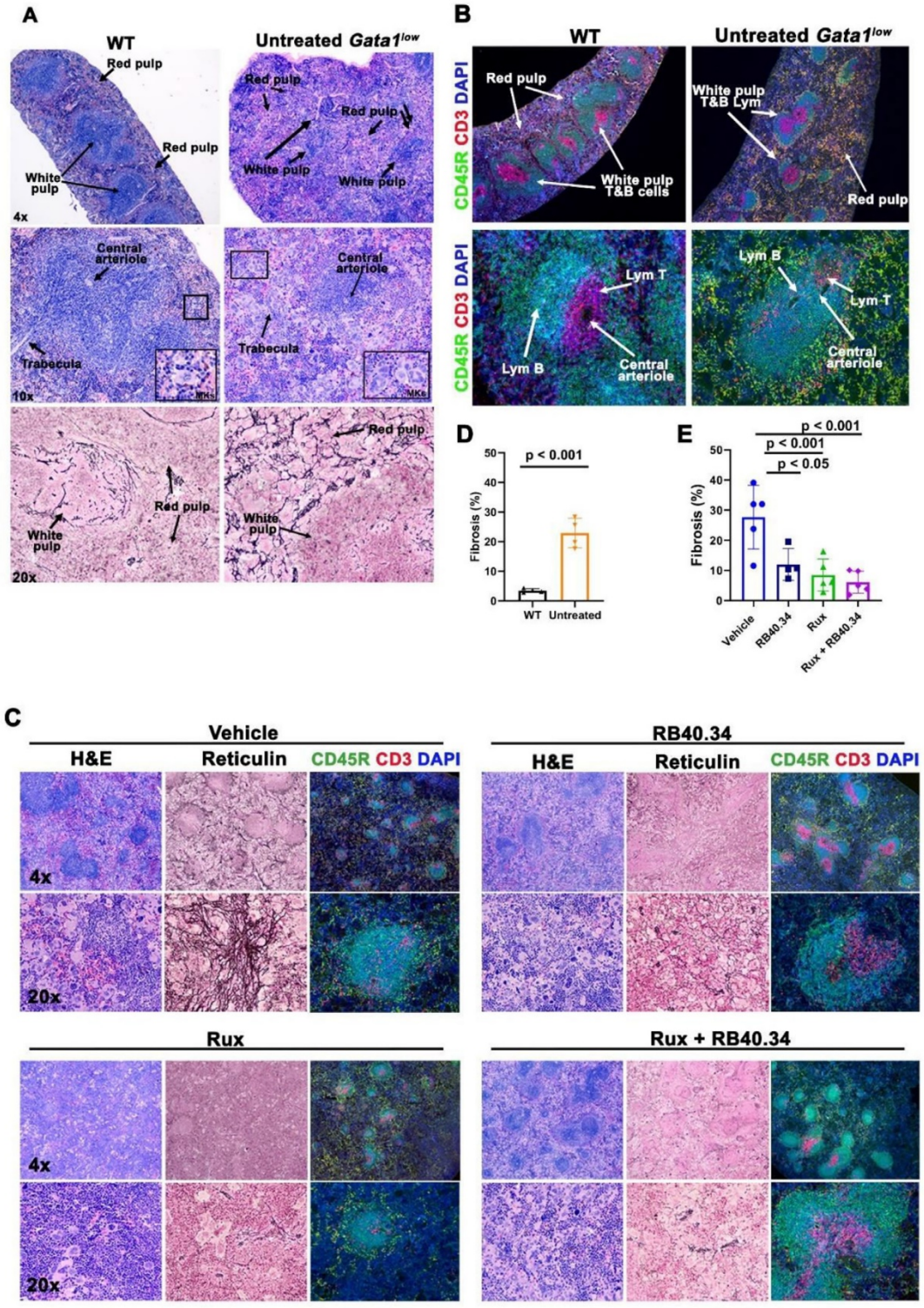

Figure 8 Treatment for 54 days with RB40.34 in combination with Rux decreases fibrosis and restores the architecture of the spleen of *Gata1*^{low} mice. **(A)** Hematoxylin and Eosin (H&E) and reticulin staining of spleen from representative 8- to 11-month-old WT and

greater levels of P-SEL on the cell surface of *Gata1^{low}* MKs as they mature. In addition, increases in MFI were also observed among MKs of comparable maturation stages analyzed on days 5 and 12, a possible reflection of the increased bioavailability of the antibody in the microenvironment due to the reduction of fibrosis induced by the treatments. By contrast, PE–Cy7–streptavidin was found barely bound to MKs from BM and spleen of mice treated with RB40.34 alone or in combination with Rux by day 54. These results indicate that the improved MK maturation induced by these two drugs in combination may include reduced localization of P-SEL on the DMS. By day 54, PE–Cy7–streptavidin binding was also barely detectable in the non-MK populations of mice treated with RB40.34 alone or in combination with Rux. Because the cells responsible for binding PE–Cy7–streptavidin in the non-MK population are probably endothelial cells and P-SEL expression in endothelial cells is upregulated by inflammation [49], these data provide further support for the hypothesis that the treatments reduce the inflammatory milieu of the BM and spleen of *Gata1^{low}* mice.

Treatment with Rux Increases the Frequency of MKs Expressing Detectable Levels of GATA1 in the BM of *Gata1^{low}* Mice

The abnormal maturation of MKs, which is thought to drive MF in patients and mouse models, is driven by defective content of GATA1 [6,9,10], the transcription factor that plays a pivotal role in supporting MK maturation [6,11]. As expected, confocal microscopy analyses with antibodies against GATA1 and CD42b (as a marker of MK) indicated that BM of *Gata1^{low}* mice contained large numbers of MKs, the nuclei of which were not stained by the GATA1 antibody (Supplementary Figure E10). To generate insights on the possible mechanism (s) that rescue MK maturation in mice treated with RB40.34 and Rux, alone or in combination, we performed confocal microscopy analyses with the same antibodies of the BM section of mice treated for 54 days with vehicle, RB40.34 alone, Rux alone, or the two drugs in combination (Figure 10). These analyses confirmed the indications provided by flow cytometry (Figure 9) that none of the treatments affected the number of MKs (as CD42bpos cells) present in the BM, which remained high. As expected, very few of the MKs of mice treated with the vehicle contained GATA1. By contrast, a significant number of MKs in the BM of mice treated with either RB40.34 or Rux alone contained detectable levels of GATA1 in their nuclei (Figure 10 and Supplementary Figure E11). It is surprising instead that GATA1 was not detected in MKs from the BM of mice treated with RB40.34 and Rux in combination.

Treatment with RB40.34 in Combination with Rux Reduces the TGF-β and CXCL1 Content of the BM of *Gata1^{low}* Mice

Increased bioavailability of the proinflammatory cytokines TGF-β and CXCL1, the murine equivalent of human IL-8, has been suggested to represent the driver for fibrosis and hematopoietic failure in BM of patients with MF and MF mouse models [4,50,51]. In previous studies, we demonstrated that abnormal MKs are the cells responsible for increasing the bioavailability of these two cytokines in the BM (and spleen) of *Gata1^{low}* mice [35]. To test whether treatment with RB40.34 in combination with Rux decreases the proinflammatory milieu of the BM microenvironment of *Gata1^{low}* mice, we performed histochemical evaluations with antibodies against TGF-β and CXCL1 of BM sections from four groups of *Gata1^{low}* mice treated for 54 days with vehicle, RB4034 alone, Rux alone, and the two drugs in combination (Figure 11).As expected, BM of *Gata1^{low}* mice treated with vehicle contained large levels of TGF-β and CXCL1. The levels of TGF-β were significantly decreased by treatment with both Rux alone and in combination with RB40.34 (Figure 11A, B). Morphological analyses of the cells that expressed TGF-β indicated that the reductions were mainly due to reduced numbers of MKs expressing this factor (Figure 11C). CXCL1 instead was reduced only by RB40.34 in combination with Rux, and the number of MKs, which express this factor, remained high in all the groups (Figure 11A–C). Because in addition to MK, CXCL1 is expressed by many other cell types, we suggest that the two drugs in combination reduce the proinflammatory milieu of *Gata1^{low}* mice by targeting not only MKs but also additional cells in the microenvironment.

DISCUSSION

The hypomorphic *Gata1^{low}* mutation deletes only one of the three major hypersensitive sites, which regulate the expression of the gene [52].

Gata1^{low} mice. WT spleens are characterized by the presence of large aggregates of lymphoid cells, well-developed white pulp, with the presence of RBCs embedded in reticular connective tissue containing few megakaryocytes (MKs) and supporting trabeculae. By contrast, *Gata1^{low}* spleen is characterized by hypoplastic white pulp and red pulp rich in MKs. Reticulin staining of the consecutive section indicates that fibrosis is localized mostly in the red pulp. Results are representative of those observed in at least three WT and three *Gata1^{low}* littermates, all of whom were 11 months old. **(B)** Triple immunofluorescent analyses for CD3 (as a marker of T cells, red), CD45R (B220, as a marker for B cells, green), and DAPI (nuclei) of spleen sections from representative WT and *Gata1^{low}* mice, as indicated. As expected [50], the white pulp of the WT spleen contains numerous T and B lymphocytes, organized around central arterioles. T lymphocytes form a sleeve around the central arteriole, the periarteriolar lymphoid sheath, whereas B cells are mainly localized in the outer white pulp region, the marginal zone. In *Gata1^{low}* spleens, the white pulp is smaller than that in the WT organ and the periarteriolar lymphoid sheath contains a markedly reduced number of T cells. Magnification 4 ×, 10 ×, and 20 ×, as indicated. **(C)** H&E, reticulin staining, and triple staining with CD45R (green), CD3 (red), and DAPI (blue) of sections from the spleen of representative *Gata1^{low}* mice treated for 54 days with the various drug combinations, as indicated. Images are presented at 4 × and 20 × magnification. **(D)** Levels of fibrosis quantified by image analyses of the reticulin staining of spleen sections from untreated 8- to 11-month-old WT and *Gata1^{low}* littermates, as indicated. **(E)** Levels of fibrosis, quantified by image analyses of the reticulin staining, in spleen sections, of *Gata1^{low}* mice treated for 54 days, as indicated. In **(D, E),** results are presented as mean (±SD) and as values per individual mice (each symbol a mouse) and were analyzed by *t* test. Statistically significant groups are indicated within the panels.

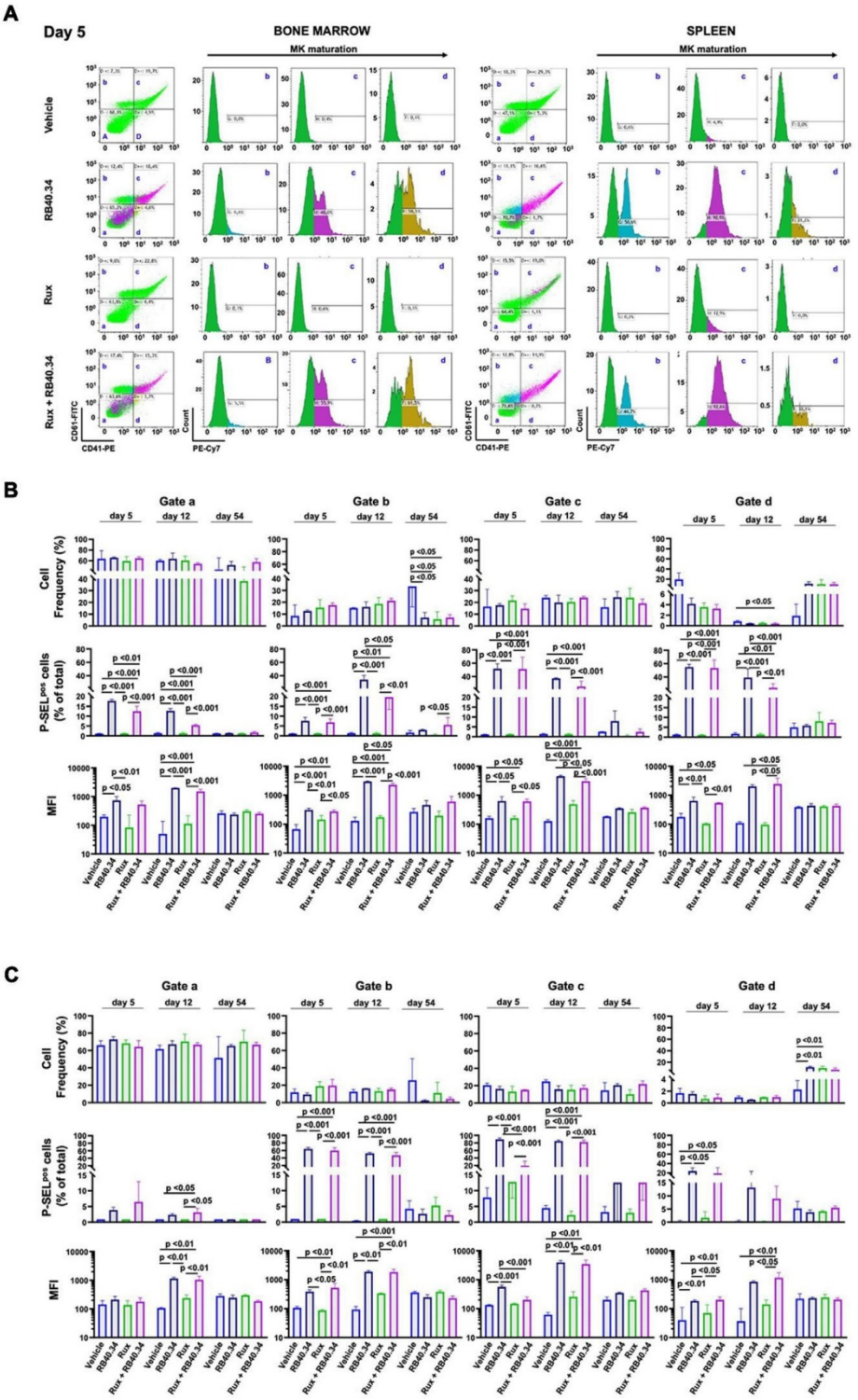

Figure 9 Treatment for 54 days with RB40.34 and Rux alone in combination improves the maturation profile of the megakaryocytes (MKs) from the bone marrow and spleen of *Gata1^{low}* mice. **(A)** Representative dot-plots and histograms of MKs from the bone

After birth, the hematopoietic cells of these mice activate the expression of the gene from the two regulatory sites not affected by the mutation so that the levels of Gata1 mRNA in the hematopoietic cells are overall normal [39]. However, the thrombocytopenia induced by the mutation activates the TPO/Mpl axis [32], which results in an RSP14 ribosomopathy, similar to that observed in patients with MF [10], which reduces the efficiency of the translation of *Gata1* mRNA, reducing the content of the protein. The mechanism(s) linking the TPO/Mpl axis to the RSP14 ribosomopathy in MF and in animal models including *Gata1^{low}* mice is still unknown. It has been suggested that it is represented by aurora kinases because their inhibition increases GATA1 in the MKs while reducing fibrosis in animal models and in patients with MF [53].

Although *Gata1^{low}* mice do not carry any of the MF driver mutations, they are considered a bona fide animal model of MF because their HSCs express an activated TPO/MPL axis, which may be drugged by JAK inhibitors, and an RSP14 ribosomopathy, which is responsible for low GATA1 content and altered MK maturation and P-SEL expression. In turn, altered P-SEL expression on the MK is responsible for the pathologic cell interaction that increases the bioavailability of proinflammatory cytokines and drives fibrosis. Over the years, we and others [54–56] have extensively used *Gata1^{low}* mice as a tool to identify lesions, which may be targeted to normalize their MF phenotype. Based on previous observations indicating that deletion of *P-sel* prevents *Gata1^{low}* mice from developing myelofibrosis [27], in this study, we established whether inhibition of P-SEL, alone or in combination with Rux, may also normalize the phenotype of *Gata1^{low}* mice that have already established myelofibrosis. A summary of the results is presented in Supplementary Table E2.

We first demonstrated that after short-term treatment, RB40.34 is bound to the platelets and the MKs from the BM of *Gata1^{low}* mice, suggesting that the drug is retained in the circulation for at least 5 hours and that, despite fibrosis, reaches the BM of the animals. We also found that after 5 days, RB40.34 in combination with Rux normalizes not only the abnormal noncanonical TGF-β signals, which is a signature of a profibrotic microenvironment, but also the abnormal canonical TGF-β signature, which indicates reduced hematopoiesis in the BM. These data suggest that after only 5 days, the combination of RB40.34 and Rux is more effective than any of the two drugs alone in suppressing the cells responsible for fibrosis while reactivating hematopoiesis in the BM. The drug combination was also more effective than the two drugs as single agents in reducing JAK2 in the spleen of the mutant mice, suggesting that it reduces extramedullary hematopoiesis in this organ.

Encouraged by these results, we analyzed the effects of long-term treatments with RB40.34 and Rux, alone and in combination, on the myelofibrotic phenotype expressed by *Gata1^{low}* mice using a vast range of clinically relevant end points. The results indicate that none of the treatments induce anemia nor rescue the thrombocytopenia of *Gata1^{low}* mice. However, treatment for 54 days with RB40.34 in combination with Rux, and to a less extent the two drugs alone, reduced anisocytosis, expression of P-SEL on MKs and probably on endothelial cells, and lymphocyte counts. Because the iron metabolism of old *Gata1^{low}* mice is normal (Rivella S, unpublished data) and the mean corpuscular volume and hemoglobin content of RBCs remained within normal values in all the treated mice (Supplementary Table E3), it is unlikely that the high RDW detected in *Gata1^{low}* mice is a sign of impaired iron metabolism. Anisocytosis without an increase in the mean corpuscular volume is induced by proinflammatory cytokines in several benign and malignant disorders, including MF, where it has been proposed as a marker that predicts inferior survival [57]. We hypothesize that the reduction in anisocytosis observed on day 54 in the RB40.34 alone or in combination with Rux groups reflects reductions in the proinflammatory cytokines TGF-β and/or CXCL1, which drive MF in this model. Because TGF-β and CXCL1 are widely known to directly (TGF-β) or indirectly (through neutrophil activation, CXCL1) affect lymphocyte counts [58–61], this hypothesis is also consistent with the reduced lymphocyte counts observed by day 54 in the mice treated with the two drugs in combination. Reduction in microenvironment bioavailability of proinflammatory cytokines was directly tested by showing that RB40.34 and Rux in combination significantly reduce the TGF-β and CXCL1 content of BM.

Finally, treatment for 54 days with RB40.34 in combination with Rux also reduced fibrosis in BM and spleen while improving effective hematopoiesis in the BM and reducing extramedullary hematopoiesis, restoring the architecture of the spleen.

Treatments for 54 days with RB40.34 and Rux, alone or in combination, were ineffective in reducing the proliferation of the MKs, which may be driven in our model as well as in patients by the activated TPO/Mpl axis. They were, however, all effective in improving the maturation profile of the MKs, including reducing their abnormally high level of cell surface expression of P-SEL and TGF-β content. RB40.34 and Rux alone were also effective in increasing the GATA1 content in a proportion of CD42bpos MKs. The mechanistic interpretation of these data is complicated by the recent single-cell profiling indicating that murine (and human) BM contains four distinctive MK subpopulations, each one exerting a different function [47,62–64]. The BM of adult mice and humans contains at least three subpopulations: platelet-producing MKs, niche-supportive MKs, and immune MKs. Only platelet-producing MKs have the morphology of mature MKs. Niche-supportive MKs and immune MKs have instead the

marrow (left quadrant) and spleen (right quadrant) of one representative mouse from each experimental group treated for 5 days. MKs were labeled with CD41, CD61, and PE–Cy7–streptavidin. The a, b, c, and d gates identify non-MKs, immature MKs, mature MKs, and very mature MKs, respectively. The levels of APC–Cy7–streptavidin bound to the MKs at their different stages of maturation are presented by histograms. Because P-sel is abnormally expressed at high levels on the surface of *Gata1^{low}* MK, the APC–Cy7-streptavidin signal identifies the MK expressing P-sel, which has bound the biotinylated RB40.34 injected 5 hours earlier in the mice. **(B, C)** Frequency of cells in the non-MK (a), immature (b), mature (c), and very mature (d) MK gate (%of total cell number) and percentage and mean fluorescence intensity (MFI) of the events positive for PE–Cy7–streptavidin staining in each gate in the BM **(A)** and spleen **(B)** of *Gata1^{low}* mice treated for 5, 12, and 54 days with either vehicle or the different drug combinations, as indicated. Values were reported as means (±SD) of those detected in at least three mice per experimental group. Data were analyzed using Tukey's multiple comparisons and statistically significant differences among groups are indicated within the panels.

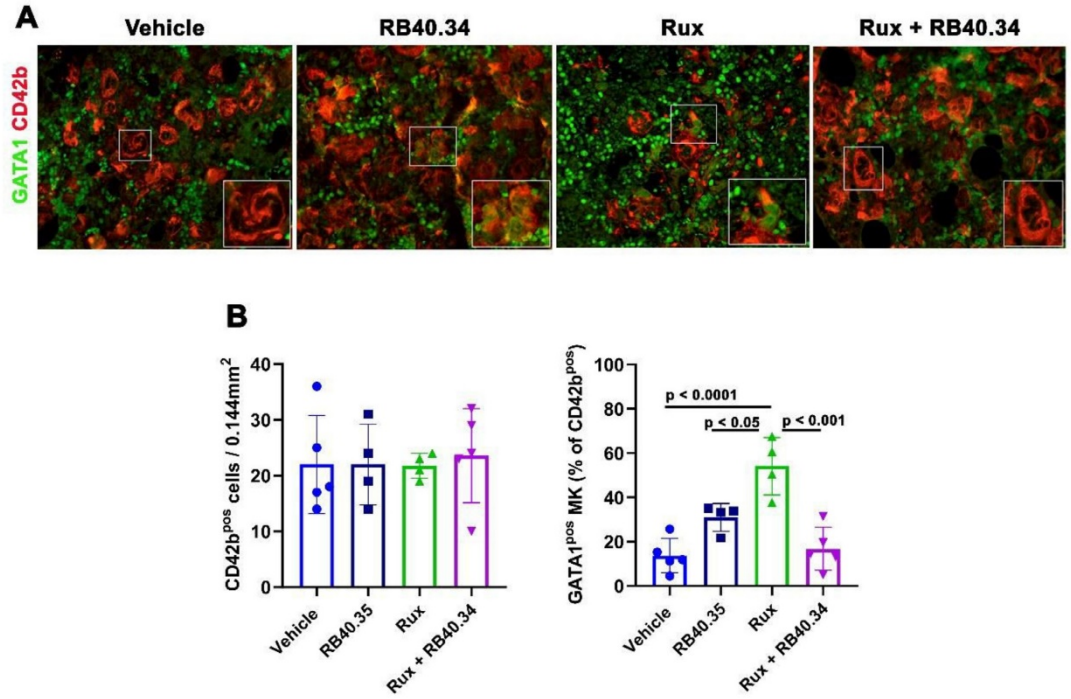

Figure 10 Treatment for 54 days with RB40.34 or Rux alone, but not in combination, increases the GATA1 content in the megakaryocytes (MKs) from the bone marrow (BM) of *Gata1^{low}* mice. **(A)** Merged GATA1 (FITCH-green) and CD42b (TRITCH-red, as a marker of MKs) images of the confocal microscopy analyses with the corresponding antibodies in BM sections from representative *Gata1^{low}* mice treated for 54 days with vehicle, RB40.34 alone, Rux alone, and the two drugs in combination, as indicated. The corresponding images acquired in the single channels, in the channel for DAPI (as an indication of the nuclear localization of GATA1), and in the bright field (to exclude autofluorescence) are presented in **Supplementary Figure E11.** Magnification 40 × . **(B)** Frequency of MKs (CD42b-positive cells) and percentage of MK positive for GATA1 in BM sections of *Gata1^{low}* mice treated for 54 days, as indicated. Data are presented as mean (±SD) and as values in individual mice (each symbol a mouse). Results were analyzed using Tukey's multiple comparisons test and significant differences among groups are indicated within the panels.

morphology of immature MKs. In addition, by characterizing the MK subpopulations present in the embryos, Wang et al. [63] identified a fourth subpopulation, which they defined as niche-poised MKs, having an immature morphology and characterized by a high expression of extracellular matrix genes, such as *COL1A1*, *COL3A1*, and *COL6A2*, and enrichment of the "response to TGF-β signature," which indicate that this subpopulation is sustained by TGF-β. Of interest for this study is that reduced GATA1 content blocks the maturation of platelet-producing MKs but does not favor the maturation of the other three subpopulations [47,62–64]. This new information indicates that the nature of the immature *GATA1^{low}* MKs found in large numbers in MF is presently not known. Preliminary observations indicating that large numbers of the morphologically immature MKs in the BM of *Gata1^{low}* mice, as well as that of patients with MF, express collagen [65,66] suggest that at least some of these MKs are represented by niche-poised MKs, the maturation of which is reactivated by TGF-β [19]. It is therefore possible that low levels of GATA1 drive the disease not only by retaining platelet-forming immature MKs (leading to thrombocytopenia) but also by increasing the frequency of other MK subtypes. According to this hypothesis, although RB40.34 and Rux in combination did not induce a detectable increase in GATA1 content in MKs (and did not increase the platelet counts), they reduced the frequency of MKs containing TGF-β, which may correspond to the niche-supporting MKs. Reduced TGF-β bioavailability may have then limited the number of niche MKs, which are sustained by these growth factors and are responsible for. On the other hand, Rux alone, which induced a greater increase of GATA1 in MKs, also reduced the number of TGF-β-containing MKs but did not alter fibrosis, suggesting that the number of MKs expressing collagen was not significantly affected. These data support the need for further studies, clearly outside the purpose of the current article, to clarify the MK subpopulations that are altered in MF, that is, which of them is responsible for the different traits of the MF phenotype and how they are affected by RB40.34 and Rux alone or in combination.

In conclusion, these data provide preclinical evidence that treatment with the RB40.34 antibody in combination with Rux is more effective than the use of Rux alone for reverting the myelofibrotic

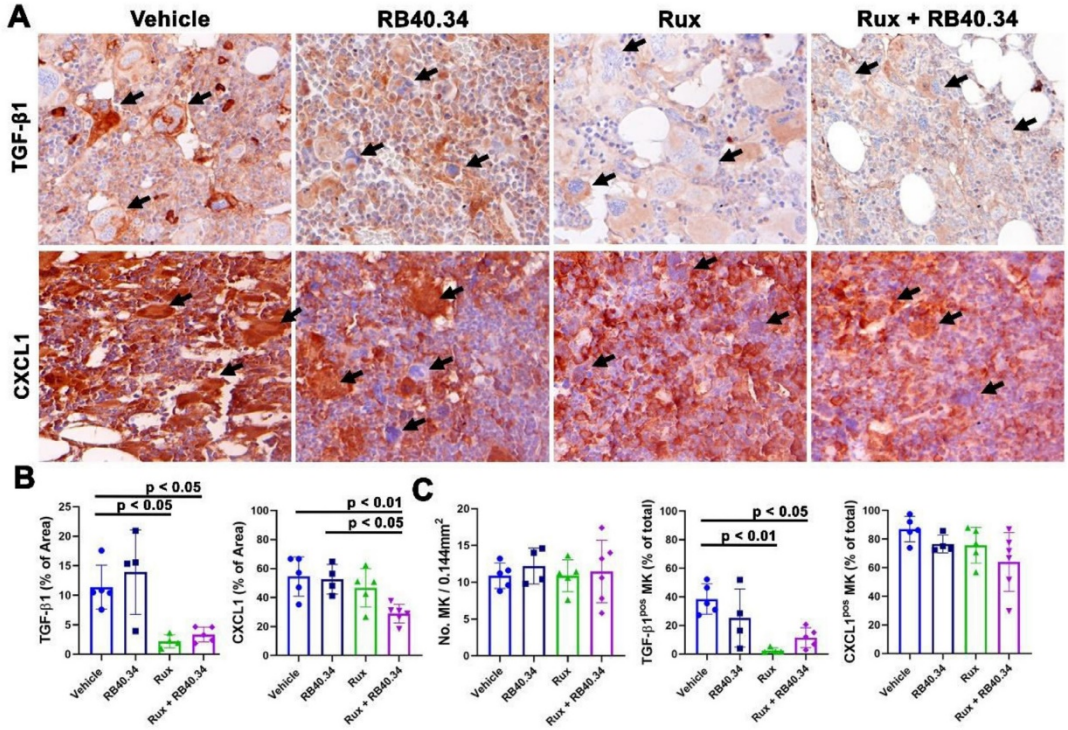

Figure 11 Treatment for 54 days with RB40.34 and Rux in combination decreases the TGF-β, mainly in the megakaryocytes (MKs), and CXCL1 content of bone marrow (BM) of *Gata1^{low}* mice. **(A)** BM sections from representative mice treated for 54 days with vehicle, RB40.34, Rux, and the two drugs in combination immune-stained for TGF-β or CXCL1, as indicated. Representative MKs are indicated by arrows. Magnification 40 $\times$. **(B)** Quantification by computer-assisted imaging of the TGF-β1 and CXCL1 content in the BM of *Gata1^{low}* mice treated for 54 days as indicated. **(C)** Frequency of MKs and percentage of MKs expressing high levels of TGF-β1 and CXCL1 in BM sections of *Gata1^{low}* mice treated, as indicated. MKs were identified based on size (10 times greater than that of any other cell type in the section) and the polylobate morphology of their nuclei. In **(B, C)**, data are presented as mean ($\pm$SD) and as values per individual mice (each symbol a different mouse) and were analyzed using Tukey's multiple comparisons test. Values statistically different are indicated within the panels.

trait in the *Gata1^{low}* mouse model and encourage clinical studies to validate the effects of crizanlizumab, in combination with Rux, for the treatment of human primary myelofibrosis.

Conflict of Interest

P.V., F.G., F.M., M.F., A.V., G.S., and M.Z. declare no conflict. C.W., A.B., and A.P. are employees of Novartis Pharmaceutical Corporation. A.R.M. received research funds from Novartis Pharmaceutical Corporation.

Author Contributions

P.V., F.G., F.M., M.F., F.A., and AV performed experiments and analyzed the data. P.V. and F.G. performed statistical analyses. G.S. reviewed all the histopathologic determinations. A.R.M. and M.Z. designed the study, interpreted the data, and wrote the manuscript. C.W., A.B., and A.P. revised the data and wrote the manuscript. All the authors read the manuscript and concur with its content.

Disclosure

The content of the manuscript was presented as a poster at the 62nd ASH Annual Meeting & Exposition, December 10th–13th, 2022, New Orleans, USA (Verachi P, Martelli F, Zingariello M, et al. Preclinical rationale for the use of crizanlizumab (SEG101) in myelofibrosis. Blood 2020;136(Suppl 1):26–27. https://doi.org/10.1182/blood-2020-133896). The data are unpublished and have not been submitted for publication to any other journal.

Funding

This study was supported by grants from the National Cancer Institute (P01-CA108671), Bethesda, MD, USA, the National Heart, Lung and Blood Institute (1R01-HL134684), Bethesda, MD, USA,

Associazione Italiana Ricerca Cancro (AIRC, IG23525), Milano, Italy and Novartis Pharmaceutical Corporation, East Hanover, NJ, USA.

Acknowledgments

The technical support of Mrs. Yvan Gilardi, Enrico Cardarelli, and Andrea Giovannelli of the Center for Animal Experimentation and Well-Being, Istituto Superiore di Sanità, Rome, Italy, and the editorial assistance of Dr. Gisella Gaspari, Università Campus Biomedico, Rome, Italy, are gratefully acknowledged.

DATA AVAILABILITY STATEMENT

The individual data for each mouse are available on request.

SUPPLEMENTARY MATERIALS

Supplementary material associated with this article can be found in the online version at https://doi.org/10.1016/j.exphem.2022.09.004.

REFERENCES

1. Zahr AA, Salama ME, Carreau N, et al. Bone marrow fibrosis in myelofibrosis: pathogenesis, prognosis and targeted strategies. Haematologica 2016;101:660–71.
2. Barbui T, Tefferi A, Vannucchi AM, et al. Philadelphia chromosome-negative classical myeloproliferative neoplasms: revised management recommendations from European LeukemiaNet. Leukemia 2018;32:1057–69.
3. Marcellino BK, Verstovsek S, Mascarenhas J. The myelodepletive phenotype in myelofibrosis: clinical relevance and therapeutic implication. Clin Lymphoma Myeloma Leuk 2020;20:415–21.
4. Dunbar AJ, Rampal RK, Levine R. Leukemia secondary to myeloproliferative neoplasms. Blood 2020;136:61–70.
5. Vainchenker W, Constantinescu SN. JAK/STAT signaling in hematological malignancies. Oncogene 2013;32:2601–13.
6. Malara A, Abbonante V, Zingariello M, Migliaccio A, Balduini A. Megakaryocyte contribution to bone marrow fibrosis: many arrows in the quiver. Mediterr J Hematol Infect Dis 2018;10:e2018068.
7. Schmitt A, Jouault H, Guichard J, Wendling F, Drouin A, Cramer EM. Pathologic interaction between megakaryocytes and polymorphonuclear leukocytes in myelofibrosis. Blood 2000;96:1342–7.
8. Centurione L, Di Baldassarre A, Zingariello M, et al. Increased and pathologic emperipolesis of neutrophils within megakaryocytes associated with marrow fibrosis in *GATA-1low* mice. Blood 2004;104:3573–80.
9. Vannucchi AM, Pancrazzi A, Guglielmelli P, et al. Abnormalities of GATA-1 in megakaryocytes from patients with idiopathic myelofibrosis. Am J Pathol 2005;167:849–58.
10. Gilles L, Arslan AD, Marinaccio C, et al. Downregulation of GATA1 drives impaired hematopoiesis in primary myelofibrosis. J Clin Invest 2017;127:1316–20.
11. Crispino JD, Weiss MJ. Erythro-megakaryocytic transcription factors associated with hereditary anemia. Blood 2014;123:3080–8.
12. Vannucchi AM, Bianchi L, Cellai C, et al. Development of myelofibrosis in mice genetically impaired for GATA-1 expression (GATA-1(low) mice). Blood 2002;100:1123–32.
13. Woods B, Chen W, Chiu S, et al. Activation of JAK/STAT signaling in megakaryocytes sustains myeloproliferation in vivo. Clin Cancer Res 2019;25:5901–12.
14. Zhang Y, Lin CHS, Kaushansky K, Zhan H. JAK2V617F megakaryocytes promote hematopoietic stem/progenitor cell expansion in mice through thrombopoietin/MPL signaling. Stem Cells 2018;36:1676–84.
15. Ciurea SO, Merchant D, Mahmud N, et al. Pivotal contributions of megakaryocytes to the biology of idiopathic myelofibrosis. Blood 2007;110:986–93.
16. Campanelli R, Rosti V, Villani L, et al. Evaluation of the bioactive and total transforming growth factor β1 levels in primary myelofibrosis. Cytokine 2011;53:100–6.
17. Chagraoui H, Komura E, Tulliez M, Giraudier S, Vainchenker W, Wendling F. Prominent role of TGF-beta 1 in thrombopoietin-induced myelofibrosis in mice. Blood 2002;100:3495–503.
18. Gastinne T, Vigant F, Lavenu-Bombled C, et al. Adenoviral-mediated TGF-beta1 inhibition in a mouse model of myelofibrosis inhibit bone marrow fibrosis development. Exp Hematol 2007;35:64–74.
19. Zingariello M, Martelli F, Ciaffoni F, et al. Characterization of the TGF-beta1 signaling abnormalities in the Gata1^{low} mouse model of myelofibrosis. Blood 2013;121:3345–63.
20. Varricchio L, Iancu-Rubin C, Upadhyaya B, et al. TGF-β1 protein trap AVID200 beneficially affects hematopoiesis and bone marrow fibrosis in myelofibrosis. JCI Insight 2021;6:e145651.
21. Gerds AT, Vannucchi AM, Passamonti F, et al. Duration of response to luspatercept in patients (Pts) requiring red blood cell (RBC) transfusions with myelofibrosis (MF) – updated data from the Phase 2 ACE-536-MF-001 Study. Blood 2020;136(Suppl 1):47–8.
22. Zetterberg E, Verrucci M, Martelli F, et al. Abnormal P-selectin localization during megakaryocyte development determines thrombosis in the gata1-low model of myelofibrosis. Platelets 2014;25:539–47.
23. Moore KL, Stults NL, Diaz S, et al. Identification of a specific glycoprotein ligand for P-selectin (CD62) on myeloid cells. J Cell Biol 1992;118:445–56.
24. Evangelista V, Manarini S, Sideri R, et al. Platelet/polymorphonuclear leukocyte interaction: P-selectin triggers protein-tyrosine phosphorylation-dependent CD11b/CD18 adhesion: role of PSGL-1 as a signaling molecule. Blood 1999;93:876–85.
25. Thiele J, Lorenzen J, Manich B, Kvasnicka HM, Zirbes TK, Fischer R. Apoptosis (programmed cell death) in idiopathic (primary) osteo-/myelofibrosis: naked nuclei in megakaryopoiesis reveal features of para-apoptosis. Acta Haematol 1997;97:137–43.
26. Zingariello M, Ruggeri A, Martelli F, et al. A novel interaction between megakaryocytes and activated fibrocytes increases TGF-β bioavailability in the *Gata1low* mouse model of myelofibrosis. Am J Blood Res 2015;5:34–61.
27. Spangrude GJ, Lewandowski D, Martelli F, et al. P-Selectin sustains extramedullary hematopoiesis in the *Gata1low* model of myelofibrosis. Stem Cells 2016;34:67–82.
28. Ceglia I, Dueck AC, Masiello F, et al. Preclinical rationale for TGF-β inhibition as a therapeutic target for the treatment of myelofibrosis. Exp Hematol 2016;44:1138–55.
29. Ataga KI, Kutlar A, Kanter J, et al. Crizanlizumab for the prevention of pain crises in sickle cell disease. N Engl J Med 2017;376:429–39.
30. Embury SH, Matsui NM, Ramanujam S, et al. The contribution of endothelial cell P-selectin to the microvascular flow of mouse sickle erythrocytes in vivo. Blood 2004;104:3378–85.
31. Martelli F, Ghinassi B, Panetta B, et al. Variegation of the phenotype induced by the *Gata1low* mutation in mice of different genetic backgrounds. Blood 2005;106:4102–13.
32. Zingariello M, Sancillo L, Martelli F, et al. The thrombopoietin/MPL axis is activated in the *Gata1low* mouse model of myelofibrosis and is associated with a defective RPS14 signature. Blood Cancer J 2017;7:1–11.
33. Oguro H, Ding L, Morrison SJ. SLAM family markers resolve functionally distinct subpopulations of hematopoietic stem cells and multipotent progenitors. Cell Stem Cell 2013;13:102–16.
34. Schneider CA, Rasband WS, Eliceiri KW. NIH Image to ImageJ: 25 years of image analysis. Nat Methods 2012;9:671–5.

35. Zingariello M, Verachi P, Gobbo F, et al. Resident self-tissue of proinflammatory cytokines rather than their systemic levels correlates with development of myelofibrosis in *Gata1low* mice. Biomolecules 2022; 12:234–60.
36. Vyas P, Ault K, Jackson CW, Orkin SH, Shivdasani RA. Consequences of GATA-1 deficiency in megakaryocytes and platelets. Blood 1999;93: 2867–75.
37. Fletcher K, Myant NB. Biotin in the synthesis of fatty acid and cholesterol by mammalian liver. Nature 1960;188:585.
38. Massagué J, Blain SW, Lo RS. TGFbeta signaling in growth control, cancer, and heritable disorders. Cell 2000;103:295–309.
39. Migliaccio AR, Martelli F, Verrucci M, et al. Gata1 expression driven by the alternative HS2 enhancer in the spleen rescues the hematopoietic failure induced by the hypomorphic Gata1^{low} mutation. Blood 2009; 114:2107–20.
40. Li L, Kim JH, Lu W, et al. HMGA1 chromatin regulators induce transcriptional networks involved in GATA2 and proliferation during MPN progression. Blood 2022;139:2797–815.
41. Garimella R, Kacena MA, Tague SE, Wang J, Horowitz MC, Anderson HC. Expression of bone morphogenetic proteins and their receptors in the bone marrow megakaryocytes of GATA-1(low) mice: a possible role in osteosclerosis. J Histochem Cytochem 2007;55:745–52.
42. Kacena MA, Shivdasani RA, Wilson K, et al. Megakaryocyte–osteoblast interaction revealed in mice deficient in transcription factors GATA-1 and NF-E2. J Bone Miner Res 2004;19:652–60.
43. Karagianni A, Ravid K. Myeloproliferative disorders and its effect on bone homeostasis: the role of megakaryocytes. Blood 2022;139:3127–37.
44. Stavnichuk M, Komarova SV. Megakaryocyte-bone cell interactions: lessons from mouse models of experimental myelofibrosis and related disorders. Am J Cell Physiol 2022;322:C177–84.
45. Perner F, Perner C, Ernst T, Heidel FH. Roles of JAK2 in aging, inflammation, hematopoiesis and malignant transformation. Cells 2019;8:854–73.
46. Steiniger BS. Human spleen microanatomy: why mice do not suffice. Immunology 2015;145:334–46.
47. Sun S, Jin C, Si J, et al. Single-cell analysis of ploidy and the transcriptome reveals functional and spatial divergency in murine megakaryopoiesis. Blood 2021;138:1211–24.
48. Ghinassi B, Sanchez M, Martelli F, et al. The hypomorphic *Gata1low* mutation alters the proliferation/differentiation potential of the common megakaryocytic-erythroid progenitor. Blood 2007;109:1460–71.
49. Foreman KE, Vaporciyan AA, Bonish BK, et al. C5a-induced expression of P-selectin in endothelial cells. J Clin Invest 1994;94:1147–55.
50. Verachi P, Gobbo F, Martelli F, et al. The CXCR1/CXCR2 inhibitor reparixin alters the development of myelofibrosis in the *Gata1low* mice. Front Oncol 2022;12:853484–98.
51. Emadi S, Clay D, Desterke C, et al. IL-8 and its CXCR1 and CXCR2 receptors participate in the control of megakaryocytic proliferation, differentiation, and ploidy in myeloid metaplasia with myelofibrosis. Blood 2005;105:464–73.
52. McDevitt MA, Fujiwara Y, Shivdasani RA, Orkin SH. An upstream, DNase I hypersensitive region of the hematopoietic-expressed transcription factor GATA-1 gene confers developmental specificity in transgenic mice. Proc Natl Acad Sci U S A 1997;94:7976–81.
53. Wen QJ, Yang Q, Goldenson B, et al. Targeting megakaryocytic-induced fibrosis in myeloproliferative neoplasms by AURKA inhibition. Nat Med 2015;21:1473–80.
54. Kramer F, Dernedde J, Mezheyeuski A, Tauber R, Micke P, Kappert K. Platelet-derived growth factor receptor β activation and regulation in murine myelofibrosis. Haematologica 2020;105:2083–94.
55. Corey SJ, Jha J, McCart EA, et al. Captopril mitigates splenomegaly and myelofibrosis in the *Gata1low* murine model of myelofibrosis. J Cell Mol Med 2018;22:4274–82.
56. Leiva O, Ng SK, Matsuura S, et al. Novel lysyl oxidase inhibitors attenuate hallmarks of primary myelofibrosis in mice. Int J Hematol 2019;110:699–6708.
57. Lucijanic M, Pejsa V, Jaksic O, et al. The degree of anisocytosis predicts survival in patients with primary myelofibrosis. Acta Haematol 2016;136:98–100.
58. Bommireddy R, Saxena V, Ormsby I, et al. TGF-β1 regulates lymphocyte homeostasis by preventing activation and subsequent apoptosis of peripheral lymphocytes. J Immunol 2003;170:4612–22.
59. Batlle E, Massagué J. Transforming growth factor-β signaling in immunity and cancer. Immunity 2019;50:924–40.
60. Mukaida N. Interleukin-8: an expanding universe beyond neutrophil chemotaxis and activation. Int J Hematol 2000;72:391–8.
61. Palomino DCT, Marti LC. Chemokines and immunity. Einstein (São Paulo) 2015;13:469–73.
62. Pariser DN, Hilt ZT, Ture SK, et al. Lung megakaryocytes are immune modulatory cells. J Clin Invest 2021;131:e137377.
63. Wang H, He J, Xu C, et al. Decoding human megakaryocyte development. Cell Stem Cell 2021;28:535–49. e8.
64. Yeung AK, Villacorta-Martin C, Hon S, Rock JR, Murphy GJ. Lung megakaryocytes display distinct transcriptional and phenotypic properties. Blood Adv 2020;4:6204–17.
65. Abbonante V, Di Buduo CA, Gruppi C, et al. Thrombopoietin/TGF-β1 loop regulates megakaryocyte extracellular matrix component synthesis. Stem Cells 2016;34:1123–33.
66. Malara A, Currao M, Gruppi C, et al. Megakaryocytes contribute to the bone marrow-matrix environment by expressing fibronectin, type IV collagen, and laminin. Stem Cells 2014;32:926–37.

3.2 Supplementary materials

Supplementary figures

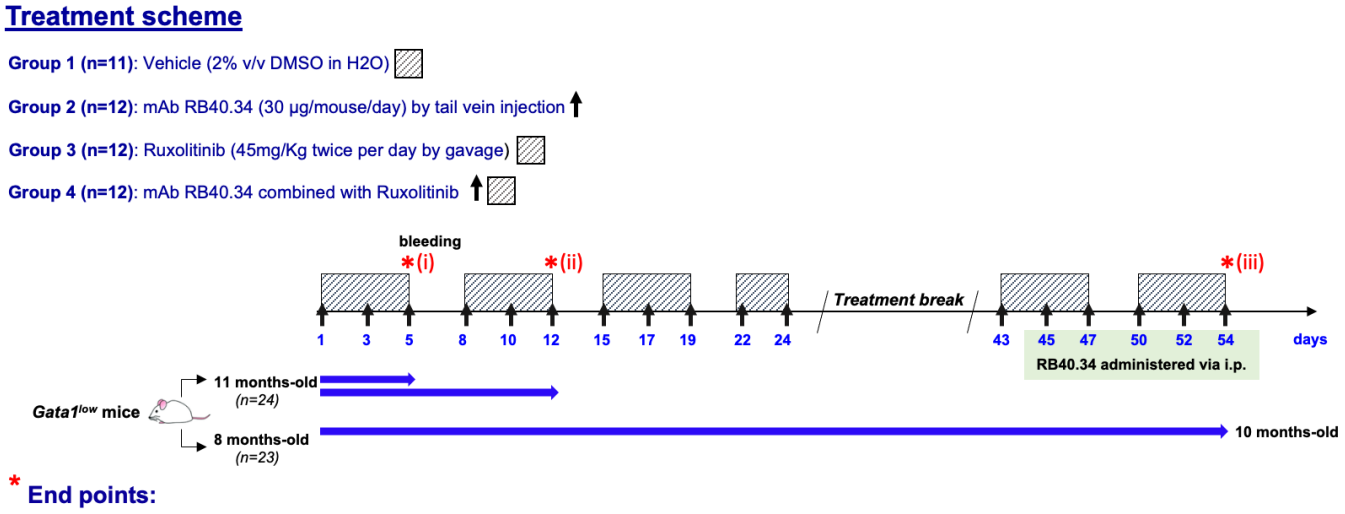

Figure S1. Scheme of the treatments. The study involved forty-seven *Gata1*^{low} mice divided into two experiments. In the first experiment, twenty-four 11-months old *Gata1*^{low} mice were divided into four treatment groups. Three mice per group were treated for 5 days and sacrificed at day 5, whereas the other mice were treated for 7 additional days and sacrificed at day 12. In the second experiment, 23 8-months old *Gata1*^{low} mice were divided in four groups and treated as described for 54 days with 2 weeks of break in between until they reach 10 months of age. Black arrows indicate day of the administrations with the antibody RB40.34, while grey boxes indicate the cycles of treatment with Rux or vehicle. Red asterisks indicate the day when mice were sacrificed and their organs harvested for end-point evaluations (day 5 (i), 12 (ii) and 54 (iii), respectively). End-points analyzed at each time point are also indicated.

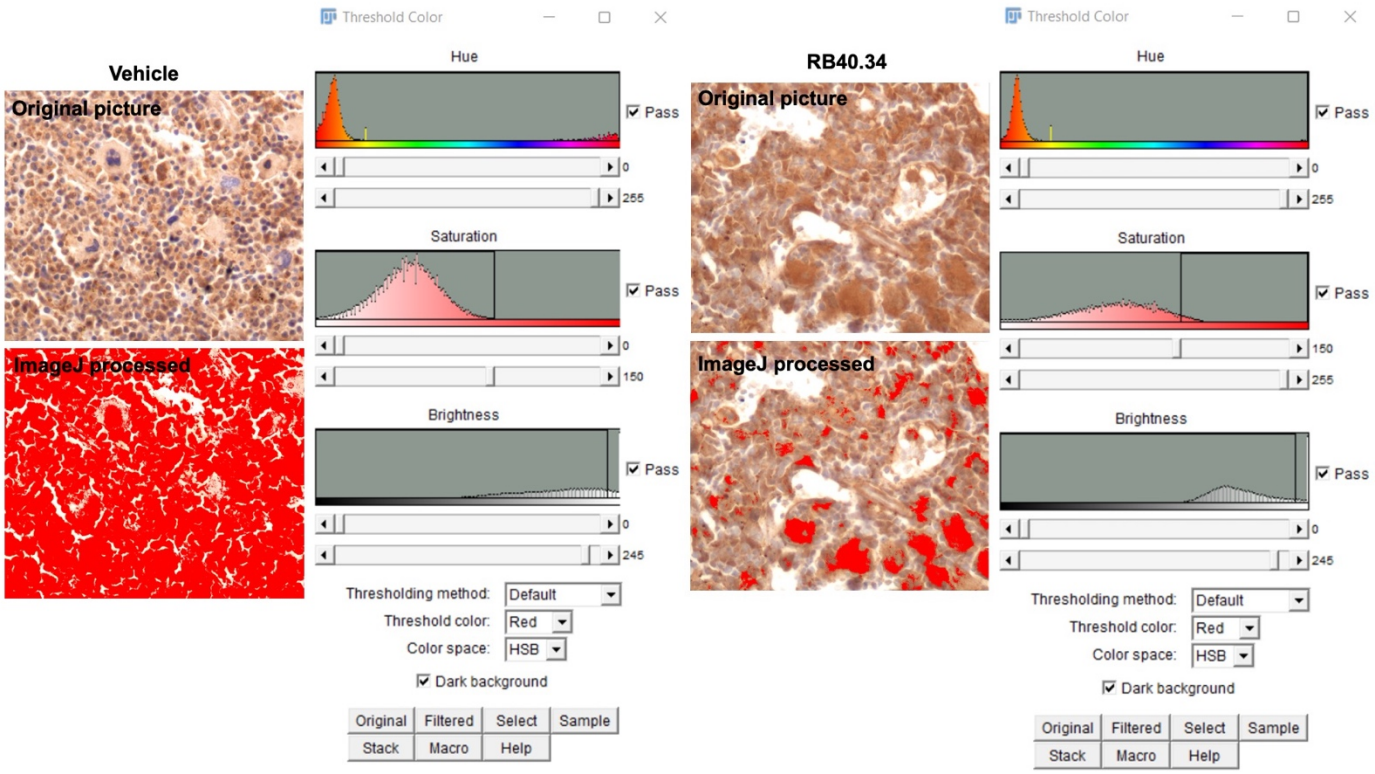

Figure S2. Computer assisted image analysis used for assessing the binding of RB40.34 antibody to the megakaryocytes of the bone marrow from mice treated with RB40.34. We first determined with the ImageJ program the level of the endogenous biotin signal above the background in the bone marrow sections from the vehicle group (saturation histogram). This level was considered as threshold in the evaluation of the biotin signal in the RB40.34 treated mice. We then identified with the ImageJ program the areas of the bone marrow sections from the RB40.34 treated mice in which the biotin signal was greater than the threshold (brightness histogram) and had the computer artificially paint these areas in red. Magnification 400X.

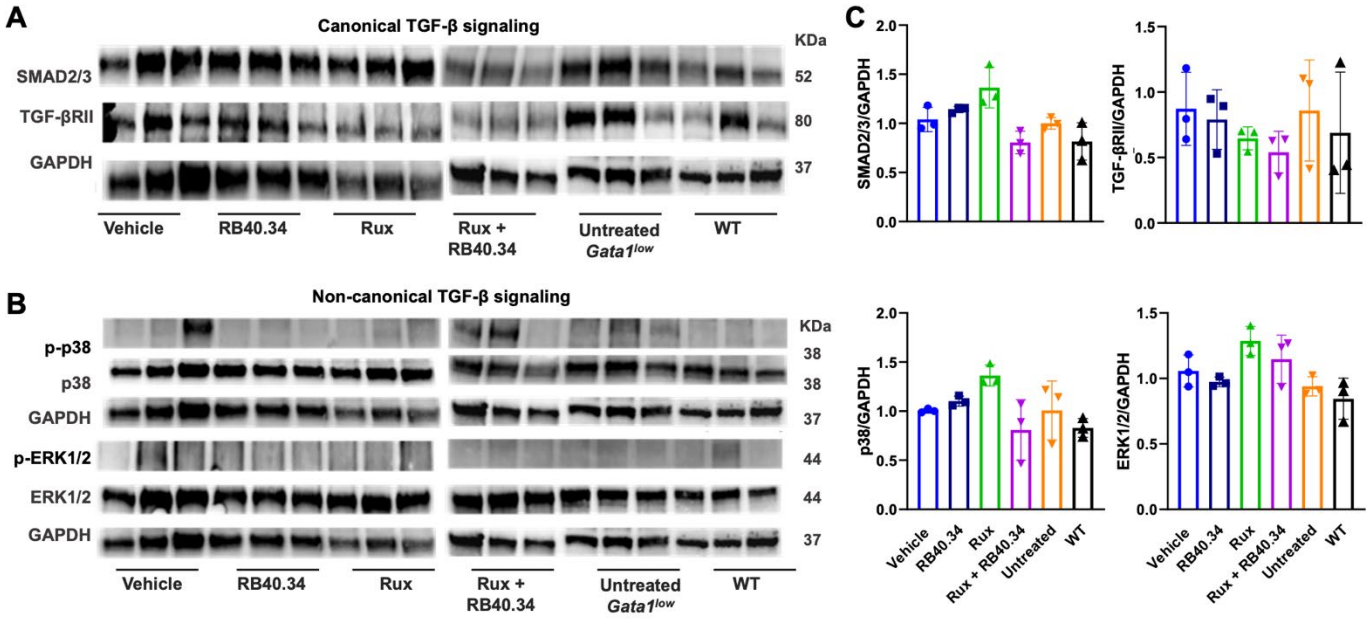

Figure S3. None of the treatments induced significant changes in canonical and non-canonical TGF-β signaling in the spleen from *Gata1*^{low} mice. (A,B) Original western blot determinations of the content of elements downstream to the canonical and non-canonical TGF-β signaling from the spleen of *Gata1*^{low} mice treated with vehicle, RB40.34, Rux or the two drugs in combination, as indicated. Each line represents one mouse, with three mice per experimental group (in the same order than in **Figure 2A,B**). GAPDH was used as loading control. (C) Levels of proteins analyzed in A,B normalized with respect to the corresponding GAPDH levels. Values are presented as Means (± SD) of values observed with multiple mice and in individual mice and were compared by Tukey multiple comparison test. The data are not significantly different among groups.

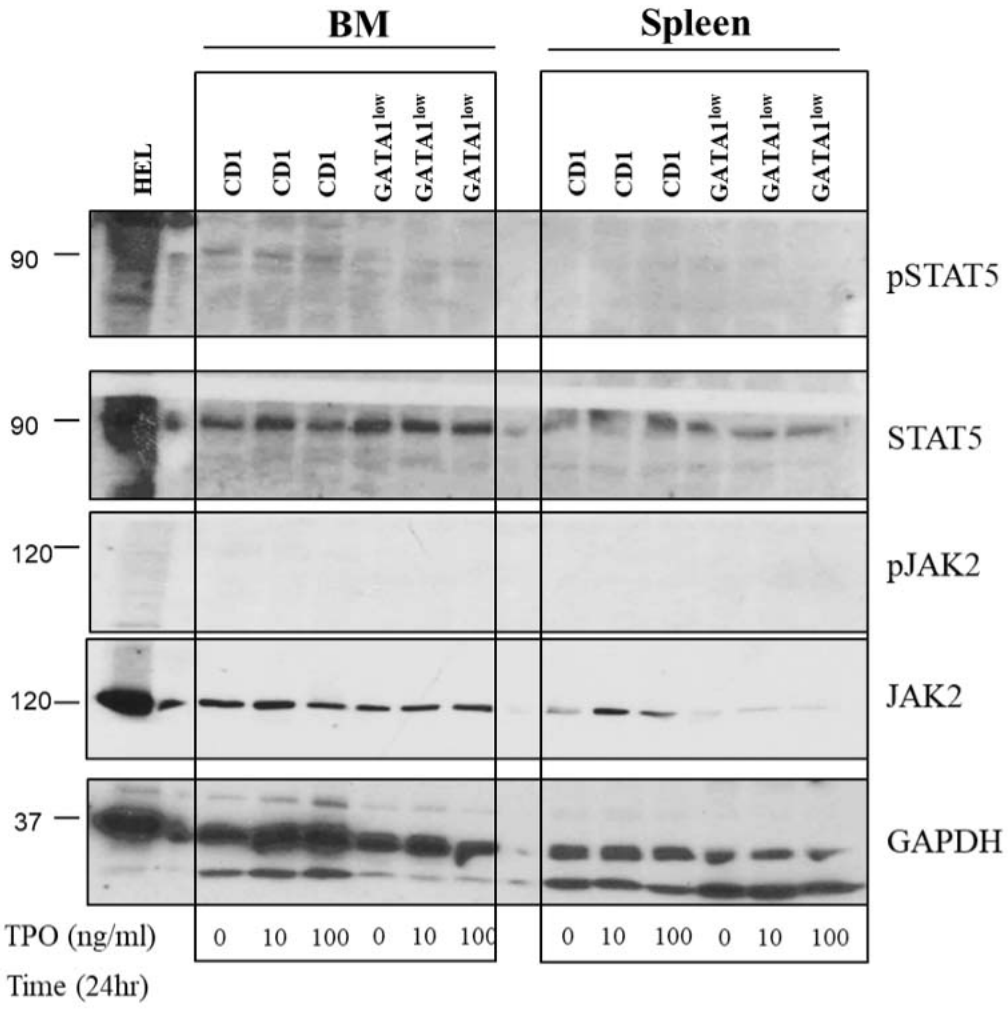

Figure S4. JAK2 and STA5 phosphorylation are barely detectable with thawed lysates of primary bone marrow cells from CD1 and *Gata1^{low}* mice even when these cells had been treated for 24hr with 10 and 100 ng/mL of thrombopoietin (TPO).

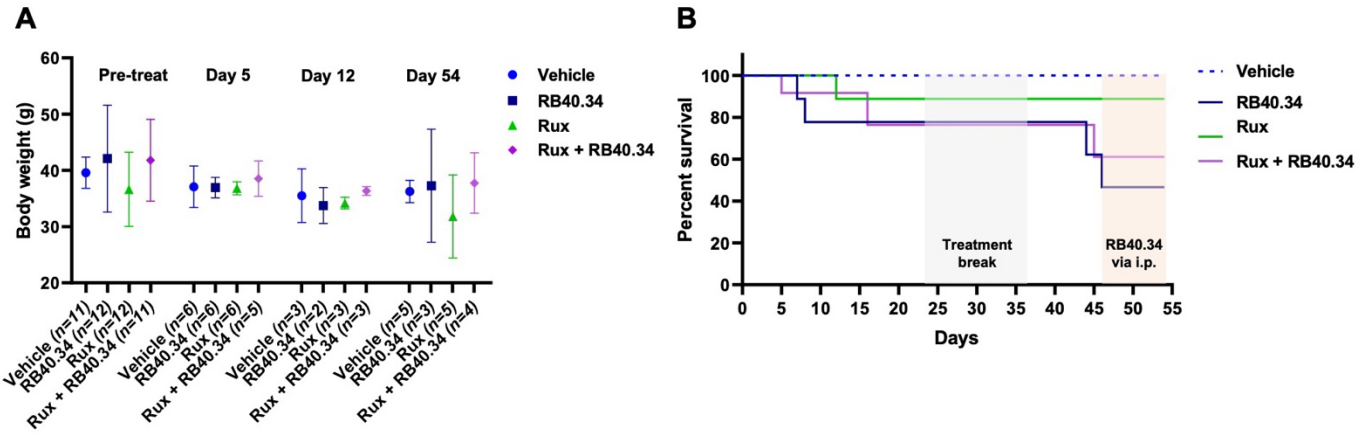

Figure S5. None of the drugs investigated induces significant changes in body weight and survival in *Gata1^{low}* mice treated for up to 54 days. (A) Body weight determinations of *Gata1*^{low} mice before (pre-treat) and after treatment for 5, 12 and 54 days. Data are presented as Mean (±SD) and are not statistically significant among groups by Tukey multiple comparison test. The number of mice included in each group is indicated by n. (B) Kaplan–Meier survival curves of *Gata1*^{low} mice treated with vehicle (dotted line, blue), RB40.34 alone (dark blue), Rux alone (green) or the two drugs in combination (lilac), as indicated. Mice sacrificed at day 5 (*n=12*) and 12 (*n=12*) were considered as censored observations. The shaded vertical lines indicate the treatment break due to the holyday season and the change of RB40.34 administration from i.v. to i.p, due to suspected mice intolerance to i.v. administration. The survival curves of the four groups are not statistically different by log-rank (Mantel-Cox) test.

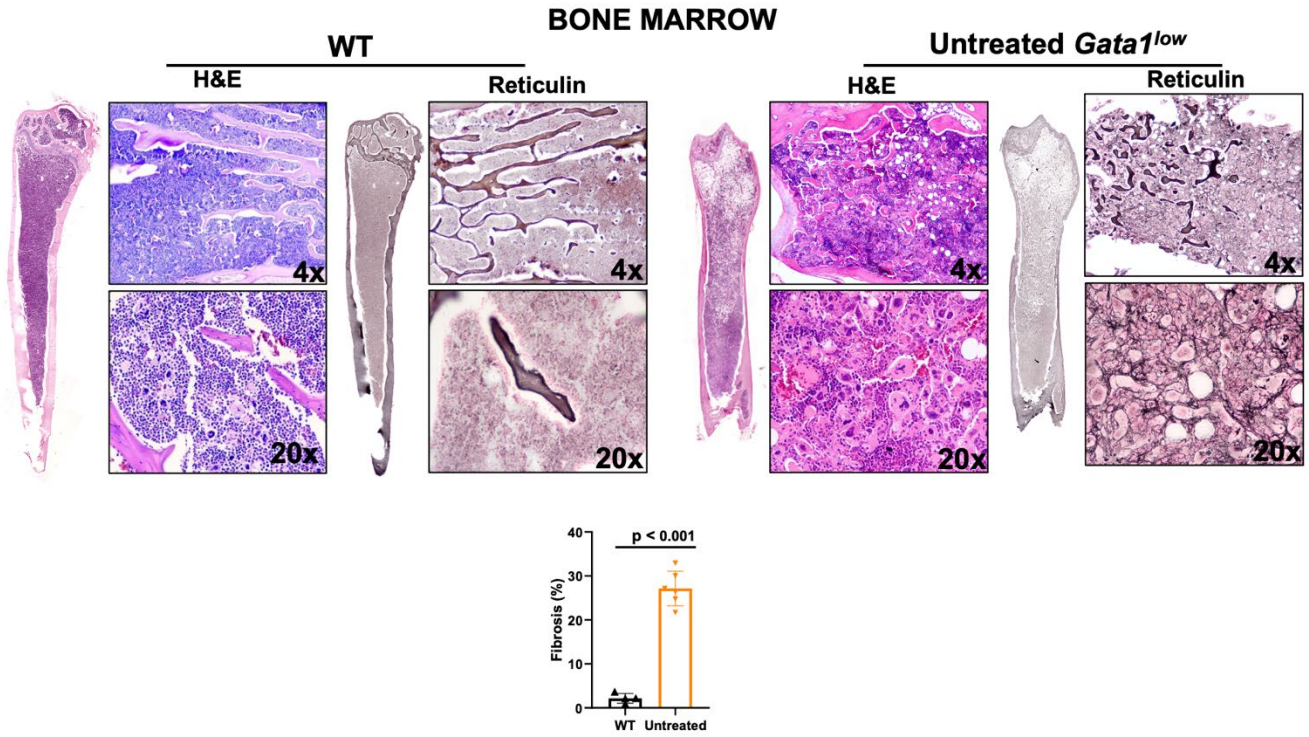

Figure S6. The femur from untreated Gata1^{low} mice contain less cells and greater levels of fibrosis than that from WT littermates. A) Hematoxylin/Eosin (H&E) and Reticulin staining of sections from the femur of representative untreated 8-11-months old *Gata1^{low}* and WT littermates, as indicated. The entire femur is presented as stack images (at 4x) and as detail at 4 and 20x magnification. B) Levels of fibrosis quantified by image analyses of the reticulin staining of BM sections from untreated WT and *Gata1^{low}* littermates, as indicated. Results are presented as Mean (±SD) and as values per individual mice (each symbol a mouse) and were analyzed by t test. The difference in the level of fibrosis between the two groups is statistically significant.

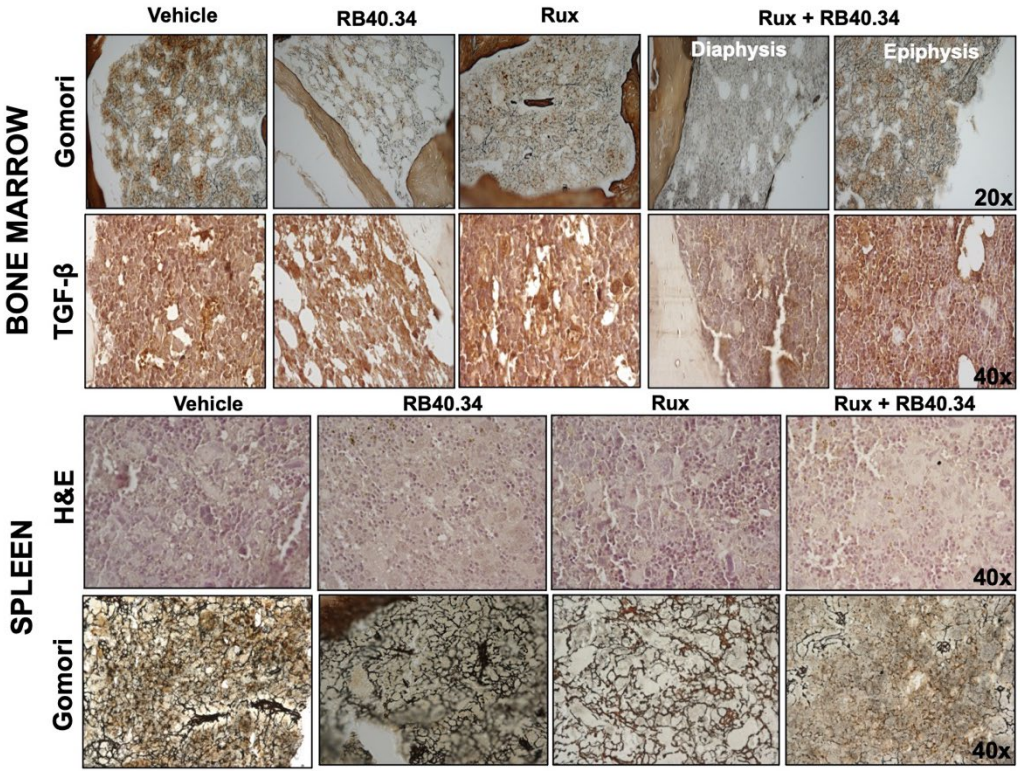

Figure S7. Treatment with RB40.34 in combination with Rux for 12 days reduced both fibrosis and TGF-β content only in the diaphysis of the femur and in the spleen from *Gata1^{low}* mice. Gomori and TGF-β immune-staining of sections from the femur and hematoxylin/eosin (H&E) and Gomori staining of sections from the spleen of representative *Gata1^{low}* mice treated for 12 days with either vehicle, RB40.34, Rux or the two drugs in combination, as indicated. Original magnification 20x or 40x, as indicated.

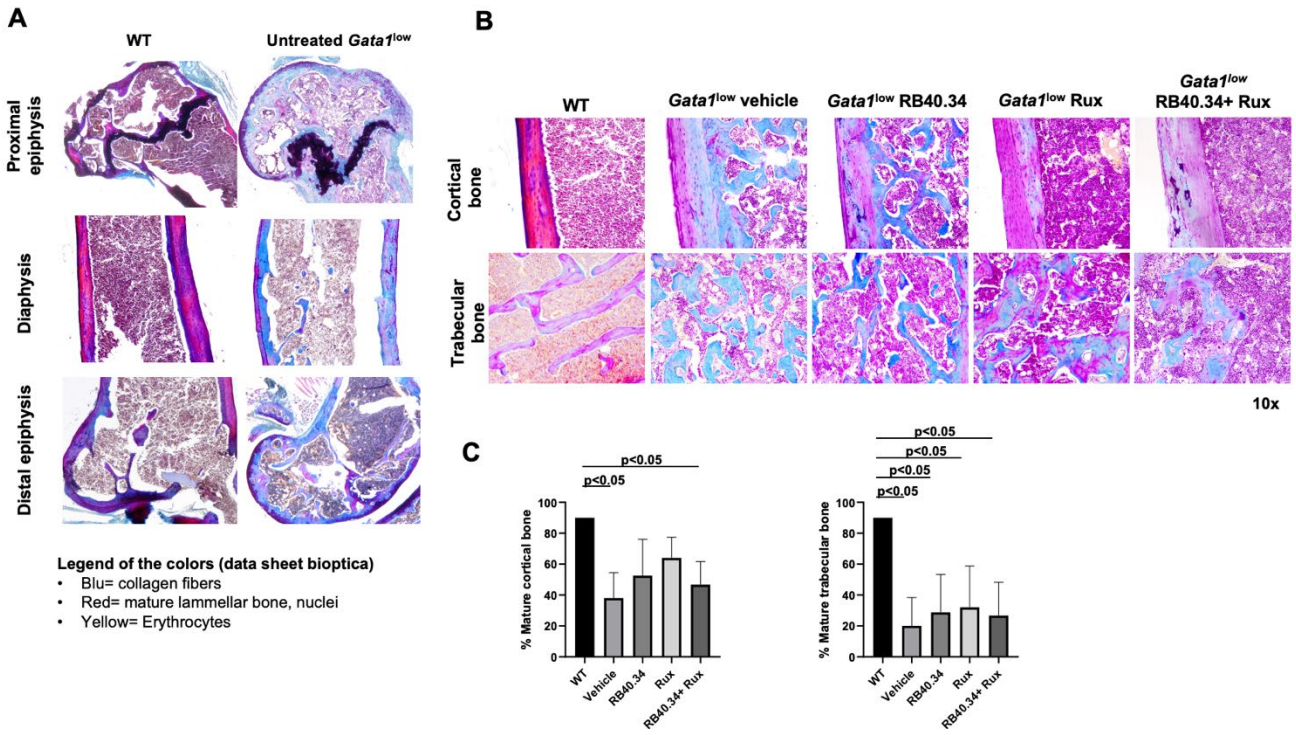

Figure S8. Treatment with Rux alone reduces the osteopetrosis and improves the maturation of the cortical bone from the femur of *Gata1^{low}* mice. A) Representative Mallory trichrome staining of the epiphysis and diaphysis of the femur from untreated 8-11-months old WT and *Gata1*^{low} littermates. Original magnification 4x. **B**) Mallory trichrome staining of the sections of the cortical and trabecular area of the femur from *Gata1*^{low} mice treated for 54 days with either vehicle, RB40.34, Rux or RB40.34+Rux in combination, as indicated. Magnification 10x. **C**) Quantification of the areas of mature bone of the cortex and the trabeculae of WT mice and of *Gata1*^{low} mice treated for 54 days with either vehicle, RB40.34, Rux or RB40.34+Rux in combinations. Data are presented as Mean(±SD) and differences among groups were analyzed by Anova. Values statistically different are presented within the panels.

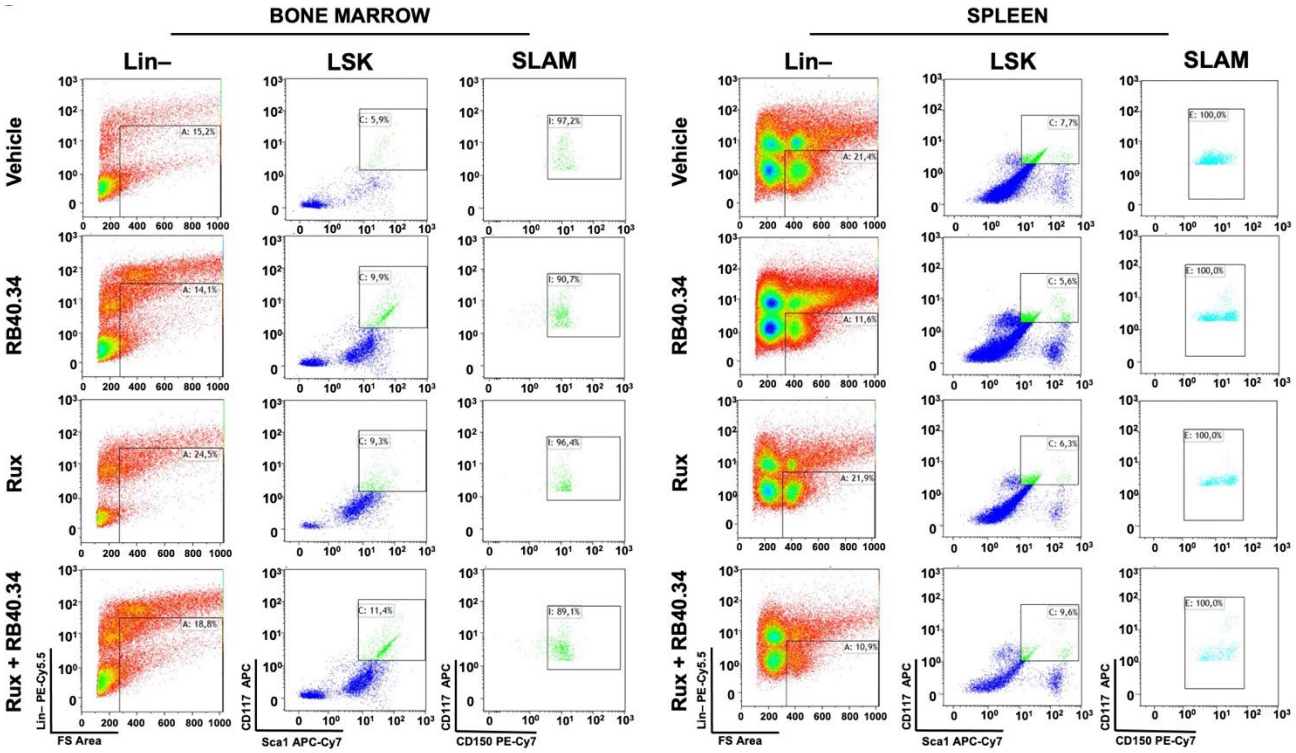

Figure S9. Representative sequence of gating used to identify the Lin-, LSK and SLAM (CD150^{pos}/CD48^{neg} LSK) cells in bone marrow (A) and spleen (B) from *Gata1^{low}* mice treated for 54 days with either vehicle, RB40.34, Rux or the two drugs in combination, as indicated.

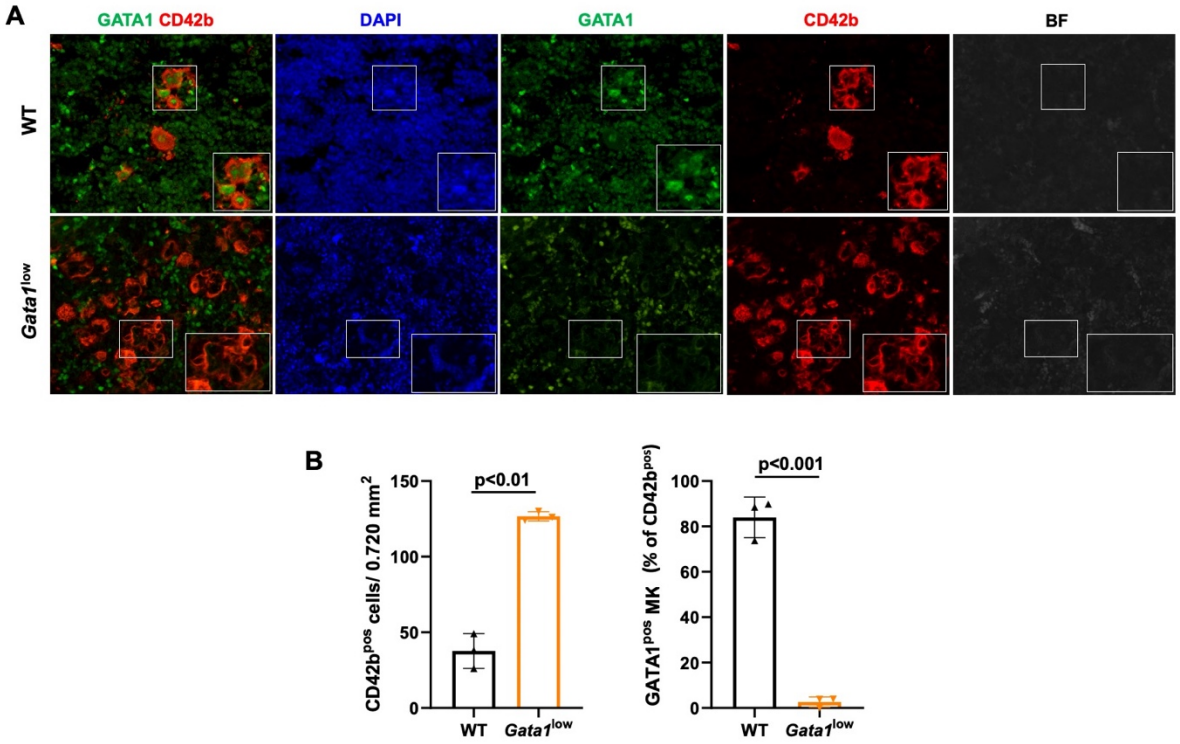

Figure S10. The bone marrow from *Gata1^{low}* mice contain great numbers of MK with barely detectable levels of GATA1. A) Triple confocal microscopy analyses with antibodies against CD42b (as MK marker, red), GATA1 (in green) and counterstained with DAPI (blue) of BM sections from representative WT and *Gata1^{low}* littermates (one mouse each) as indicated. Images were acquired in the bright field channel (to evaluate autofluorescence), and in the red (555nm), green (488nm) and DAPI (405nm) fields and are presented as single channels and in combination. B) Frequency of CD42b^{pos} cells (MK) and of CD42b^{pos} cells containing detectable levels of GATA1 in BM sections from multiple WT and *Gata1^{low}* littermates. Data are presented as Means (± SD) of values observed with three mice per experimental group and are compared by t test.

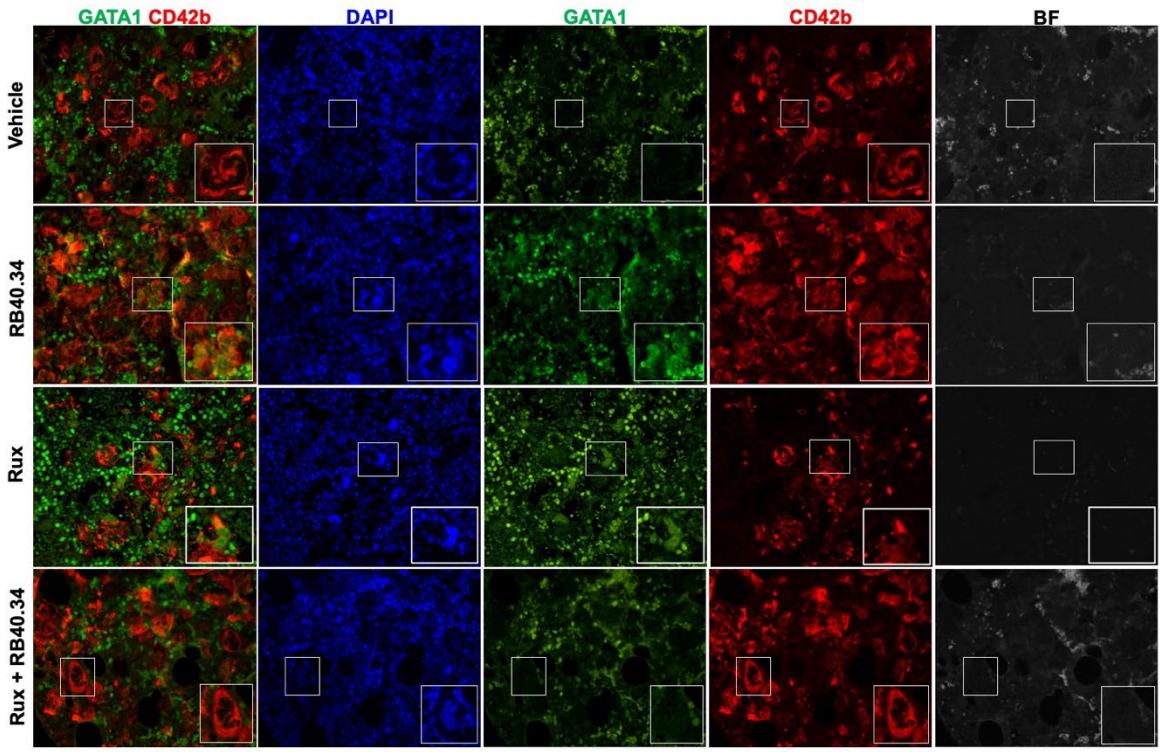

Figure S11 Treatment for 54 days with RB40.34 or Rux alone, but not in combination, increased the GATA1 content in the MK from the BM of *Gata1^{low}* mice. Triple immunofluorescence analyses with antibodies against GATA1 (FITCH-green), CD42b (TRITCH-red, as a marker of MKs), and DAPI (to identify the nuclei) of BM sections from representative *Gata1^{low}* mice treated for 54 days with either vehicle, RB40.34 alone, Rux alone, or the two drugs in combination, as indicated. The individual panels shows images acquired in the bright field (as indication of autofluorescence from red blood cells), or in the DAPI, GATA1 and CD42b channels alone and in combination. See **Figure 10** for detail.

Supplementary Tables

Table S1. Summary table of deaths recorded in *Gata1*^{low} mice treated with vehicle, RB40.34, Rux or the combination of drugs during the treatment period. In 6 out of 8 cases (3 mice treated with RB40.34 and 3 mice treated with the two drugs in combination) the cause of death remains unclear.

Treatment	Recorded deaths	Days of treatment	Cause of death
Vehicle (n=11)	0		
RB40.34 (n=12)	4	7,8, 44, 46	Improper manipulation during the injection (n=1); not established, found dead shortly after the venous injection (n=3)
Rux (n=12)	1	12	Suppressed for signs of suffering
Rux + RB40.34 (n=12)	3	5, 16, 45	not established, found dead shortly after the venous injection (n=3)

Table S2. Complete red blood cell values of *Gata1*^{low} mice 54 days post-treatment. Values among groups are not statistically significant by ANOVA multiple comparisons test. Abbreviations: $^{(n)}$: number of mice analyzed; RBC: Red Blood Cells; Hgb: Hemoglobin; MCV: Mean Cell Volume; MCH: Mean Cell Hemoglobin; MCHC: Mean Cell Hemoglobin Concentration; CHCM: Cell Hemoglobin Concentration Mean; CH: Hemoglobin Content; CHDW: Cell Hemoglobin Distribuition Width; HDW: Hemoglobin Distribution Width.

Treatment	Vehicle	RB40.34	Rux	Rux + RB40.34
RBC (10^6/µL)	6.12± 0.74 $^{(5)}$	6.32±0.10 $^{(3)}$	5.47±0.74 $^{(5)}$	5.47±0.55 $^{(3)}$
Hgb (g/dL)	10.92±1.24 $^{(5)}$	11.27 ±0.15 $^{(3)}$	9.62±1.70 $^{(5)}$	9.60±0.61 $^{(3)}$
MCV (fL)	54.80±2.28 $^{(5)}$	52.97±1.19 $^{(3)}$	53.70±3.50 $^{(5)}$	53.40±3.22 $^{(3)}$
MCH (pg)	17.82±0.48 $^{(5)}$	17.80±0.52 $^{(3)}$	17.48±1.21 $^{(5)}$	17.53±0.67 $^{(3)}$
MCHC (g/dL)	32.58±0.87 $^{(5)}$	33.63±0.25 $^{(3)}$	32.58±0.30 $^{(5)}$	32.90±0.80 $^{(3)}$
CHCM (g/dL)	32.52±1.02 $^{(5)}$	31.17 ± 0.06 $^{(3)}$	32.30±0.16 $^{(5)}$	31.47±0.25 $^{(3)}$
MCHC/CHCM	1.00±0.00 $^{(5)}$	1.07 ± 0.06 $^{(3)}$	1.00 ± 0.00 $^{(5)}$	1.03 ± 0.06 $^{(3)}$
CH (pg)	16.66±1.03 $^{(5)}$	16.47±0.32 $^{(3)}$	16.64±1.00 $^{(5)}$	16.03±0.55 $^{(3)}$
CHDW (pg)	2.82±0.22 $^{(5)}$	2.83±0.06 $^{(3)}$	3.02±0.20 $^{(5)}$	2.93±0.32 $^{(3)}$
HDW (g/dL)	2.34±0.23 $^{(5)}$	2.50±0.00 $^{(3)}$	2.32±0.22 $^{(5)}$	2.53±0.06 $^{(3)}$

Table S3. Summary of the response of *Gata1*^{low} mice to the various treatments.

			Treatment groups			
		End Points	**Vehicle**	**RB40.34**	**Rux**	**RB.40.34+Rux**
Blood	**Day 5**	**Hct (%)**	Normal	Normal	Normal	Normal
		Platelets (10^3/μL)	Low	Low	Low	Low
		Platelet Binding to RB40.34	-	+	-	+
	Day 54	**Hct (%)**	Normal	Normal	Normal	Normal
		Anistocytosis	+	-	+	-
		Platelets (10^3/μL)	Low	Low	Low	Low
		WBC (10^3/μL)	High	High	Normal	Normal
		Lymphocytes (10^3/μL)	High	High	Normal	Normal
Bone Marrow	**Day 5**	**Binding of RB40.34 to MK**	-	+	-	+
		Cellularity	Low	Low	Low	Low
		TGF-β Signaling	Activated	Activated	Activated	Normal
	Day 54	**MK maturation**	Immature	Mature	Mature	Mature
		Cellularity	Low	Low	Low	Normal
		Binding of RB40.34 to MK	?	-	?	-
		Fibrosis	High	Low	High	Low
		Hematopoiesis	Low	Low	Low	Improved
		GATA1pos MK	Few	Increased	Increased	Few
		TGF-β/CXCL1	High	High	Low	Low
		Neoangiogensis	High	Reduced	Reduced	Reduced
		Osteopetrosis	High	High	Reduced	High
Spleen	**Day 5**	**Size**	Enlarged	Enlarged	Enlarged	Enlarged
		Binding of RB40.34 to MK	-	+	-	+
		JAK2 Signaling	Increased	Normal	Increased	Normal
	Day 54	**Size**	Enlarged	Enlarged	Enlarged	Normal
		Binding of RB40.34 to MK	?	-	?	-
		Fibrosis	High	Low	Low	Low
		Hematopoiesis	High	High	High	Low
		Architecture	Altered	Normal	Altered	Normal
		Neoangiogensis	High	Reduced	Reduced	Reduced

4. Discussion

The discovery of the *JAK2*^{V617F} driver mutation, which is expressed by ≈ 50-60% of PMF patients, led to the development of several pharmacological JAK1/2 inhibitors for the treatment of the disease. Although the pivotal role of JAK-STAT activation in MPN has been widely recognized, PMF is characterized by a secondary inflammatory response with aberrant cytokine expression. Moreover, the activate JAK-STAT signaling is a non-specific phenomenon in cancer and pharmacological inhibition of JAK has proven to be ineffective in inducing selective suppression of the malignant clone [99]. Indeed, JAK1/2 inhibitors, like Rux, reduce splenomegaly and ameliorate constitutional symptoms but do not halt the natural course of the disease.

At present, AHSCT remains the only treatment in PMF that secures disease-free remission state and prolonged survival. Thus, the scenario requires urgent attention to genetic characterization of clinical observations followed by *in vivo* animal studies that may lead to the development of new therapeutic drugs targeting the malignant cells and the microenvironmental abnormalities and not only the constitutional effects of the disease.

The hypomorphic *Gata1*^{low} mutation deletes one of the three major hypersensitive sites which regulate the expression of the gene [87,100]. After birth, the expression of the gene in HSCs is activated by the alternative HS2 enhancer as demonstrated by the fact that the levels of *Gata1* mRNA are overall normal in these cells [101]. However, the *Gata1*^{low} mutation induces thrombocytopenia and hyperactivation of the TPO/MPL axis, which was associated with a RSP14 deficiency and a discordant microarray ribosome signature (reduced RPS24, RPS26 and SBDS expression) [102]. The resulting RSP14 ribosomopathy is thought to be responsible of the defective post-transcriptional events that lead to the reduced content of the of GATA1 protein in *Gata1*^{low} mice, similarly to what observed in PMF patients [14].

Despite *Gata1*^{low} mice do not carry any of the most common driver mutation of PMF, they recapitulate all the pathological features of human PMF. The relevance of this animal model has been provided by the observation that, independently from the driver mutation, the MKs from all the patients affected by PMF contain low levels of GATA1 and by the fact that *Gata1*^{low} mice respond to treatment with the JAK2 inhibitor Rux in a fashion extremely similar to that of PMF patients (significant reduction of spleen size without detectable effects on the natural history of the disease). Over the years, the *Gata1*^{low} model has been used to characterize the pathogenic mechanisms underlying PMF and to identify new targets to cure the disease. In particular, our previous studies demonstrated that malignant MKs released a high content of TGFβ-1 in the microenvironment, leading to fibrocytes activation and to collagen/reticulin deposition in the BM of *Gata1*^{low} mice. In

addition, we demonstrated that this massive release of TGF-β1 and other pro-inflammatory cytokines was initiated by a pathologic emperipolesis between MKs and neutrophils, which is in turn triggered by abnormal expression of P-sel to the DMS of MKs [28]. Based on previous observations indicating that deletion of the P-sel gene prevented the development of myelofibrosis in *Gata1*^{low} mice, in this study we assessed whether pharmacological inhibition of P-sel, alone or in combination with Rux, may prevent the development of the myelofibrotic phenotype in these mice.

Firstly, by flow cytometry and immunohistochemistry determinations we demonstrated that after five days of treatment the monoclonal antibody RB40.34 was able to reach the myelofibrotic organs of *Gata1*^{low} mice, binding to the MKs. In addition, we found that after 5 days the combined therapy, but not the drugs alone, restored the typical abnormalities in the canonical and non-canonical TGF-β1 signaling.

We previously demonstrated that fibrosis in PMF is driven by the activation of the non-canonical TGF-β1 signaling, whereas defects of the canonical TGF-β1 signaling were associated with impaired hematopoiesis in the BM [103]. Further evidence that the signals that induce hematopoietic niche disruption in BM were distinct from those that induce the fibrosis program were provided by Yao et al., who reported that BM fibrosis was mediated by a SMAD4-independent TGF-β signaling in a mouse model of the disease [104].

Thus, our data suggested that the combined therapy could be effective both in reducing the fibrosis and in restoring normal hematopoiesis in the BM. Moreover, the drug combination was effective in reducing the JAK2 content in the spleen, consistently with our previous report indicating that Rux was able to reduce the EMH in the spleen [102].

Encouraged by these preliminary results, we analyzed the effects of long-term treatments with RB40.34 and Rux, alone or in combination, on the myelofibrotic phenotype expressed by *Gata1*^{low} mice. First, the results indicated that none of the treatments induced anemia nor rescued the thrombocytopenia of *Gata1*^{low} mice. However, treatment for 54 days with RB40.34 in combination with Rux, and to a less extent with the two drugs alone, reduced anisocytosis and lymphocyte counts. Since anisocytosis with high Red blood cell Distribution Width (RDW) values has been correlated with an increase of inflammatory cytokines in a wide spectrum of benign and malignant disorders, including PMF [105], we hypothesized that the reduction in anisocytosis observed on day 54 in the RB40.34 alone or in combination with Rux groups reflected the reductions in the pro-inflammatory cytokines TGF-β1 and/or CXCL1, which drive MF in this model. This hypothesis was consistent with the reduced lymphocyte counts observed by day 54 in the mice treated with the two drugs in combination. Indeed, several studies demonstrated that TGF-β1 regulates lymphocytes homeostasis

[106], whereas CXCL1 has been proven to have diverse actions on various types of leukocytic and non-leukocytic cells besides neutrophils, including lymphocytes [107].

The content of TGF-β1 and CXCL1 in BM microenvironment was directly tested, demonstrating that the combined therapy significantly reduced the bioavailability of these two pro-inflammatory cytokines in the BM of *Gata1*^{low} mice. Consistently, RB40.34 in combination with Rux significantly reduced the fibrosis in the BM and the spleen, restored hematopoiesis in the BM and reduced the EMH in the spleen.

None of the treatments reduced the frequency of MKs, which remained high. A possible explanation may be provided by our previous observations indicating that MKs abnormalities in our murine model, as well as in PMF patients, were driven by the TPO/MPL axis [102]. Conversely, all the treatments were effective in reducing the levels of P-sel on the MKs cell surface and the TGF-β1 content. The two drugs alone, mostly Rux alone, were also effective in increasing the GATA1 content in CD42pos MKs in the BM of *Gata1*^{low} mice. It is peculiar instead that the levels of GATA1 were not increased in MKs from the BM of mice treated with RB40.34 and Rux in combination.

The mechanistic interpretation of these data is difficult and need to take account of the increasing recent studies indicating the existence of specialized MKs subpopulations, each one exerting different functions. To this regard, Sun et al., by single-cell analysis of ploidy and the transcriptome identified three distinct subpopulations with gene signatures related to platelet generation, HSCs niche interaction, and inflammatory responses, respectively. Only platelet-producing MKs exhibited the morphology of mature MKs and were high ploidy cells (≥8N), whereas niche-supporting MKs and immune-MKs had the morphology of immature MKs [61].

Of particular interest for our study, Wang et al., described a human embryonic MKs subpopulation having an immature morphology and characterized by high expression of extracellular matrix genes, such as *COL1A1*, *COL3A1*, and *COL6A2*, and enrichment in the gene sets of "response to TGF-β" [60]. In addition, the above-mentioned studies reported that the distinct MKs subpopulations expressed different levels of the key traditional regulators of megakaryopoiesis, and in particular that *GATA1* was highly expressed in the platelet-poised MKs whereas was not found to be upregulated in the population associated with "extracellular matrix organization" and "neutrophil activation" [60]. Of note, Balduini et al., reported that malignant MKs from PMF patients showed increased expression of type III collagen and fibronectin compared to healthy controls [108].

Collectively, these data suggest that PMF may be driven by a specific MKs subpopulation and that low levels of GATA1 may block the maturation of platelet-poised MKs and may promote the MKs differentiation towards other MKs subtypes that are sustained by high levels of TGF-β1.

According to this hypothesis, we suggested that RB40.34 and Rux exerted their effects by reducing the content of TGF-β1 and thus frequency of niche-poised MKs. On the other hand, Rux alone was able to increase the GATA1 content in CD42pos MKs and to normalize the levels of TGF-β1, but did not reduced the fibrosis in the BM and spleen from *Gata1*^{low} mice, suggesting that the drug alone did not target the niche-poised MKs.
Taken toghether, these data indicated that treatment with RB40.34 in combination with Rux was more effective than the use of Rux alone in rescuing the myelofibrotic traits of *Gata1*^{low} mice.

Finally, we found an interesting link between the abnormal high levels of TGF-β1 and of CXCL1 expressed by *Gata1*^{low} mice. In recent studies, we demonstrated that the allosteric CXCR1/R2 inhibitor Reparixin reduced the fibrosis by reducing TGF-β1 and collagen III expression in MKs from *Gata1*^{low} mice [98]. These effects were observed in parallel with decreased neutrophil infiltration and reduced number of neutrophils engulfed by malignant MKs [97]. On the other hand, P-sel inhibition reduced both TGF-β1 and CXCL1 levels.
Several studies demonstrated that TGF-β1 and CXCL1 drive disease progression by triggering the fibrotic deposition and altering the HCSs niches. Beyond its well-known role in promoting fibrosis by activating MSCs, dysregulated TGF-β1 signaling can also alter the hematopoietic microenvironment supporting the predominance of MF-HSCs and inducing the quiescence of the reservoir of wild-type HSCs. In addition, TGF-β1 activates MSCs which participate in the amplification and differentiation of hematopoietic clones as a consequence of altered HSCs-niche cross talk [109]. On the other hand, Levine and colleagues demonstrated that IL-8 enhanced the colony-forming capacity of primary CD34pos cells from PMF patients while CXCR1/2 inhibitors inverted this effects. In addition, MKs from PMF patients cultured in vitro displayed increased IL-8 secretion. The authors observed an increased expression of CXCR1/R2 in the malignant CD34pos cells, suggesting that these cells could be both the source and the target of IL-8. Finally, they reported that administration of exogenous IL-8 to malignant CD34pos cells induced cell proliferation and a significant increase in the number of monocytes and MKs [58]. Moreover, the authors demonstrated that splenocytes from hMPL^{W515L} mice, a mouse model of PMF, with targeted deletion of CXCR2 receptor showed a significant reduction of agonists toll-like receptor 4 (TLR4) S100A8/S100A9, suggesting a role for CXCR2 in modulating pro-inflammatory signaling [58]. The alarmin S100A8/S100A9 heterocomplex [110] is highly expressed by pre-fibrotic MSCs and act through the inflammatory activating endogenous TLR4 as a mediator of myelofibrosis, favoring MSCs proliferation and myofibroblast differentiation in early stage of the disease.

Thus, we hypothesize that HSCs- and MKs-derived CXCL1 may contribute to the progression toward the fibrotic phase by modulating pro-inflammatory signaling and by triggering neutrophil chemotaxis, an event that precedes the P-sel-driven emperipolesis between MKs and neutrophils. As a result, this pathological cell interaction leads to the death of MKs by para-apoptosis and to the massive release of TGF-β1 in the microenvironment (**Figure 1**).

In conclusion, taking into account the well-established role of TGF-β1 in the progression of MF, and the emergent role of IL-8 in sustaining malignant HCSs and MKs through a self-fuel circuit, we believe that inhibition of the P-sel/TGF-β1 and IL-8/CXCR1/R2 axes may represent an attractive therapeutic opportunity to intercept MF progression and therefore warrants further study in the clinical context.

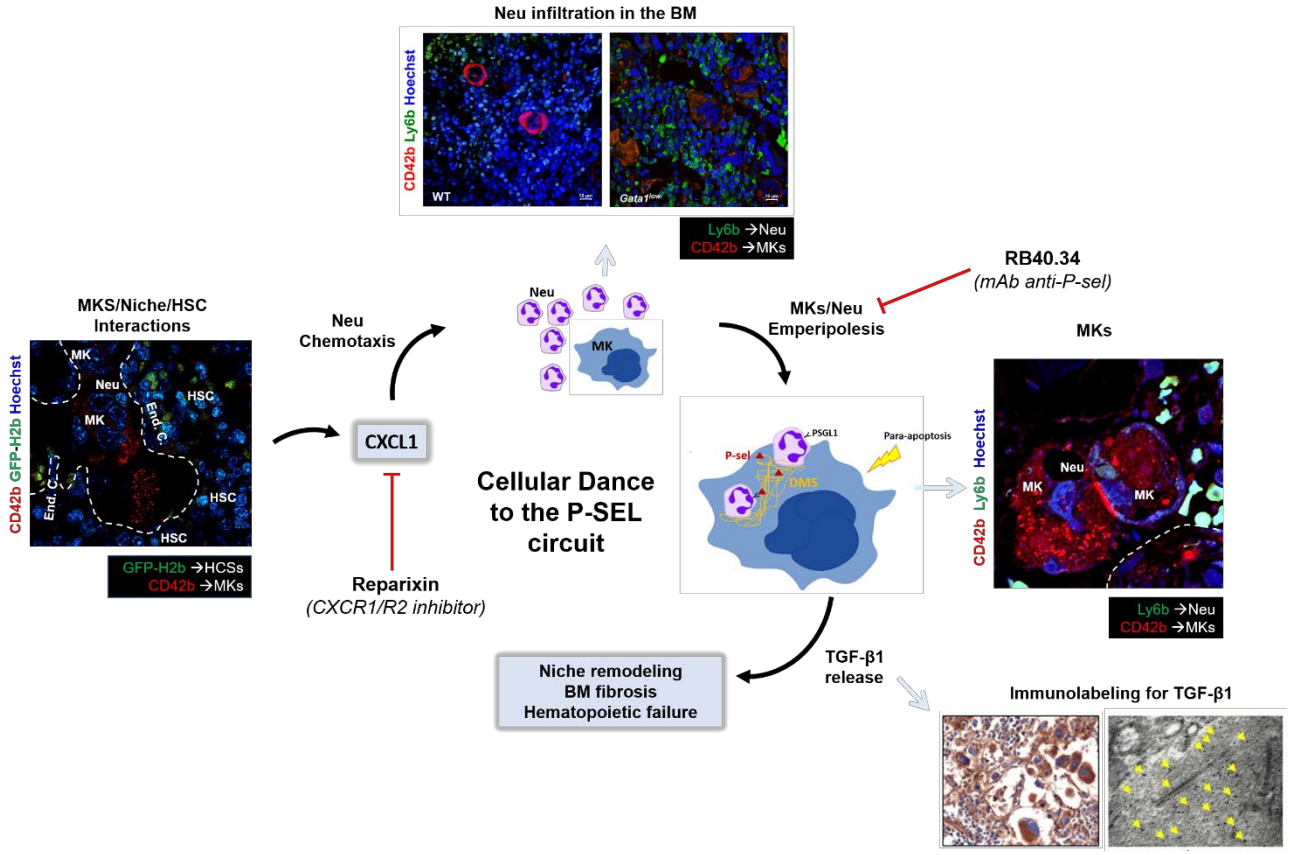

Figure 1. Graphical representation of the mechanism underlying the fibrotic progression triggered by the malignant megakaryocytes (MKs) in *Gata1*^{low} mice. High levels of CXCL1 secreted by malignant HSCs and MKs trigger the chemotaxis of neutrophils (Neu) in the BM, an event that precedes the pathological MK-Neu emperipolesis. This destructive cell-cell interaction is promoted by abnormal high levels of P-selectin (P-sel) expressed on the cell surface of malignant MKs instead of within the α-granules. The consequential death of MKs by para-apoptosis leads to the massive release of MKs content in the microenvironment, including TGF-β1 that promotes fibrotic deposition, niche remodeling with resulting hematopoietic failure. Representative panels of immunofluorescence analysis on BM sections to detect MKs (CD42b), Neu (Ly6b)

and GFP-tagged HSCs interactions are shown. Representative images of TGF-β1 immunolabeling show the high levels of this cytokine in the BM microenvironment. Red arrows indicate the targets of the CXCR1/R2 inhibitor Reparixin and the anti-Psel antibody RB40.34.

5. Conclusions

MKs are multifunctional hematopoietic cells that produce platelets, regulate the BM niches supporting the development of HSCs and provide inflammatory signals to respond to opportunistic infections in the lung. During the embryogenesis, a specific MK subpopulation is responsible to synthesize the extracellular matrix of the organs. The MKs subpopulations produced in the bone marrow can dynamically change during homeostasis and under stress condition, thereby regulating HSCs functions. PMF is a progressive chronic MPN characterized by hyperactivation of JAK/STAT signaling which sustains MKs abnormalities that include an aberrant pro-inflammatory signature. Several studies on PMF patients and murine models of the disease demonstrated that malignant MKs represent the main source of pro-inflammatory cytokines, including TGF-β1 and CXCL1. These MK-derived factors promote the emergence of disease and its progression by corrupting the microenvironment, inducing fibrosis, e by turning the hematopoietic niche into a malignant-HSCs sustaining niche. Conventional treatments for MF, such as treatment with JAK1/2 inhibitors, are effective in controlling the symptoms but do not halt the progression of PMF and new therapeutic approaches aiming to target mechanisms downstream to the driver mutations are badly needed. During my PhD, I have demonstrated that treatment with P-sel and JAK1/2 inhibitors in combination is more effective than any of the two drugs as single agent in rescuing the myelofibrosis phenotype of the *Gata1*^{low} mouse model by significantly decreasing the content of TGF-β1 and CXCL1 in the microenvironment, normalizing the MK-driven microenvironmental abnormalities, restoring hematopoiesis in the BM and the architecture of the spleen. In conclusion, my study provided preclinical evidence that combination therapies are more effective than the use of the single agents for the cure of PMF.

6. Bibliography

1. Tefferi, A.; Gangat, N.; Pardanani, A.; Crispino, J.D. Myelofibrosis: Genetic Characteristics and the Emerging Therapeutic Landscape. *Cancer Res.* **2022**, *82*, 749–763, doi:10.1158/0008-5472.CAN-21-2930.
2. Vainchenker, W.; Constantinescu, S.N.; Plo, I. Recent advances in understanding myelofibrosis and essential thrombocythemia. *F1000Research* **2016**, *5*, doi:10.12688/f1000research.8081.1.
3. Levine, R.L.; Wadleigh, M.; Cools, J.; Ebert, B.L.; Wernig, G.; Huntly, B.J.P.; Boggon, T.J.; Wlodarska, I.; Clark, J.J.; Moore, S.; et al. Activating mutation in the tyrosine kinase JAK2 in polycythemia vera, essential thrombocythemia, and myeloid metaplasia with myelofibrosis. *Cancer Cell* **2005**, *7*, 387–397, doi:10.1016/j.ccr.2005.03.023.
4. James, C.; Ugo, V.; Le Couédic, J.-P.; Staerk, J.; Delhommeau, F.; Lacout, C.; Garçon, L.; Raslova, H.; Berger, R.; Bennaceur-Griscelli, A.; et al. A unique clonal JAK2 mutation leading to constitutive signalling causes polycythaemia vera. *Nature* **2005**, *434*, 1144–1148, doi:10.1038/nature03546.
5. Kralovics, R.; Passamonti, F.; Buser, A.S.; Teo, S.-S.; Tiedt, R.; Passweg, J.R.; Tichelli, A.; Cazzola, M.; Skoda, R.C. A gain-of-function mutation of JAK2 in myeloproliferative disorders. *N. Engl. J. Med.* **2005**, *352*, 1779–1790, doi:10.1056/NEJMoa051113.
6. Baxter, E.J.; Scott, L.M.; Campbell, P.J.; East, C.; Fourouclas, N.; Swanton, S.; Vassiliou, G.S.; Bench, A.J.; Boyd, E.M.; Curtin, N.; et al. Acquired mutation of the tyrosine kinase JAK2 in human myeloproliferative disorders. *Lancet (London, England)* **2005**, *365*, 1054–1061, doi:10.1016/S0140-6736(05)71142-9.
7. Hu, X.; Li, J.; Fu, M.; Zhao, X.; Wang, W. The JAK/STAT signaling pathway: from bench to clinic. *Signal Transduct. Target. Ther.* **2021**, *6*, 402, doi:10.1038/s41392-021-00791-1.
8. Tefferi, A. Somatic JAK2 mutations and their tumor phenotypes. *Blood* **2016**, *128*, 748–749, doi:10.1182/blood-2016-06-722645.
9. Schmitz, B.; Thiele, J.; Otto, F.; Farahmand, P.; Henze, F.; Frimpong, S.; Wickenhauser, C.; Fischer, R. Evidence for integrin receptor involvement in megakaryocyte-fibroblast interaction: a possible pathomechanism for the evolution of myelofibrosis. *J. Cell. Physiol.* **1998**, *176*, 445–455, doi:10.1002/(SICI)1097-4652(199809)176:3<445::AID-JCP1>3.0.CO;2-O.
10. Mesa, R.A.; Hanson, C.A.; Rajkumar, S. V; Schroeder, G.; Tefferi, A. Evaluation and clinical correlations of bone marrow angiogenesis in myelofibrosis with myeloid metaplasia. *Blood* **2000**, *96*, 3374–3380.
11. Carbuccia, N.; Murati, A.; Trouplin, V.; Brecqueville, M.; Adélaïde, J.; Rey, J.; Vainchenker, W.; Bernard, O.A.; Chaffanet, M.; Vey, N.; et al. Mutations of ASXL1 gene in myeloproliferative neoplasms. *Leukemia* 2009, *23*, 2183–2186.
12. Delhommeau, F.; Dupont, S.; Della Valle, V.; James, C.; Trannoy, S.; Massé, A.; Kosmider, O.; Le Couedic, J.-P.; Robert, F.; Alberdi, A.; et al. Mutation in TET2 in myeloid cancers. *N. Engl. J. Med.* **2009**, *360*, 2289–2301, doi:10.1056/NEJMoa0810069.
13. Abdel-Wahab, O.; Pardanani, A.; Rampal, R.; Lasho, T.L.; Levine, R.L.; Tefferi, A. DNMT3A mutational analysis in primary myelofibrosis, chronic myelomonocytic leukemia and advanced phases of myeloproliferative neoplasms. *Leukemia* 2011, *25*, 1219–1220.
14. Gilles, L.; Arslan, A.D.; Marinaccio, C.; Wen, Q.J.; Arya, P.; McNulty, M.; Yang, Q.; Zhao, J.C.; Konstantinoff, K.; Lasho, T.; et al. Downregulation of GATA1 drives impaired hematopoiesis in primary myelofibrosis. *J. Clin. Invest.* **2017**, *127*, 1316–1320, doi:10.1172/JCI82905.
15. Tefferi, A. Myelofibrosis with myeloid metaplasia. *N. Engl. J. Med.* **2000**, *342*, 1255–1265,

doi:10.1056/NEJM200004273421706.
16. Barbui, T.; Thiele, J.; Gisslinger, H.; Kvasnicka, H.M.; Vannucchi, A.M.; Guglielmelli, P.; Orazi, A.; Tefferi, A. The 2016 WHO classification and diagnostic criteria for myeloproliferative neoplasms: document summary and in-depth discussion. *Blood Cancer J.* **2018**, *8*, 15, doi:10.1038/s41408-018-0054-y.
17. Ballen, K.K.; Shrestha, S.; Sobocinski, K.A.; Zhang, M.-J.; Bashey, A.; Bolwell, B.J.; Cervantes, F.; Devine, S.M.; Gale, R.P.; Gupta, V.; et al. Outcome of transplantation for myelofibrosis. *Biol. blood marrow Transplant. J. Am. Soc. Blood Marrow Transplant.* **2010**, *16*, 358–367, doi:10.1016/j.bbmt.2009.10.025.
18. Tefferi, A. Primary myelofibrosis: 2021 update on diagnosis, risk-stratification and management. *Am. J. Hematol.* **2021**, *96*, 145–162, doi:10.1002/ajh.26050.
19. Harrison, C.; Kiladjian, J.-J.; Al-Ali, H.K.; Gisslinger, H.; Waltzman, R.; Stalbovskaya, V.; McQuitty, M.; Hunter, D.S.; Levy, R.; Knoops, L.; et al. JAK inhibition with Rux versus best available therapy for myelofibrosis. *N. Engl. J. Med.* **2012**, *366*, 787–798, doi:10.1056/NEJMoa1110556.
20. Tefferi, A. JAK inhibitors for myeloproliferative neoplasms: clarifying facts from myths. *Blood* **2012**, *119*, 2721–2730, doi:10.1182/blood-2011-11-395228.
21. Coltro, G.; Mannelli, F.; Guglielmelli, P.; Pacilli, A.; Bosi, A.; Vannucchi, A.M. A life-threatening Rux discontinuation syndrome. *Am. J. Hematol.* **2017**, *92*, 833–838, doi:10.1002/ajh.24775.
22. Palandri, F.; Palumbo, G.A.; Elli, E.M.; Polverelli, N.; Benevolo, G.; Martino, B.; Abruzzese, E.; Tiribelli, M.; Tieghi, A.; Latagliata, R.; et al. Rux discontinuation syndrome: incidence, risk factors, and management in 251 patients with myelofibrosis. *Blood Cancer J.* 2021, *11*, 4.
23. Tefferi, A. Primary myelofibrosis: 2023 update on diagnosis, risk-stratification, and management. *Am. J. Hematol.* **2023**, *98*, 801–821, doi:10.1002/ajh.26857.
24. Guo, T.; Wang, X.; Qu, Y.; Yin, Y.; Jing, T.; Zhang, Q. Megakaryopoiesis and platelet production: insight into hematopoietic stem cell proliferation and differentiation. *Stem cell Investig.* **2015**, *2*, 3, doi:10.3978/j.issn.2306-9759.2015.02.01.
25. Doré, L.C.; Crispino, J.D. Transcription factor networks in erythroid cell and megakaryocyte development. *Blood* **2011**, *118*, 231–239, doi:10.1182/blood-2011-04-285981.
26. Bianchi, E.; Norfo, R.; Pennucci, V.; Zini, R.; Manfredini, R. Genomic landscape of megakaryopoiesis and platelet function defects. *Blood* **2016**, *127*, 1249–1259, doi:10.1182/blood-2015-07-607952.
27. Antony-Debré, I.; Manchev, V.T.; Balayn, N.; Bluteau, D.; Tomowiak, C.; Legrand, C.; Langlois, T.; Bawa, O.; Tosca, L.; Tachdjian, G.; et al. Level of RUNX1 activity is critical for leukemic predisposition but not for thrombocytopenia. *Blood* **2015**, *125*, 930–940, doi:10.1182/blood-2014-06-585513.
28. Centurione, L.; Di Baldassarre, A.; Zingariello, M.; Bosco, D.; Gatta, V.; Rana, R.A.; Langella, V.; Di Virgilio, A.; Vannucchi, A.M.; Migliaccio, A.R. Increased and pathologic emperipolesis of neutrophils within megakaryocytes associated with marrow fibrosis in GATA-1low mice. *Blood* **2004**, *104*, 3573–3580, doi:10.1182/blood-2004-01-0193.
29. Patel, S.R.; Hartwig, J.H.; Italiano, J.E.J. The biogenesis of platelets from megakaryocyte proplatelets. *J. Clin. Invest.* **2005**, *115*, 3348–3354, doi:10.1172/JCI26891.
30. Coppinger, J.A.; Cagney, G.; Toomey, S.; Kislinger, T.; Belton, O.; McRedmond, J.P.; Cahill, D.J.; Emili, A.; Fitzgerald, D.J.; Maguire, P.B. Characterization of the proteins released from activated platelets leads to localization of novel platelet proteins in human atherosclerotic lesions. *Blood* **2004**, *103*, 2096–2104, doi:10.1182/blood-2003-08-2804.
31. Ciurea, S.O.; Merchant, D.; Mahmud, N.; Ishii, T.; Zhao, Y.; Hu, W.; Bruno, E.; Barosi, G.; Xu, M.; Hoffman, R. Pivotal contributions of megakaryocytes to the biology of idiopathic

myelofibrosis. *Blood* **2007**, *110*, 986–993, doi:10.1182/blood-2006-12-064626.
32. Juvonen, E. Megakaryocyte colony formation in chronic myeloid leukemia and myelofibrosis. *Leuk. Res.* **1988**, *12*, 751–756, doi:10.1016/0145-2126(88)90008-2.
33. Balduini, A.; Badalucco, S.; Pugliano, M.T.; Baev, D.; De Silvestri, A.; Cattaneo, M.; Rosti, V.; Barosi, G. In vitro megakaryocyte differentiation and proplatelet formation in Ph-negative classical myeloproliferative neoplasms: distinct patterns in the different clinical phenotypes. *PLoS One* **2011**, *6*, e21015, doi:10.1371/journal.pone.0021015.
34. Nam, A.S.; Kim, K.-T.; Chaligne, R.; Izzo, F.; Ang, C.; Taylor, J.; Myers, R.M.; Abu-Zeinah, G.; Brand, R.; Omans, N.D.; et al. Somatic mutations and cell identity linked by Genotyping of Transcriptomes. *Nature* **2019**, *571*, 355–360, doi:10.1038/s41586-019-1367-0.
35. Psaila, B.; Wang, G.; Rodriguez-Meira, A.; Li, R.; Heuston, E.F.; Murphy, L.; Yee, D.; Hitchcock, I.S.; Sousos, N.; O'Sullivan, J.; et al. Single-Cell Analyses Reveal Megakaryocyte-Biased Hematopoiesis in Myelofibrosis and Identify Mutant Clone-Specific Targets. *Mol. Cell* **2020**, *78*, 477-492.e8, doi:10.1016/j.molcel.2020.04.008.
36. de Sauvage, F.J.; Hass, P.E.; Spencer, S.D.; Malloy, B.E.; Gurney, A.L.; Spencer, S.A.; Darbonne, W.C.; Henzel, W.J.; Wong, S.C.; Kuang, W.J. Stimulation of megakaryocytopoiesis and thrombopoiesis by the c-Mpl ligand. *Nature* **1994**, *369*, 533–538, doi:10.1038/369533a0.
37. Gurney, A.L.; Carver-Moore, K.; de Sauvage, F.J.; Moore, M.W. Thrombocytopenia in c-mpl-deficient mice. *Science* **1994**, *265*, 1445–1447, doi:10.1126/science.8073287.
38. Alexander, W.S.; Roberts, A.W.; Nicola, N.A.; Li, R.; Metcalf, D. Deficiencies in progenitor cells of multiple hematopoietic lineages and defective megakaryocytopoiesis in mice lacking the thrombopoietic receptor c-Mpl. *Blood* **1996**, *87*, 2162–2170.
39. Wang, J.C.; Chen, C.; Novetsky, A.D.; Lichter, S.M.; Ahmed, F.; Friedberg, N.M. Blood thrombopoietin levels in clonal thrombocytosis and reactive thrombocytosis. *Am. J. Med.* **1998**, *104*, 451–455, doi:10.1016/s0002-9343(98)00090-4.
40. Griesshammer, M.; Hornkohl, A.; Nichol, J.L.; Hecht, T.; Raghavachar, A.; Heimpel, H.; Schrezenmeier, H. High levels of thrombopoietin in sera of patients with essential thrombocythemia: cause or consequence of abnormal platelet production? *Ann. Hematol.* **1998**, *77*, 211–215, doi:10.1007/s002770050445.
41. Vannucchi, A.M.; Pancrazzi, A.; Guglielmelli, P.; Di Lollo, S.; Bogani, C.; Baroni, G.; Bianchi, L.; Migliaccio, A.R.; Bosi, A.; Paoletti, F. Abnormalities of GATA-1 in megakaryocytes from patients with idiopathic myelofibrosis. *Am. J. Pathol.* **2005**, *167*, 849–858, doi:10.1016/S0002-9440(10)62056-1.
42. Vannucchi, A.M.; Bianchi, L.; Paoletti, F.; Pancrazzi, A.; Torre, E.; Nishikawa, M.; Zingariello, M.; Di Baldassarre, A.; Rana, R.A.; Lorenzini, R.; et al. A pathobiologic pathway linking thrombopoietin, GATA-1, and TGF-β1 in the development of myelofibrosis. *Blood* **2005**, *105*, 3493–3501, doi:10.1182/blood-2004-04-1320.
43. Skoda, R.C.; Duek, A.; Grisouard, J. Pathogenesis of myeloproliferative neoplasms. *Exp. Hematol.* **2015**, *43*, 599–608, doi:10.1016/j.exphem.2015.06.007.
44. Zhan, H.; Ma, Y.; Lin, C.H.S.; Kaushansky, K. JAK2(V617F)-mutant megakaryocytes contribute to hematopoietic stem/progenitor cell expansion in a model of murine myeloproliferation. *Leukemia* **2016**, *30*, 2332–2341, doi:10.1038/leu.2016.114.
45. Kuter, D.J.; Mufti, G.J.; Bain, B.J.; Hasserjian, R.P.; Davis, W.; Rutstein, M. Evaluation of bone marrow reticulin formation in chronic immune thrombocytopenia patients treated with romiplostim. *Blood* **2009**, *114*, 3748–3756, doi:10.1182/blood-2009-05-224766.
46. Villeval, J.L.; Cohen-Solal, K.; Tulliez, M.; Giraudier, S.; Guichard, J.; Burstein, S.A.; Cramer, E.M.; Vainchenker, W.; Wendling, F. High thrombopoietin production by hematopoietic cells induces a fatal myeloproliferative syndrome in mice. *Blood* **1997**, *90*, 4369–4383.

47. Vannucchi, A.M.; Bianchi, L.; Cellai, C.; Paoletti, F.; Rana, R.A.; Lorenzini, R.; Migliaccio, G.; Migliaccio, A.R. Development of myelofibrosis in mice genetically impaired for GATA-1 expression (GATA-1(low) mice). *Blood* **2002**, *100*, 1123–1132, doi:10.1182/blood-2002-06-1913.
48. Jantunen, E.; Hänninen, A.; Naukkarinen, A.; Vornanen, M.; Lahtinen, R. Gray platelet syndrome with splenomegaly and signs of extramedullary hematopoiesis: a case report with review of the literature. *Am. J. Hematol.* **1994**, *46*, 218–224, doi:10.1002/ajh.2830460311.
49. Le Bousse-Kerdilès, M.C.; Martyré, M.C. Dual implication of fibrogenic cytokines in the pathogenesis of fibrosis and myeloproliferation in myeloid metaplasia with myelofibrosis. *Ann. Hematol.* **1999**, *78*, 437–444, doi:10.1007/s002770050595.
50. Wang, J.C.; Novetsky, A.; Chen, C.; Novetsky, A.D. Plasma matrix metalloproteinase and tissue inhibitor of metalloproteinase in patients with agnogenic myeloid metaplasia or idiopathic primary myelofibrosis. *Br. J. Haematol.* **2002**, *119*, 709–712, doi:10.1046/j.1365-2141.2002.03874.x.
51. Erba, B.G.; Gruppi, C.; Corada, M.; Pisati, F.; Rosti, V.; Bartalucci, N.; Villeval, J.-L.; Vannucchi, A.M.; Barosi, G.; Balduini, A.; et al. Endothelial-to-Mesenchymal Transition in Bone Marrow and Spleen of Primary Myelofibrosis. *Am. J. Pathol.* **2017**, *187*, 1879–1892, doi:10.1016/j.ajpath.2017.04.006.
52. Zingariello, M.; Martelli, F.; Ciaffoni, F.; Masiello, F.; Ghinassi, B.; D'Amore, E.; Massa, M.; Barosi, G.; Sancillo, L.; Li, X.; et al. Characterization of the TGF-beta1 signaling abnormalities in the Gata1low mouse model of myelofibrosis. *Blood* **2013**, *121*, 3345–3363, doi:10.1182/blood-2012-06-439661.
53. Chagraoui, H.; Komura, E.; Tulliez, M.; Giraudier, S.; Vainchenker, W.; Wendling, F. Prominent role of TGF-beta 1 in thrombopoietin-induced myelofibrosis in mice. *Blood* **2002**, *100*, 3495–3503, doi:10.1182/blood-2002-04-1133.
54. Yue, L.; Bartenstein, M.; Zhao, W.; Ho, W.T.; Han, Y.; Murdun, C.; Mailloux, A.W.; Zhang, L.; Wang, X.; Budhathoki, A.; et al. Efficacy of ALK5 inhibition in myelofibrosis. *JCI insight* **2017**, *2*, e90932, doi:10.1172/jci.insight.90932.
55. Gastinne, T.; Vigant, F.; Lavenu-Bombled, C.; Wagner-Ballon, O.; Tulliez, M.; Chagraoui, H.; Villeval, J.-L.; Lacout, C.; Perricaudet, M.; Vainchenker, W.; et al. Adenoviral-mediated TGF-beta1 inhibition in a mouse model of myelofibrosis inhibit bone marrow fibrosis development. *Exp. Hematol.* **2007**, *35*, 64–74, doi:10.1016/j.exphem.2006.08.016.
56. Ceglia, I.; Dueck, A.C.; Masiello, F.; Martelli, F.; He, W.; Federici, G.; Petricoin, E.F. 3rd; Zeuner, A.; Iancu-Rubin, C.; Weinberg, R.; et al. Preclinical rationale for TGF-β inhibition as a therapeutic target for the treatment of myelofibrosis. *Exp. Hematol.* **2016**, *44*, 1138-1155.e4, doi:10.1016/j.exphem.2016.08.007.
57. Tefferi, A.; Vaidya, R.; Caramazza, D.; Finke, C.; Lasho, T.; Pardanani, A. Circulating interleukin (IL)-8, IL-2R, IL-12, and IL-15 levels are independently prognostic in primary myelofibrosis: a comprehensive cytokine profiling study. *J Clin Oncol* **2011**, *29*, 1356–1363, doi:10.1200/JCO.2010.32.9490.
58. Dunbar, A.J.; Kim, D.; Lu, M.; Farina, M.; Bowman, R.L.; Yang, J.L.; Park, Y.; Karzai, A.; Xiao, W.; Zaroogian, Z.; et al. CXCL8/CXCR2 signaling mediates bone marrow fibrosis and is a therapeutic target in myelofibrosis. *Blood* **2023**, *141*, 2508–2519, doi:10.1182/blood.2022015418.
59. Malara, A.; Abbonante, V.; Zingariello, M.; Migliaccio, A.; Balduini, A. Megakaryocyte Contribution to Bone Marrow Fibrosis: many Arrows in the Quiver. *Mediterr. J. Hematol. Infect. Dis.* **2018**, *10*, e2018068, doi:10.4084/MJHID.2018.068.
60. Wang, H.; He, J.; Xu, C.; Chen, X.; Yang, H.; Shi, S.; Liu, C.; Zeng, Y.; Wu, D.; Bai, Z.; et al. Decoding Human Megakaryocyte Development. *Cell Stem Cell* **2021**, *28*, 535-549.e8, doi:10.1016/j.stem.2020.11.006.

61. Sun, S.; Jin, C.; Si, J.; Lei, Y.; Chen, K.; Cui, Y.; Liu, Z.; Liu, J.; Zhao, M.; Zhang, X.; et al. Single-cell analysis of ploidy and the transcriptome reveals functional and spatial divergency in murine megakaryopoiesis. *Blood* **2021**, *138*, 1211–1224, doi:10.1182/blood.2021010697.
62. Pariser, D.N.; Hilt, Z.T.; Ture, S.K.; Blick-Nitko, S.K.; Looney, M.R.; Cleary, S.J.; Roman-Pagan, E.; Saunders, J. 2nd; Georas, S.N.; Veazey, J.; et al. Lung megakaryocytes are immune modulatory cells. *J. Clin. Invest.* **2021**, *131*, doi:10.1172/JCI137377.
63. Yeung, A.K.; Villacorta-Martin, C.; Hon, S.; Rock, J.R.; Murphy, G.J. Lung megakaryocytes display distinct transcriptional and phenotypic properties. *Blood Adv.* **2020**, *4*, 6204–6217, doi:10.1182/bloodadvances.2020002843.
64. Bruns, I.; Lucas, D.; Pinho, S.; Ahmed, J.; Lambert, M.P.; Kunisaki, Y.; Scheiermann, C.; Schiff, L.; Poncz, M.; Bergman, A.; et al. Megakaryocytes regulate hematopoietic stem cell quiescence through CXCL4 secretion. *Nat. Med.* **2014**, *20*, 1315–1320, doi:10.1038/nm.3707.
65. Zhao, M.; Perry, J.M.; Marshall, H.; Venkatraman, A.; Qian, P.; He, X.C.; Ahamed, J.; Li, L. Megakaryocytes maintain homeostatic quiescence and promote post-injury regeneration of hematopoietic stem cells. *Nat. Med.* **2014**, *20*, 1321–1326, doi:10.1038/nm.3706.
66. Dominici, M.; Rasini, V.; Bussolari, R.; Chen, X.; Hofmann, T.J.; Spano, C.; Bernabei, D.; Veronesi, E.; Bertoni, F.; Paolucci, P.; et al. Restoration and reversible expansion of the osteoblastic hematopoietic stem cell niche after marrow radioablation. *Blood* **2009**, *114*, 2333–2343, doi:10.1182/blood-2008-10-183459.
67. Olson, T.S.; Caselli, A.; Otsuru, S.; Hofmann, T.J.; Williams, R.; Paolucci, P.; Dominici, M.; Horwitz, E.M. Megakaryocytes promote murine osteoblastic HSC niche expansion and stem cell engraftment after radioablative conditioning. *Blood* **2013**, *121*, 5238–5249, doi:10.1182/blood-2012-10-463414.
68. Zhao, M.; Ross, J.T.; Itkin, T.; Perry, J.M.; Venkatraman, A.; Haug, J.S.; Hembree, M.J.; Deng, C.-X.; Lapidot, T.; He, X.C.; et al. FGF signaling facilitates postinjury recovery of mouse hematopoietic system. *Blood* **2012**, *120*, 1831–1842, doi:10.1182/blood-2011-11-393991.
69. Khatib-Massalha, E.; Méndez-Ferrer, S. Megakaryocyte Diversity in Ontogeny, Functions and Cell-Cell Interactions. *Front. Oncol.* **2022**, *12*, 840044, doi:10.3389/fonc.2022.840044.
70. Varricchio, L.; Iancu-Rubin, C.; Upadhyaya, B.; Zingariello, M.; Martelli, F.; Verachi, P.; Clementelli, C.; Denis, J.-F.; Rahman, A.H.; Tremblay, G.; et al. TGF-β1 protein trap AVID200 beneficially affects hematopoiesis and bone marrow fibrosis in myelofibrosis. *JCI insight* **2021**, *6*, doi:10.1172/jci.insight.145651.
71. Mascarenhas, J.; Kosiorek, H.E.; Bhave, R.; Palmer, J.M.; Kuykendall, A.T.; Mesa, R.A.; Rampal, R.; Gerds, A.T.; Yacoub, A.; Pettit, K.M.; et al. Treatment of Myelofibrosis Patients with the TGF-β 1/3 Inhibitor AVID200 (MPN-RC 118) Induces a Profound Effect on Platelet Production. *Blood* **2021**, *138*, 142, doi:10.1182/blood-2021-148995.
72. Zingariello, M.; Verachi, P.; Gobbo, F.; Martelli, F.; Falchi, M.; Mazzarini, M.; Valeri, M.; Sarli, G.; Marinaccio, C.; Melo-Cardenas, J.; et al. Resident Self-Tissue of Proinflammatory Cytokines Rather Than Their Systemic Levels Correlates with Development of Myelofibrosis in Gata1(low) Mice. *Biomolecules* **2022**, *12*, doi:10.3390/biom12020234.
73. Shen, Q.; Zhu, S.; Hu, J.; Geng, N.; Zou, S. Recombinant human bone morphogenetic protein-4 (BMP-4)-stimulated cell differentiation and bone formation within the expanding calvarial suture in rats. *J. Craniofac. Surg.* **2009**, *20*, 1561–1565, doi:10.1097/SCS.0b013e3181b09cc1.
74. Nguyen, J.; Tang, S.Y.; Nguyen, D.; Alliston, T. Load regulates bone formation and Sclerostin expression through a TGFβ-dependent mechanism. *PLoS One* **2013**, *8*, e53813, doi:10.1371/journal.pone.0053813.
75. Lin, S.; Xie, J.; Gong, T.; Shi, S.; Zhang, T.; Fu, N.; Ye, L.; Wang, M.; Lin, Y. TGFβ signalling pathway regulates angiogenesis by endothelial cells, in an adipose-derived stromal cell/endothelial cell co-culture 3D gel model. *Cell Prolif.* **2015**, *48*, 729–737, doi:10.1111/cpr.12222.

76. Karagianni, A.; Ravid, K. Myeloproliferative disorders and their effects on bone homeostasis: the role of megakaryocytes. *Blood* **2022**, *139*, 3127–3137, doi:10.1182/blood.2021011480.
77. Schmitt, A.; Jouault, H.; Guichard, J.; Wendling, F.; Drouin, A.; Cramer, E.M. Pathologic interaction between megakaryocytes and polymorphonuclear leukocytes in myelofibrosis. *Blood* **2000**, *96*, 1342–1347.
78. Pevny, L.; Simon, M.C.; Robertson, E.; Klein, W.H.; Tsai, S.F.; D'Agati, V.; Orkin, S.H.; Costantini, F. Erythroid differentiation in chimaeric mice blocked by a targeted mutation in the gene for transcription factor GATA-1. *Nature* **1991**, *349*, 257–260, doi:10.1038/349257a0.
79. Fujiwara, Y.; Browne, C.P.; Cunniff, K.; Goff, S.C.; Orkin, S.H. Arrested development of embryonic red cell precursors in mouse embryos lacking transcription factor GATA-1. *Proc. Natl. Acad. Sci. U. S. A.* **1996**, *93*, 12355–12358, doi:10.1073/pnas.93.22.12355.
80. Nichols, K.E.; Crispino, J.D.; Poncz, M.; White, J.G.; Orkin, S.H.; Maris, J.M.; Weiss, M.J. Familial dyserythropoietic anaemia and thrombocytopenia due to an inherited mutation in GATA1. *Nat. Genet.* **2000**, *24*, 266–270, doi:10.1038/73480.
81. Freson, K.; Devriendt, K.; Matthijs, G.; Van Hoof, A.; De Vos, R.; Thys, C.; Minner, K.; Hoylaerts, M.F.; Vermylen, J.; Van Geet, C. Platelet characteristics in patients with X-linked macrothrombocytopenia because of a novel GATA1 mutation. *Blood* **2001**, *98*, 85–92, doi:10.1182/blood.v98.1.85.
82. Mehaffey, M.G.; Newton, A.L.; Gandhi, M.J.; Crossley, M.; Drachman, J.G. X-linked thrombocytopenia caused by a novel mutation of GATA-1. *Blood* **2001**, *98*, 2681–2688, doi:10.1182/blood.v98.9.2681.
83. Yu, C.; Niakan, K.K.; Matsushita, M.; Stamatoyannopoulos, G.; Orkin, S.H.; Raskind, W.H. X-linked thrombocytopenia with thalassemia from a mutation in the amino finger of GATA-1 affecting DNA binding rather than FOG-1 interaction. *Blood* **2002**, *100*, 2040–2045, doi:10.1182/blood-2002-02-0387.
84. Vyas, P.; Ault, K.; Jackson, C.W.; Orkin, S.H.; Shivdasani, R.A. Consequences of GATA-1 deficiency in megakaryocytes and platelets. *Blood* **1999**, *93*, 2867–2875.
85. Chang, A.N.; Cantor, A.B.; Fujiwara, Y.; Lodish, M.B.; Droho, S.; Crispino, J.D.; Orkin, S.H. GATA-factor dependence of the multitype zinc-finger protein FOG-1 for its essential role in megakaryopoiesis. *Proc. Natl. Acad. Sci. U. S. A.* **2002**, *99*, 9237–9242, doi:10.1073/pnas.142302099.
86. Shivdasani, R.A.; Fujiwara, Y.; McDevitt, M.A.; Orkin, S.H. A lineage-selective knockout establishes the critical role of transcription factor GATA-1 in megakaryocyte growth and platelet development. *EMBO J.* **1997**, *16*, 3965–3973, doi:10.1093/emboj/16.13.3965.
87. McDevitt, M.A.; Shivdasani, R.A.; Fujiwara, Y.; Yang, H.; Orkin, S.H. A "knockdown" mutation created by cis-element gene targeting reveals the dependence of erythroid cell maturation on the level of transcription factor GATA-1. *Proc. Natl. Acad. Sci.* **1997**, *94*, 6781–6785, doi:10.1073/pnas.94.13.6781.
88. Massagué, J. TGFbeta in Cancer. *Cell* **2008**, *134*, 215–230, doi:10.1016/j.cell.2008.07.001.
89. Funaba, M.; Zimmerman, C.M.; Mathews, L.S. Modulation of Smad2-mediated signaling by extracellular signal-regulated kinase. *J. Biol. Chem.* **2002**, *277*, 41361–41368, doi:10.1074/jbc.M204597200.
90. Seay, U.; Sedding, D.; Krick, S.; Hecker, M.; Seeger, W.; Eickelberg, O. Transforming growth factor-beta-dependent growth inhibition in primary vascular smooth muscle cells is p38-dependent. *J. Pharmacol. Exp. Ther.* **2005**, *315*, 1005–1012, doi:10.1124/jpet.105.091249.
91. Larsen, T.E. Emperipolesis of granular leukocytes within megakaryocytes in human hemopoietic bone marrow. *Am. J. Clin. Pathol.* **1970**, *53*, 485–489, doi:10.1093/ajcp/53.4.485.
92. Cunin, P.; Bouslama, R.; Machlus, K.R.; Martínez-Bonet, M.; Lee, P.Y.; Wactor, A.; Nelson-Maney, N.; Morris, A.; Guo, L.; Weyrich, A.; et al. Megakaryocyte emperipolesis mediates

membrane transfer from intracytoplasmic neutrophils to platelets. *Elife* **2019**, *8*, doi:10.7554/eLife.44031.
93. Evangelista, V.; Manarini, S.; Sideri, R.; Rotondo, S.; Martelli, N.; Piccoli, A.; Totani, L.; Piccardoni, P.; Vestweber, D.; de Gaetano, G.; et al. Platelet/polymorphonuclear leukocyte interaction: P-selectin triggers protein-tyrosine phosphorylation-dependent CD11b/CD18 adhesion: role of PSGL-1 as a signaling molecule. *Blood* **1999**, *93*, 876–885.
94. Thiele, J.; Lorenzen, J.; Manich, B.; Kvasnicka, H.M.; Zirbes, T.K.; Fischer, R. Apoptosis (programmed cell death) in idiopathic (primary) osteo-/myelofibrosis: naked nuclei in megakaryopoiesis reveal features of para-apoptosis. *Acta Haematol.* **1997**, *97*, 137–143, doi:10.1159/000203671.
95. Zingariello, M.; Fabucci, M.E.; Bosco, D.; Migliaccio, A.R.; Martelli, F.; Rana, R.A.; Zetterberg, E. Differential localization of P-selectin and von Willebrand factor during megakaryocyte maturation. *Biotech. Histochem. Off. Publ. Biol. Stain Comm.* **2010**, *85*, 157–170, doi:10.3109/10520290903149612.
96. Spangrude, G.J.; Lewandowski, D.; Martelli, F.; Marra, M.; Zingariello, M.; Sancillo, L.; Rana, R.A.; Migliaccio, A.R. P-Selectin Sustains Extramedullary Hematopoiesis in the Gata1low Model of Myelofibrosis. *Stem Cells* **2016**, *34*, 67–82, doi:10.1002/stem.2229.
97. Arciprete, F.; Verachi, P.; Martelli, F.; Valeri, M.; Balliu, M.; Guglielmelli, P.; Vannucchi, A.M.; Migliaccio, A.R.; Zingariello, M. Inhibition of CXCR1/2 reduces the emperipolesis between neutrophils and megakaryocytes in the Gata1(low) model of myelofibrosis. *Exp. Hematol.* **2023**, *121*, 30–37, doi:10.1016/j.exphem.2023.02.003.
98. Verachi, P.; Gobbo, F.; Martelli, F.; Martinelli, A.; Sarli, G.; Dunbar, A.; Levine, R.L.; Hoffman, R.; Massucci, M.T.; Brandolini, L.; et al. The CXCR1/CXCR2 Inhibitor Reparixin Alters the Development of Myelofibrosis in the Gata1 (low) Mice. *Front. Oncol.* **2022**, *12*, 853484, doi:10.3389/fonc.2022.853484.
99. Tefferi, A. Challenges facing JAK inhibitor therapy for myeloproliferative neoplasms. *N. Engl. J. Med.* 2012, *366*, 844–846.
100. McDevitt, M.A.; Fujiwara, Y.; Shivdasani, R.A.; Orkin, S.H. An upstream, DNase I hypersensitive region of the hematopoietic-expressed transcription factor GATA-1 gene confers developmental specificity in transgenic mice. *Proc. Natl. Acad. Sci. U. S. A.* **1997**, *94*, 7976–7981, doi:10.1073/pnas.94.15.7976.
101. Migliaccio, A.R.; Martelli, F.; Verrucci, M.; Sanchez, M.; Valeri, M.; Migliaccio, G.; Vannucchi, A.M.; Zingariello, M.; Di Baldassarre, A.; Ghinassi, B.; et al. Gata1 expression driven by the alternative HS2 enhancer in the spleen rescues the hematopoietic failure induced by the hypomorphic Gata1low mutation. *Blood* **2009**, *114*, 2107–2120, doi:10.1182/blood-2009-03-211680.
102. Zingariello, M.; Sancillo, L.; Martelli, F.; Ciaffoni, F.; Marra, M.; Varricchio, L.; Rana, R.A.; Zhao, C.; Crispino, J.D.; Migliaccio, A.R. The thrombopoietin/MPL axis is activated in the gata1low mouse model of myelofibrosis and is associated with a defective RPS14 signature. *Blood Cancer J.* **2017**, *7*, 1–11, doi:10.1038/bcj.2017.51.
103. Ciaffoni, F.; Cassella, E.; Varricchio, L.; Massa, M.; Barosi, G.; Migliaccio, A.R. Activation of non-canonical TGF-β1 signaling indicates an autoimmune mechanism for bone marrow fibrosis in primary myelofibrosis. *Blood Cells. Mol. Dis.* **2015**, *54*, 234–241, doi:10.1016/j.bcmd.2014.12.005.
104. Yao, J.-C.; Oetjen, K.A.; Wang, T.; Xu, H.; Abou-Ezzi, G.; Krambs, J.R.; Uttarwar, S.; Duncavage, E.J.; Link, D.C. TGF-β signaling in myeloproliferative neoplasms contributes to myelofibrosis without disrupting the hematopoietic niche. *J. Clin. Invest.* **2022**, *132*, doi:10.1172/JCI154092.
105. Lucijanic, M.; Pejsa, V.; Jaksic, O.; Mitrovic, Z.; Tomasovic-Loncaric, C.; Stoos-Veic, T.; Prka, Z.; Pirsic, M.; Haris, V.; Vasilj, T.; et al. The Degree of Anisocytosis Predicts Survival

in Patients with Primary Myelofibrosis. *Acta Haematol.* **2016**, *136*, 98–100, doi:10.1159/000445247.
106. Bommireddy, R.; Saxena, V.; Ormsby, I.; Yin, M.; Boivin, G.P.; Babcock, G.F.; Singh, R.R.; Doetschman, T. TGF-beta 1 regulates lymphocyte homeostasis by preventing activation and subsequent apoptosis of peripheral lymphocytes. *J. Immunol.* **2003**, *170*, 4612–4622, doi:10.4049/jimmunol.170.9.4612.
107. Mukaida, N. Interleukin-8: an expanding universe beyond neutrophil chemotaxis and activation. *Int. J. Hematol.* **2000**, *72*, 391–398.
108. Abbonante, V.; Di Buduo, C.A.; Gruppi, C.; Malara, A.; Gianelli, U.; Celesti, G.; Anselmo, A.; Laghi, L.; Vercellino, M.; Visai, L.; et al. Thrombopoietin/TGF-β1 Loop Regulates Megakaryocyte Extracellular Matrix Component Synthesis. *Stem Cells* **2016**, *34*, 1123–1133, doi:10.1002/stem.2285.
109. Varricchio, L.; Hoffman, R. Megakaryocytes Are Regulators of the Tumor Microenvironment and Malignant Hematopoietic Progenitor Cells in Myelofibrosis. *Front. Oncol.* **2022**, *12*, 906698, doi:10.3389/fonc.2022.906698.
110. Leimkühler, N.B.; Gleitz, H.F.E.; Ronghui, L.; Snoeren, I.A.M.; Fuchs, S.N.R.; Nagai, J.S.; Banjanin, B.; Lam, K.H.; Vogl, T.; Kuppe, C.; et al. Heterogeneous bone-marrow stromal progenitors drive myelofibrosis via a druggable alarmin axis. *Cell Stem Cell* **2021**, *28*, 637-652.e8, doi:10.1016/j.stem.2020.11.004.